

**UNCLASSIFIED**

---

**AD 296 543**

*Reproduced  
by the*

**ARMED SERVICES TECHNICAL INFORMATION AGENCY  
ARLINGTON HALL STATION  
ARLINGTON 12, VIRGINIA**



---

**UNCLASSIFIED**

NOTICE: When government or other drawings, specifications or other data are used for any purpose other than in connection with a definitely related government procurement operation, the U. S. Government thereby incurs no responsibility, nor any obligation whatsoever; and the fact that the Government may have formulated, furnished, or in any way supplied the said drawings, specifications, or other data is not to be regarded by implication or otherwise as in any manner licensing the holder or any other person or corporation, or conveying any rights or permission to manufacture, use or sell any patented invention that may in any way be related thereto.

UNCLASSIFIED

CATALOGED BY ASIA  
AS AD 10  
296543

296 543

**"MILLIMETER WAVE RESEARCH"**

by

J. M. Cotton

M. Cohn

F. Sobel

J. C. Willse

Final Technical Report  
Contract No. AF 30(602)-2457



**ONIC  
UNICATIONS**

HOME OFFICE-ST. PETERSBURG, FLORIDA

Prepared  
for  
Rome Air Development Center  
Air Force Systems Command  
United States Air Force  
Griffiss Air Force Base  
New York

RESEARCH DIVISION  
1830 YORK ROAD  
TIMONIUM, MARYLAND

UNCLASSIFIED

### **PATENT NOTICE**

When Government drawings, specifications, or other data are used for any purpose other than in connection with a definitely related Government procurement operation, the United States Government thereby incurs no responsibility nor any obligation whatsoever and the fact that the Government may have formulated, furnished, or in any way supplied the said drawings, specifications or other data is not to be regarded by implication or otherwise as in any manner licensing the holder or any other person or corporation, or conveying any rights or permission to manufacture, use, or sell any patented invention that may in any way be related thereto.

### **ASTIA NOTICE**

Qualified requestors may obtain copies of this report from the ASTIA Document Service Center, Arlington Hall Station, Arlington 12, Virginia. ASTIA Services for the Department of Defense contractors are available through the "Field of Interest Register" on a "need-to-know" certified by the cognizant military agency of their project or contract.

### **OTS NOTICE**

This report has been released to the Office of Technical Services, U.S. Department of Commerce, Washington 25, D. C. for sale to the general public.

UNCLASSIFIED

**"MILLIMETER WAVE RESEARCH"**

by

J. M. Cotton

M. Cohn

F. Sobel

J. C. Wiltse

Final Technical Report

Contract No. AF 30(602)-2457

Project No. 4506

Task No. 450602



HOME OFFICE—ST. PETERSBURG, FLORIDA

Prepared  
for

Rome Air Development Center  
Air Force Systems Command  
United States Air Force  
Griffiss Air Force Base  
New York

RESEARCH DIVISION  
1830 YORK ROAD  
TIMONIUM, MARYLAND

UNCLASSIFIED

## FOREWORD

The authors would like to thank Mrs. Marcia J. King for her contributions to the analyses and computations pertaining to the several transmission methods described herein. They would like to thank Mr. John O. Wedel for his work in designing circuitry for the AFC system components. Acknowledgement is also due Mr. Frederick L. Wentworth and Mr. James D. Rodgers for assistance with the instrumentation and measurements in the experimental program.

## ABSTRACT

The report includes a study of propagation methods for possible use in the submillimeter wavelength region (1.0 to 0.1 mm) of the electromagnetic spectrum. The more promising among these (trough waveguide, oversized waveguide and Fresnel region propagation using Fresnel zone plates) are given a more comprehensive analytical treatment. Recommendations are given for some designs which would appear to have the highest probability for success.

A measurement system consisting of a harmonic generator signal source and a harmonic-mixing superheterodyne receiver was built which was used for data taking at 210, 280, 350, and 420 Gc. The fundamental signals for harmonic generation and mixing were obtained from 70 Gc klystrons. An AFC system was developed to hold the frequency of one klystron stable with respect to the frequency of the second. The theory and instrumentation of the system is presented with some data taken on standard and oversized rectangular waveguides.

## TABLE OF CONTENTS

	<u>Page</u>
1. INTRODUCTION	1
2. DISCUSSION OF AVAILABLE TRANSMISSION SYSTEMS	2
2.1 <u>Enclosed Waveguides</u>	2
2.1.1 Standard Rectangular and Circular Guides	2
2.1.2 Oversized Waveguide	4
2.2 <u>Surface Wave Transmission Lines</u>	4
2.2.1 Dielectric Waveguides, Dielectric Image Lines and Fiber Optics	4
2.2.2 Coated or Uncoated Single Conductor Transmission Lines	6
2.2.3 H-Guide or Trough Guide	10
2.3 <u>Optical and Quasi-Optical Waveguides</u>	10
2.3.1 Refractive or Reflective Methods Using Repeated Image Formation	10
2.3.2 Beam Waveguide	12
2.3.3 Propagation in the Fresnel Region	16
3. TROUGH GUIDE	18
3.1 <u>Transmission Properties of the H-Guide and Trough Guide</u>	18
3.2 <u>Excitation of the <math>PM_{11}</math> Mode on the Partially Dielectric Loaded Trough Waveguide</u>	32
3.2.1 Boundary Value Problem	32
3.2.2 Singularities in the Integrand	39
3.2.3 Evaluation of the Contour Integral	40
3.2.4 Evaluation of the Branch Cut Integral (Radiation Field)	40
3.2.5 Evaluation of the Pole Residue (Surface Wave Field)	49
3.2.6 Calculation of the $PM_{11}$ Mode Launching Efficiency	51
3.2.7 Launching Efficiency Measurements	64

## TABLE OF CONTENTS (Cont'd)

	<u>Page</u>
3.3 <u>Recommendations and Conclusions Concerning the Trough Guide</u>	67
4. FRESNEL ZONE PLATES	73
4.1 <u>Operating Principle of Zone Plates</u>	73
4.2 <u>Intensity at the Focal Point</u>	76
4.2.1 General Procedure	78
4.2.2 Contribution from the $n^{\text{th}}$ zone	78
4.2.3 Intensity Ratio for N Half-Period Zones	82
4.2.4 Intensity Ratio for N Quarter-Period Zones	83
4.2.5 Intensity Ratio for M Open Zones	86
4.3 <u>Zone Plates as Frequency Filters</u>	86
4.4 <u>Zone Plates as Antennas</u>	87
4.5 <u>Some Comments on Quasi-Optical Components</u>	89
5. OVERSIZED ENCLOSED WAVEGUIDE	94
6. MEASUREMENT SYSTEM	105
6.1 <u>Harmonic Generation</u>	105
6.1.1 Magnetron Driven Ferrite Harmonic Generator	105
6.1.2 Klystron Driven Crystal Harmonic Generator	112
6.2 <u>Harmonic Mixing</u>	117
6.3 <u>AFC System</u>	119
6.4 <u>Receiver</u>	124
6.5 <u>System Performance</u>	125
6.6 <u>Measurements</u>	130
7. CONCLUSIONS	140

# LIST OF ILLUSTRATIONS

	<u>Page</u>
Figure 1 - Theoretical Attenuation for $TE_{10}$ Mode Propagation in Silver Waveguides of Rectangular Cross Section	3
Figure 2 - Transmission Loss of $TM_{01}$ Mode on Copper Wires of Radius "a"	7
Figure 3 - Radius of Area Around Wire Within Which 90% of the Power is Propagated	8
Figure 4 - Maximum Power Transmissible on Copper Wires of Radius "a"	9
Figure 5 - Suggested Transmission Methods (After Damon and Chang)	11
Figure 6 - (a) Field Configuration of the $PM_{11}$ Mode, (b) Graph of the Magnitude of the Field Components of the $PM_{11}$ Mode	19
Figure 7 - View of the Partially Dielectric Loaded Trough Waveguide	20
Figure 8 - Curves of the Normalized Cutoff Spacing Between the Parallel Walls for the $PM_{1n}$ Modes	22
Figure 9 - Attenuation of the $PM_{11}$ Mode of the Partially Dielectric Loaded Trough Guide vs Frequency	24
Figure 10 - Attenuation of the $PM_{11}$ Mode of the Partially Dielectric Loaded Trough Guide vs Frequency	25
Figure 11 - Attenuation of the $PM_{11}$ Mode of the Partially Dielectric Loaded Trough Guide vs Frequency	26
Figure 12 - Attenuation of the $PM_{11}$ Mode of the Partially Dielectric Loaded Trough Guide vs Frequency	27
Figure 13 - Attenuation of the $PM_{11}$ Mode of the Partially Dielectric Loaded Trough Guide vs Frequency	28
Figure 14 - Attenuation of the $PM_{11}$ Mode of the Partially Dielectric Loaded Trough Guide vs Frequency	29
Figure 15 - (a) End View, and (b) Side View of the Partially Dielectric Loaded Trough Guide Excited by a Magnetic Line Source	34
Figure 16 - Contour of Integration in the $\xi$ -Plane	41
Figure 17 - Path of Integration in the $\tau$ -Plane	43

# LIST OF ILLUSTRATIONS (Cont'd)

	<u>Page</u>
Figure 18 - Power Radiation Patterns due to a Magnetic Line Source Loacted Above the Strip of a Dielectric Loaded Trough Guide	47
Figure 19 - Power Radiation Patterns due to a Magnetic Line Source Located Above the Dielectric Strip of a Dielectric Loaded Trough Guide	48
Figure 20 - Launching Efficiency ( $\eta_L$ ) vs Normalized Dielectric Strip Thickness ( $2a/\lambda_o$ ), $d/a = 1.0$	52
Figure 21 - Launching Efficiency ( $\eta_L$ ) vs Normalized Dielectric Strip Thickness ( $2a/\lambda_o$ ), $d/a = 1.5$	53
Figure 22 - Launching Efficiency ( $\eta_L$ ) vs Normalized Dielectric Strip Thickness ( $2a/\lambda_o$ ), $d/a = 2.0$	54
Figure 23 - Launching Efficiency ( $\eta_L$ ) vs Normalized Dielectric Strip Thickness ( $2a/\lambda_o$ ), $d/a = 2.5$	55
Figure 24 - Launching Efficiency ( $\eta_L$ ) vs Normalized Dielectric Strip Thickness ( $2a/\lambda_o$ ), $d/a = 3.0$	56
Figure 25 - Launching Efficiency ( $\eta_L$ ) vs Normalized Dielectric Strip Thickness ( $2a/\lambda_o$ ), $d/a = 4.0$	57
Figure 26 - Launching Efficiency ( $\eta_L$ ) vs Normalized Dielectric Strip Thickness ( $2a/\lambda_o$ ), $d/a = 6.0$	58
Figure 27 - Launching Efficiency ( $\eta_L$ ) vs Normalized Dielectric Strip Thickness ( $2a/\lambda_o$ ), $d/a = 8.0$	59
Figure 28 - Launching Efficiency ( $\eta_L$ ) vs Normalized Dielectric Strip Thickness ( $2a/\lambda_o$ ), $d/a = 10.0$	60
Figure 29 - Launching Efficiency ( $\eta_L$ ) vs Normalized Dielectric Strip Thickness ( $2a/\lambda_o$ ), $d/a = 15.0$	61
Figure 30 - Launching Efficiency ( $\eta_L$ ) vs Normalized Dielectric Strip Thickness ( $2a/\lambda_o$ ), $d/a = 20.0$	62
Figure 31 - Launching Efficiency ( $\eta_L$ ) vs Normalized Dielectric Strip Thickness ( $2a/\lambda_o$ ), $d/a = 25.0$	63
Figure 32 - Launching Efficiency vs Frequency and Height of Launching Slot	66
Figure 33 - Measured and Calculated Launching Efficiency vs Height of Launching Slot, $f = 29$ Gc	68
Figure 34 - Measured and Calculated Launching Efficiency vs Height of Launching Slot, $f = 35$ Gc	69

# LIST OF ILLUSTRATIONS (Cont'd)

	<u>Page</u>
Figure 35 - Ray Geometry of Zone Plate	74
Figure 36 - Relation Between Lenses and Zone Plates	77
Figure 37 - Geometry of the $n^{\text{th}}$ Zone	79
Figure 38 - Intensity Ratios for Zone Plates with $f = 50\lambda_0$	85
Figure 39 - Double Prism Coupler (and Attenuator)	92
Figure 40 - Geometry for Direct and Indirect Rays in Oversized Waveguide	103
Figure 41 - Submillimeter Wave Propagation Measurement System	106
Figure 42 - Crossguide Crystal Harmonic Generator and Mixer	113
Figure 43 - Crystal Harmonic Generator and Mixer	114
Figure 44 - Harmonic Generation Conversion Loss to Third Harmonic	116
Figure 45 - Block Diagram of AFC System	120
Figure 46 - Schematic of IF Amplifier	122
Figure 47 - Schematic of DC Converter	123
Figure 48 - Submillimeter Wavelength Measurement System	126
Figure 49 - Attenuation in RG-139/U Waveguide	132
Figure 50 - Experimental Arrangement for Measurement on RG-48/U Waveguide	134
Figure 51 - Measured Losses in RG-48/U Waveguide at 210 and 280 Gc	135
Figure 52 - Measured Losses in RG-48/U Waveguide at 350 Gc	138

## 1. INTRODUCTION

The objective of this contract was the study and investigation of techniques applicable in effecting the efficient transfer of energy in the submillimeter wavelength region (1.0 to 0.1 mm) of the electromagnetic spectrum.

The investigation covered a wide range of possible transmission systems. The significant ones among these, i. e., standard and oversized enclosed waveguides, surface wave transmission lines (such as dielectric waveguides, single conductor lines, H-guides and trough guides) and quasi-optical Fresnel region transmission systems are described in the report. Among these, the more promising for submillimeter wave transmission were found to be the trough waveguide, Fresnel region optical transmission, and oversized waveguide. These are given a more comprehensive theoretical treatment. Some recommendations for component design are given which, based on the theoretical investigations, would appear to have the highest probability for success.

In the experimental phase of the investigation it was agreed that measurements would be made where possible and desirable to check experimental and theoretical agreement. In spite of numerous difficulties encountered, a measurement system was completed which was used for obtaining data at 210, 280, 350, and 420 Gc. A description of the theory and instrumentation of the system as well as the data obtained is also presented.

## 2. DISCUSSION OF AVAILABLE TRANSMISSION SYSTEMS

### 2.1 Enclosed Waveguides

#### 2.1.1 Standard Rectangular and Circular Guides.

At frequencies above 300 Gc, dominant mode hollow metal waveguide is impracticable for most applications because of high attenuation, very small size, and low power handling ability. The theoretical attenuation factors for several standard waveguides have been calculated and are plotted in Figure 1. (A conductivity for silver of  $6.17 \times 10^7$  mhos per meter was used in the calculations.) Measured attenuations are generally considerably larger than those shown because of further losses due to surface roughness, losses at the junctions, etc. This was verified in this investigation by measurements on RG-139/U waveguide. The results are given in Section 6. One would obviously want to use only very short lengths of these guides.

#### Rectangular Waveguide Data

<u>Designation</u>	<u>Size (ID) inches</u>	<u>TE<sub>10</sub> Cutoff Frequency (Gc)</u>
RG 135/U	0.051 x 0.0255	116
RG 137/U	.043 x .0215	138
RG 139/U	.034 x .017	173
E - Guide	.033 x .0165	184

Circular waveguide propagating the low-loss circular electric mode (TE<sub>01</sub>) is not now practical for frequencies above 300 Gc. In this waveguide, several (or many) other modes may propagate. These are ordinarily eliminated by the use of mode suppressors inside the guide. This structure requires dimensional tolerances on the order of 0.001 inch at 50 Gc, and tolerances on the order of  $10^{-4}$  inch would be required above

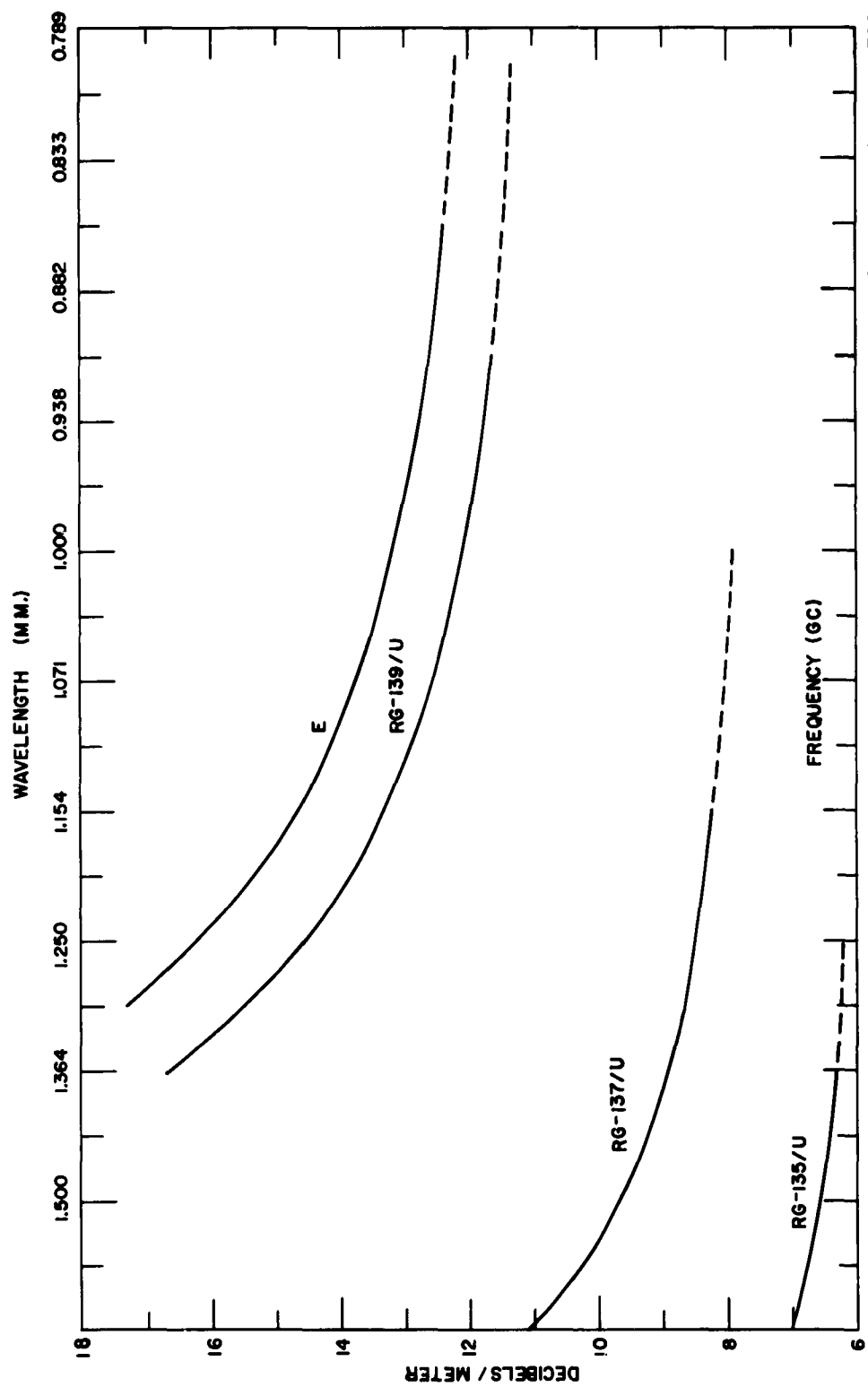


FIG. 1 - THEORETICAL ATTENUATION FOR  $TE_{10}$  MODE PROPAGATION IN SILVER WAVEGUIDES OF RECTANGULAR CROSS SECTION

300 Gc. Even if construction of such a guide were possible, it would be prohibitively expensive at the present time for most applications. As far as is known at this time, the highest frequency where this configuration is being used is the three millimeter region.\*

#### 2.1.2 Oversized Waveguide

A way of reducing attenuation and increasing power handling capabilities in waveguide is to use oversized guides. This immediately raises the issue of multi-mode propagation and its associated disadvantages. These are the possibility of signal distortion and the question of whether components could be designed to operate on all modes efficiently.

There exist situations, however, where these disadvantages can be overcome, and oversized guide could have useful application in the submillimeter region. A theoretical discussion will be presented in Section 5, and some related measurements in Section 6.

### 2.2 Surface Wave Transmission Lines

#### 2.2.1 Dielectric Waveguides, Dielectric Image Lines and Fiber Optics

At frequencies below 150 Gc, dielectric image lines have been found to exhibit lower attenuation than dominant mode hollow rectangular waveguide<sup>(1, 2, 3)</sup>. The dielectric image line consists of a thin strip of low-loss dielectric (such as polystyrene or Teflon) cemented along the centerline on one side of a flat metal (image) plane. To maintain low attenuation as one goes above 150 Gc, the dielectric cross section must be

---

\* A. J. Simmons, "TE<sub>01</sub> Mode Components in the 3mm Region" Paper to be presented at the Millimeter and Submillimeter Conference, Orlando, Florida; January 7 - 10, 1963.

reduced to a very small size (transverse dimensions on the order of a half wavelength or less) and it becomes impractical to fasten the dielectric to the image plane in a straight line.

Pure dielectric waveguides have also been used for low-loss transmission at millimeter wavelengths, but they have the disadvantage that there is no convenient way to support them. Single strands of thin plastic do, of course, exhibit considerable sag when stretched out horizontally with no support.

In the infrared and optical regions (for wavelengths shorter than 20 microns) the use of fiber optics techniques has recently been very successful. Fine glass strands (of the order of a micron in diameter) a few inches or feet in length are coated with a "spacer" material (cladding) and are laid close together in a bundle. Each strand forms a tiny light pipe and an image formed at one end of the bundle is transmitted to the other end. The "spacer" material, of lower dielectric constant than the glass core, is placed around each strand to reduce coupling and crosstalk between the fibers.

Adaptation of this technique to the submillimeter wavelength region would be desirable, but it appears, unfortunately, that the available materials are much more lossy at such frequencies than at the higher infrared and optical frequencies. As a consequence, the attenuation per unit length is undesirably high. In the optical region a fiber optics pipe typically has an attenuation on the order of 3 db per meter, whereas in the submillimeter range, the loss would be about an order of magnitude higher. The use of fiber optics lines of significant lengths therefore waits on the availability of a material which will provide low dielectric losses

### 2.2.2 Coated or Uncoated Single Conductor Transmission Lines

The properties of surface waves guided by an uncoated cylinder of finite conductivity (Sommerfeld wave) or by a perfectly conducting cylinder with a dielectric coating (Goubau wave) have recently been analyzed theoretically for frequencies in the millimeter and submillimeter wavelength regions.<sup>3</sup> (Propagation characteristics were also measured at frequencies of 105 and 140 Gc.) For wire sizes which provide low loss above about 100 Gc, the approximations used earlier by Goubau are not sufficiently accurate to provide useful results. More accurate solutions were obtained for wires of circular cross section by the use of fewer or different approximations.

Calculated values of attenuation are shown in Figure 2 for frequencies as high as 1000 Gc. It may be seen that attenuations of the order of a few tenths of a decibel per meter may be obtained for convenient wire (or rod) sizes. This figure is orders of magnitude lower than that for rectangular waveguide. Calculations of the radius of the transverse area around the wire through which 90% of the power flows shows that the field extent is moderate (see Figure 3). The power handling ability (Figure 4) is very large, on the order of hundreds or thousands of kilowatts peak power (calculated using a breakdown strength for air of 15 kilovolts per centimeter). It appears, therefore, that this might be a useful waveguide for the submillimeter wavelength region. The major technical problems arise in providing efficient launching of the wave onto the line and in supporting the line. A theoretical analysis has recently been performed for the first of these problems.<sup>4</sup> Except in the immediate vicinity of the launcher only a single mode is propagated since other modes are highly damped. The structure is not

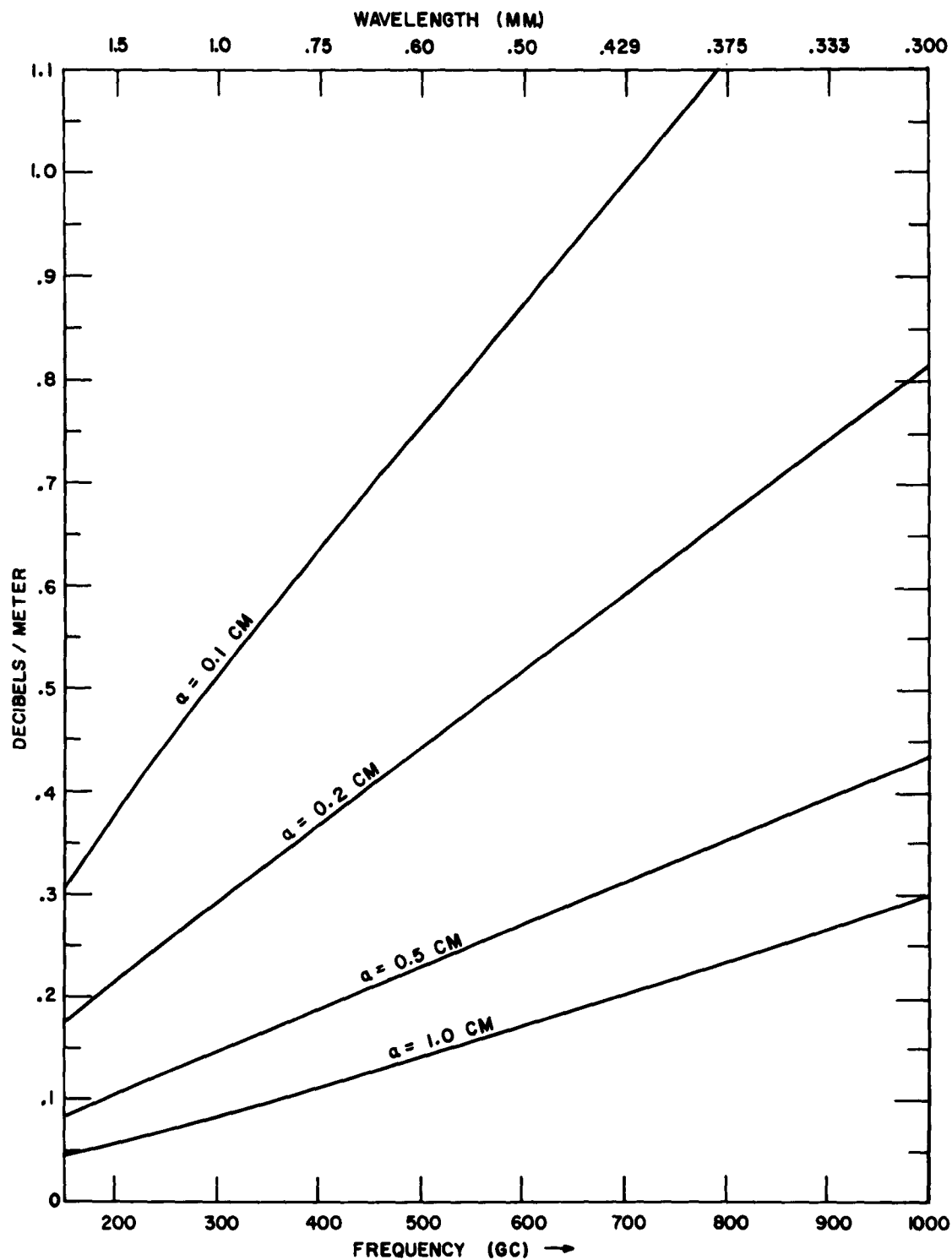


FIG. 2 - TRANSMISSION LOSS OF  $TM_{01}$  MODE ON COPPER WIRES OF RADIUS " $a$ ."

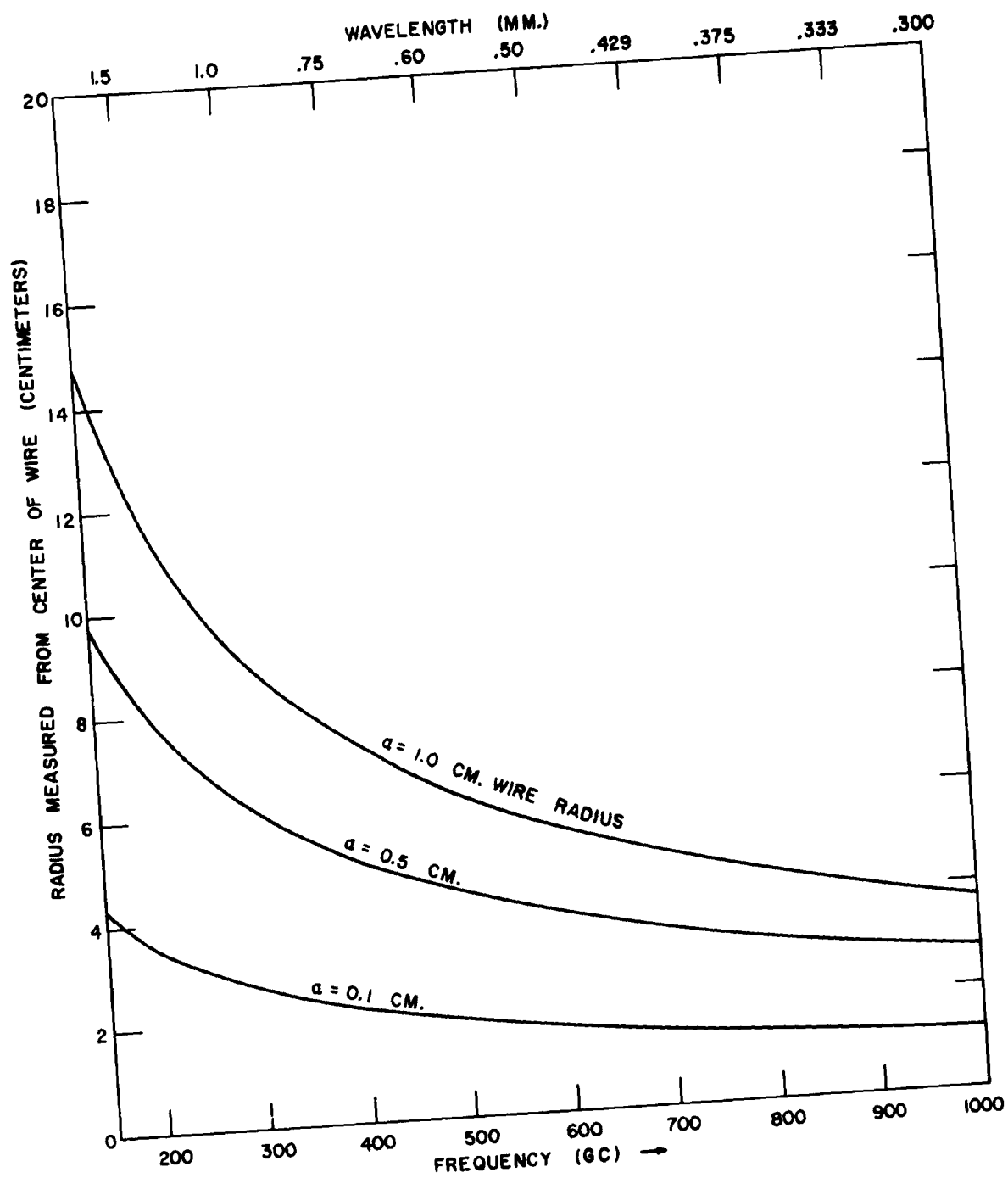
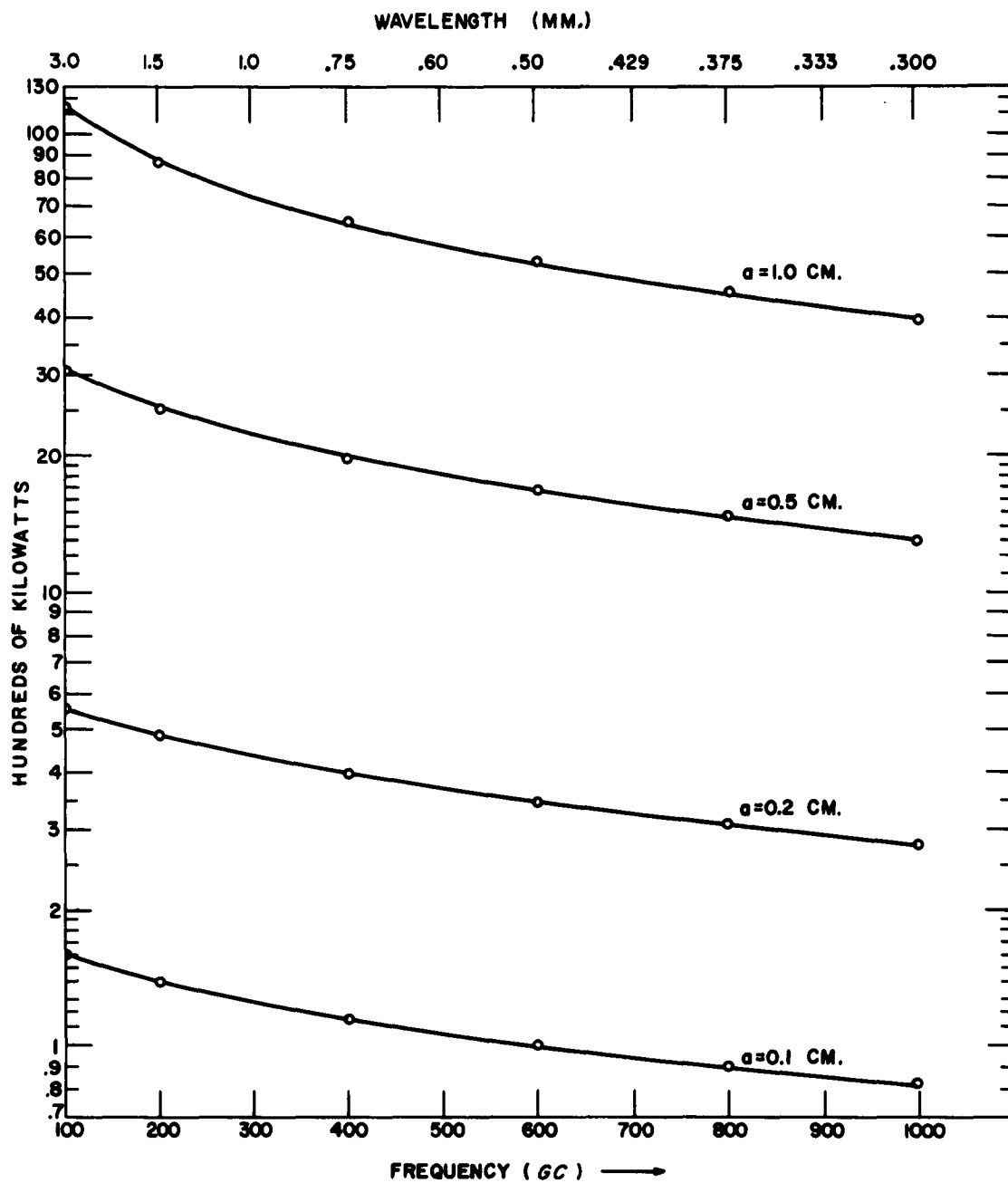


FIG. 3 - RADIUS OF AREA AROUND WIRE WITHIN WHICH 90% OF THE POWER IS PROPAGATED



MAXIMUM POWER TRANSMISSIBLE ON COPPER WIRES OF RADIUS  $a$ .

FIG. 4

physically or electrically shielded, but it has been demonstrated that shielding of surface-wave lines may be accomplished by enclosing the line in a shield of lossy material large enough in transverse dimensions to be out of the region of significant field extent.

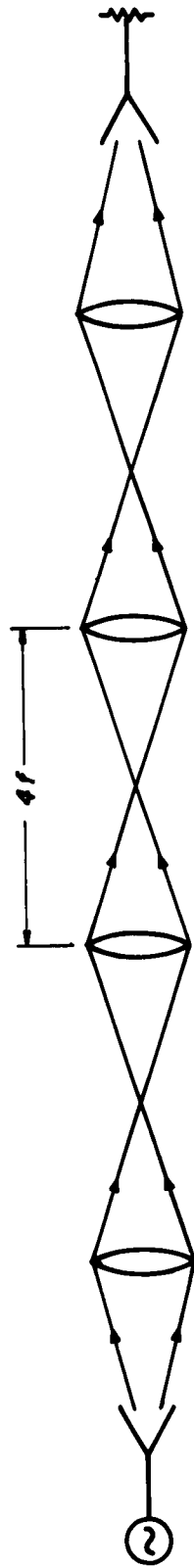
### 2.2.3 H-Guide or Trough Guide

Among surface wave structures, one of the more promising is the modified H-guide, or trough guide. This offers the advantages of low-loss transmission possibilities with a structure which is rigid, so support is not a problem. It can also be shielded physically and electrically. Description and analysis of this structure is given in detail in Section 3.

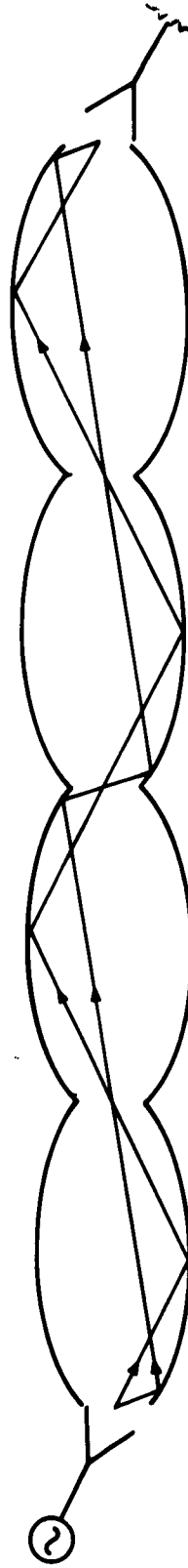
## 2.3 Optical and Quasi-Optical Waveguides

### 2.3.1 Refractive or Reflective Methods Using Repeated Image Formation.

Some examples of these transmission methods are shown in Figure 5, which is similar to a figure given in a paper by Damon and Chang.<sup>5</sup> In these cases, a collinear array of lenses or of spheroids with common foci is used for the transfer of energy. In the lens example, a point source is placed at a distance  $2f$  (where  $f$  is the focal length) behind a lens which forms an image of the source. The image serves as a source for a second lens and is reimaged. Successive images are thus formed at distance intervals of  $4f$ . Unfortunately, this approach suffers from image deformation effects, which rapidly deteriorate the quality of the image of the point source. Since the imaging process is repeated several or many times in a line of moderate length, the energy becomes spread out over a relatively large volume around the last focus, and cannot be efficiently recovered. The line also has other diffraction, scattering and transmission losses at or in the material of the lenses.



(2a) LENS TRANSMISSION LINE



(2b) SPHERICAL TRANSMISSION LINE

FIG. 5 - SUGGESTED TRANSMISSION METHODS (AFTER DAMON AND CHANG)

Somewhat similar comments appear to be applicable to the spheroidal line. Here the source is located at the first focus and the reflectors (elliptical longitudinal cross section) then concentrate most of this at the second focus, which in turn acts as the first focus of the second spheroid, etc. Image deformation occurs partly because some rays (those having a small angle with the axis of the line) can pass from the first spheroid to the second without passing through a focal point. This is possible because portions of the spheroids have been cut away near the foci. Image deterioration also occurs if the reflector surfaces are not perfect. The spheroids are presumed to have dimensions considerably greater than a wavelength (to reduce wall losses). The mechanical problems of constructing sizeable spheroids to high accuracy and of connecting a large number of them together with common foci appears to be quite serious. Our conclusion is therefore that long lengths of this line, in the form described here, will not have general usefulness for submillimeter wavelength applications.

### 2.3.2 Beam Waveguide

Goubau and his associates have recently described an optical type of transmission line called the beam waveguide.<sup>(6, 7)</sup> In this method, a transmitted beam of energy is kept well collimated by the use of weakly-correcting lenses, referred to as phase transformers, which typically are placed at intervals of several feet or tens of feet along the beam axis. Quoting from Christian and Goubau, "The beam waveguide utilizes reiterative wave beams which are guided by resetting the cross-sectional phase distributions at periodic intervals." Calculations indicate that this approach is capable of providing low loss transmission in the submillimeter wavelength region.

The iteration loss of a beam waveguide of the type described by Christian and Goubau consists of diffraction loss and the reflection and absorption losses of the lens or phase transformer. The diffraction loss can be obtained from Figure 2 of their article as a function of  $\frac{k}{D}R^2$ , where D and R are the spacing and radius respectively, of the phase transformers, and  $k = 2\pi/\lambda$ . Christian and Goubau give approximate expressions for the reflection loss and the absorption loss for  $\epsilon \geq 1.2$ , where  $\epsilon$  is the relative dielectric constant. The reflection loss is

$$(1) \quad L_R = -2 \left[ 10 \log_{10} (1 - \Gamma) \right] \text{ db}$$

where

$$(2) \quad \Gamma \approx \left( \frac{\epsilon - 1}{\epsilon + 1} \right)^2 + \left( \frac{1}{4} - \frac{1}{\epsilon \sqrt{\epsilon}} \frac{[4\sqrt{\epsilon} - \epsilon - 1]}{(\epsilon - 1)^2} \frac{1}{(kD)^2} \frac{1 - \left[ 1 + a^2 + \frac{a^4}{2} \right] e^{-a^2}}{1 - \epsilon^{-a^2}} \right)$$

and

$$(3) \quad a = \sqrt{\frac{k}{D}} R,$$

while the absorption loss is

$$(4) \quad L_A = -10 [\log_{10} (1 - \eta)] \text{ db}$$

where

$$(5) \quad \eta \approx \frac{\epsilon_r (a^2 - 1)}{\sqrt{\epsilon - 1}}$$

and  $\epsilon_r$  is the dissipation factor. The value of  $\epsilon_r = .001$  was selected for computation.

If k and D are chosen such that  $kD \gg 1$ , the second term in equation (2) can be neglected, and  $\Gamma$  can be written

$$(6) \quad \Gamma \approx \left( \frac{\sqrt{\epsilon} - 1}{\sqrt{\epsilon} + 1} \right)^2 \quad (\text{if } kD \gg 1)$$

Thus, if the frequency increases as D remains constant the reflection loss becomes a function of the dielectric constant alone.

Assuming  $kD \gg 1$ , values of  $a$  and  $\epsilon$  may be chosen so as to fix the total loss (diffraction loss plus reflection loss plus absorption loss) per section of length. Since  $a = \sqrt{\frac{k}{D}} R =$  constant, it is seen that if, at a given frequency, the lens radius is halved, the distance between the lenses must be quartered for the loss to remain the same.

On the other hand, keeping R and D the same and increasing the frequency increases  $a^2 = \frac{k}{D} R^2$ , which decreases the diffraction loss (as can be seen from their Figure 2). However, as  $a^2$  increases,  $\eta$  increases and as it becomes closer to unity, the absorption loss increases. For increasing frequency, the total loss may drop rapidly at first. It will then begin to increase due to the increase in absorption loss. Calculations for  $\epsilon = 1.4$  and 2.56, for  $R^2/D = 0.9 \times 10^{-3}$  and frequencies between 100 and 500 Gc showed a sudden drop in total loss at first, and then a very slow increase as frequency went up.

Calculations also showed that at the higher relative dielectric constant,  $\epsilon = 2.56$ , the reflection loss by far dominates the other losses providing  $a$  is chosen properly to keep the diffraction loss low. Therefore, it would be desirable to use a nonreflective coating on the lens or to choose a large lens size so as to increase the distance between transformers and decrease the total loss along the line.

Some typical examples have been calculated which illustrate the lens spacings and attenuations for lenses of specific diameters and dielectric constants at frequencies in the range of 100 to 500 Gc. These are given in the tables below.

Table I  
Beam Waveguide Losses

$\epsilon$	$R^2/D$	Frequency (Gc)	Total loss per Transformer (db)
1.4	$.9 \times 10^{-3}$	100	2.08
		150	0.71
		200	.28
		250	.18
		300	.18
		350	.20
		400	.22
		450	.24
		500	.27
2.56	$.9 \times 10^{-3}$	100	2.48
		150	1.09
		200	0.64
		250	.53
		300	.52
		350	.52
		400	.52
		450	.53
		500	.54

Table II  
Typical Sizes (R) and Spacings (D) for Phase Transformers

$R^2/D$	R(cm)	D (meters)
$.9 \times 10^{-3}$	7	5.4
	5	2.8
	4	1.8

### 2.3.3 Propagation in the Fresnel Region

Relatively low loss transmission can be accomplished by using antennas which have apertures so large that their Fresnel regions are of considerable length. Such transmission can occur over an appreciable fraction of the Rayleigh distance ( $D^2/\lambda$ , where  $D$  = diameter and  $\lambda$  = wavelength) of the aperture. This is certainly a possibility for use at the wavelengths of light where optical communication methods are under study. For such a system, workers at Bell Telephone Laboratories are considering using a tightly collimated light beam within a pipe. The pipe would be a few inches in diameter and painted dull black on the inside. Repeater amplifiers would be spaced several thousand feet apart along the line. The diameter of the waveguide would be about  $10^5$  wavelengths. For a lens or antenna 2 1/2 inches in diameter, the Rayleigh distance is about 20,000 feet. Propagation between such lenses (at repeaters) spaced apart by a few thousand feet would be in the Fresnel region. This system is very simple, and the principle difficulty would be in maintaining the straightness of the pipe under various environmental conditions.

Although the shielding method mentioned above is still expected to be useful in the 300 to 3000 Gc region, the remainder of the waveguide system does not scale well to this frequency range if a waveguide for long-distance transmission is desired. If a waveguide having inside dimensions of at least a foot is used, this corresponds to a diameter between 300 and 3000 wavelengths. If ten-inch diameter lenses are used, the corresponding Rayleigh distances are 200 to 2000 feet, respectively, and low-loss propagation would occur over about a quarter of these distances, that is, over path lengths from 50 feet (300 Gc) to 500 feet (3000 Gc). Although these distances cannot compare

3

with those obtainable at optical wavelengths, they are still quite respectable and useful. The technique has already been utilized at millimeter wavelengths and transmission with low attenuation has been demonstrated at frequencies as high as 210 Gc.<sup>3</sup>

The large lenses required, however, present a disadvantage in that they are large in diameter and thickness (for reasonable focal lengths), which in turn results in machining problems and undesirable insertion loss and bulkiness. Here phase correcting Fresnel zone plates can be advantageously used in place of the lenses. These immediately present a much simpler machining task as well as a considerable reduction of weight. These devices and possible components compatible with such a transmission system are discussed in Section 4.

### 3. TROUGH GUIDE

#### 3.1 Transmission Properties of the H-Guide and Trough Guide

A surface wave structure which has potential application as a transmission line at the lower end of the sub-millimeter wavelength spectrum is the H-guide. The H-guide consists of two parallel conducting planes with a dielectric slab of rectangular cross-section between the two planes and contacting each of them. A disadvantage of using the H-guide at these short wavelengths is that extremely thin dielectric slabs must be used if sufficiently low losses are to be achieved. The dielectric slab is then mechanically too weak to be self supporting.

A modification of the line, which eliminates this structural defect, is the configuration referred to as the dielectric-loaded trough waveguide. A partial view of the H-guide, showing the field configuration of the low loss  $PM_{11}$  mode is shown in Figure 6(a). The magnitude of the field components is shown in Figure 6(b). It is apparent from Figures 6(a) and 6(b), that insertion of a conducting plane at  $x = 0$  will not disturb the field configuration of the  $PM_{11}$  mode. This modified line, which looks like half of the H-guide, has conducting planes on three sides of the dielectric and thus provides the necessary mechanical support for the very thin dielectric slab. See Figure 7. A further advantage of the trough guide is that the additional conducting plane causes the desired  $PM_{11}$  mode to be the dominant mode. In the case of an oversize trough waveguide (larger spacing between the parallel conducting walls than is needed for dominant mode propagation), the extra conducting wall of the trough waveguide suppresses many of the higher order modes which would have propagated on the full H-guide.

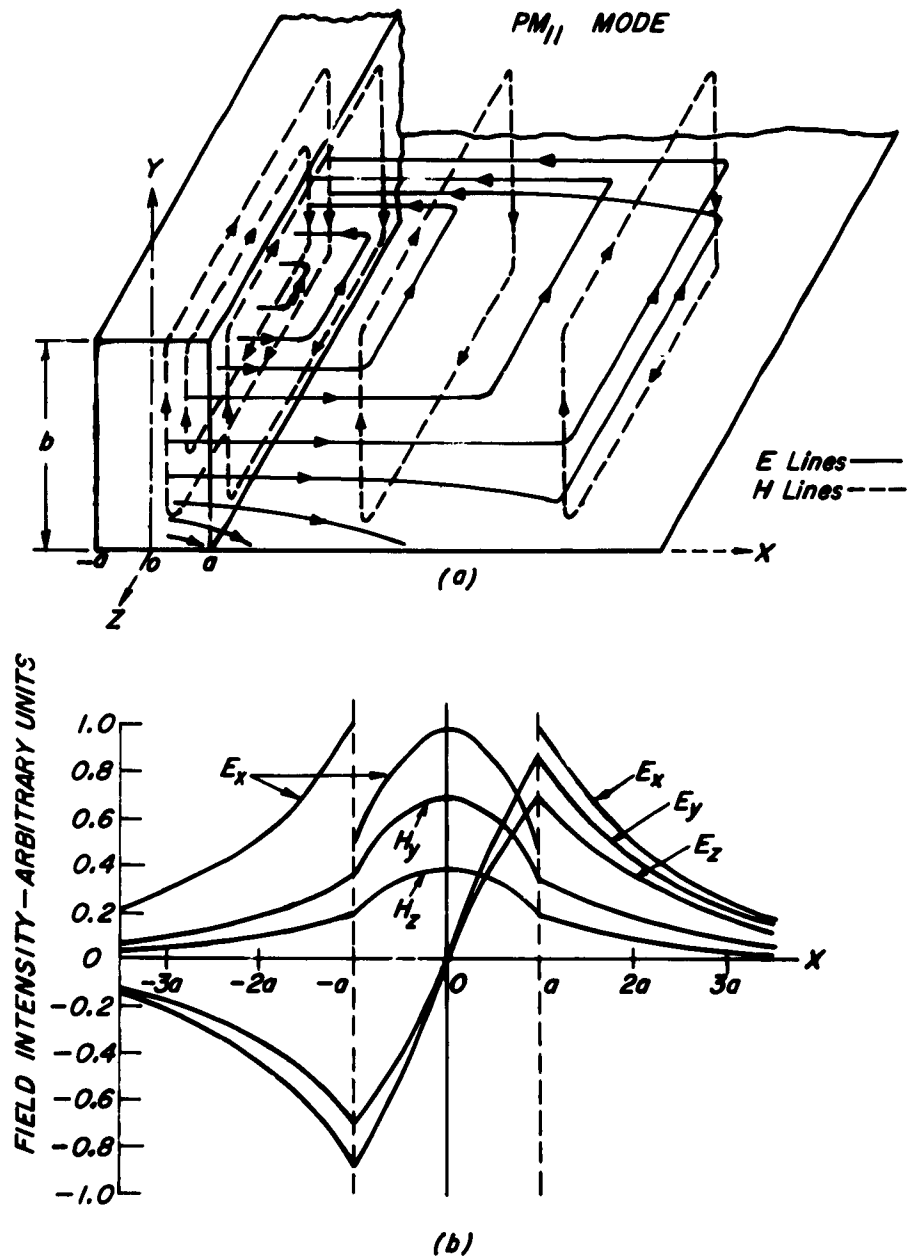


FIG. 6 — (a) FIELD CONFIGURATION OF THE  $PM_{11}$  MODE. ONLY HALF OF THE PARALLEL PLANE LINE IS SHOWN. THE UPPER CONDUCTING WALL IS REMOVED. (b) A GRAPH OF THE MAGNITUDE OF THE FIELD COMPONENTS OF THE  $PM_{11}$  MODE

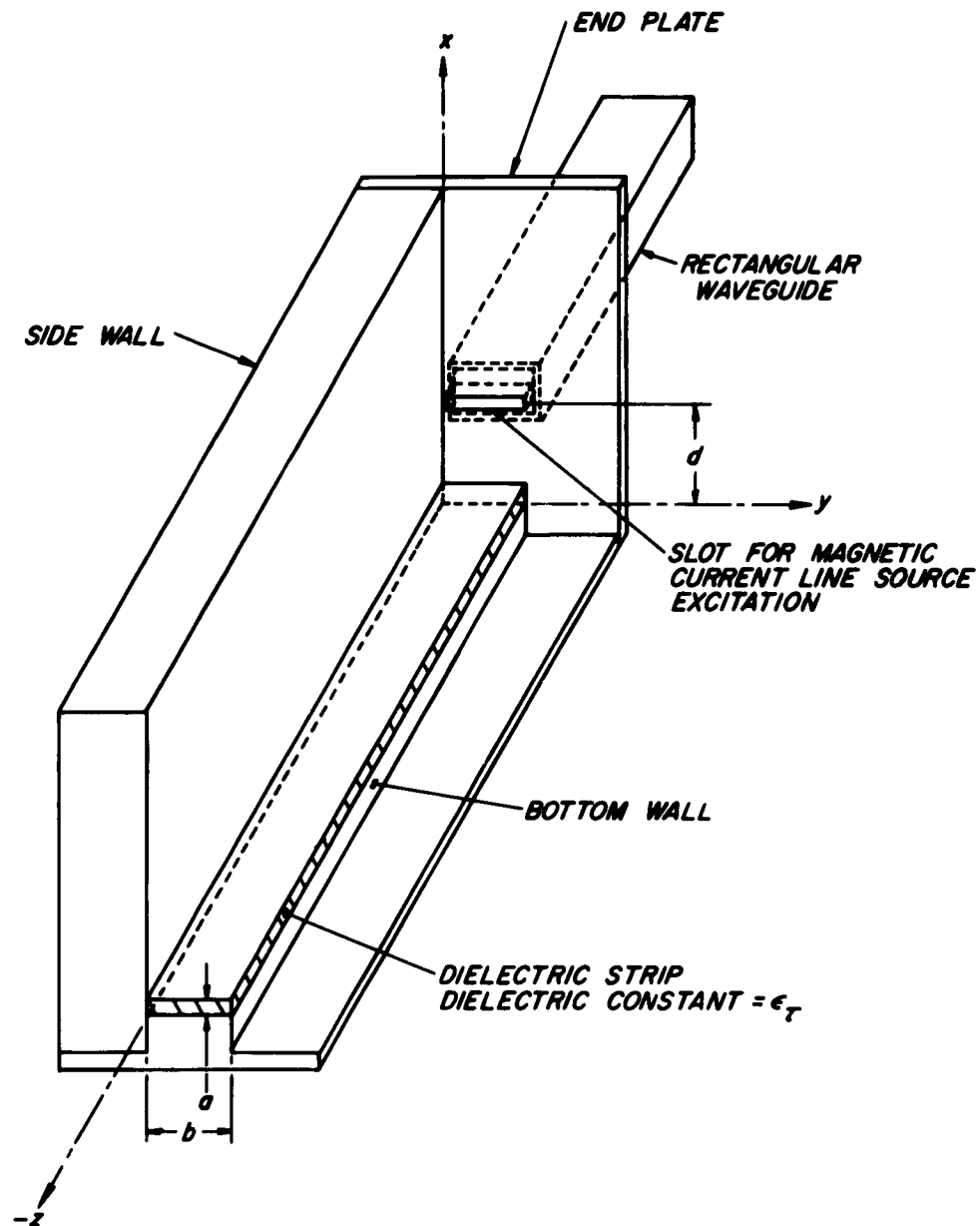


FIG. 7 -VIEW OF THE PARTIALLY DIELECTRIC LOADED TROUGH WAVEGUIDE. THE METHOD OF EXCITING THE  $PM_N$  MODE BY A MAGNETIC CURRENT LINE SOURCE IS SHOWN. ONE OF THE SIDE WALLS IS NOT SHOWN.

A previous analysis and corroborating measurements<sup>8</sup> of the H-guide and trough guide have yielded the properties of these structures. It has been shown that there are two classes of surface wave modes ( $PE_{mn}$  and  $PM_{mn}$ ) which can propagate on these structures. The designation PE, which stands for parallel electric, refers to the fact that the electric field lines of these modes lie entirely in planes parallel to the dielectric-air interface ( $E_x = 0$ ). Similarly, the designation PM, which stands for parallel magnetic, refers to the fact that the magnetic field lines of these modes lie entirely in planes parallel to the dielectric-air interface ( $H_x = 0$ ), as shown in Figure 6(a). The index m gives the rank of the mode and is indicative of the manner in which the fields in the dielectric strip vary as a function of x. The index n is the order of the mode and equals the number of half cycles of sinusoidal variation of the fields in the y-direction.

In order to assure single mode ( $PM_{11}$ ) operation, the dielectric strip thickness (a) and parallel wall spacing (b) must satisfy certain conditions

$$(1) \quad \frac{2a}{\lambda_o} < \frac{1}{2\sqrt{\epsilon_r - 1}}$$

$$(2) \quad b_c < b < 2b_c,$$

where  $b_c$  is the critical wall spacing shown in Figure 8. It should be noted in Figure 8, that for a loosely bound wave (small  $2a/\lambda_o$ ),  $b_c$  is approximately equal to  $\lambda_o/2$ .

For very thin dielectric strips, the complex equations for the attenuation due to losses in the parallel walls ( $\alpha_w$ ), in the dielectric ( $\alpha_d$ ), and in the bottom conducting wall ( $\alpha_b$ ) can be accurately represented by the following approximate relationship.

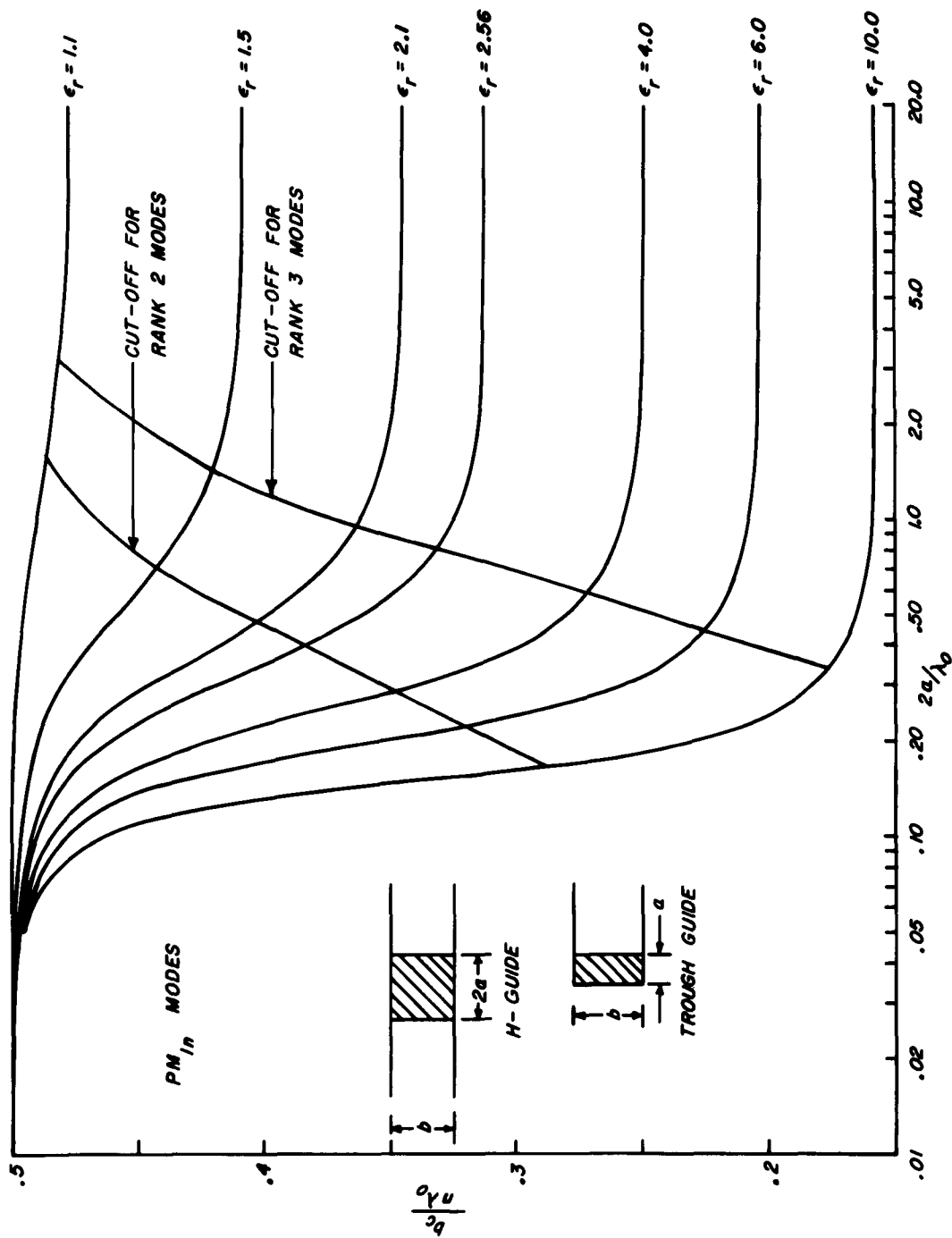


FIG. 8 - CURVES OF THE NORMALIZED CUTOFF SPACING BETWEEN THE PARALLEL WALLS FOR THE PM<sub>1n</sub> MODES

$$(3) \quad a_w b \sqrt{\lambda_o} = \frac{1825 (\lambda_o/2b)^2}{\sqrt{\sigma_w} \sqrt{1 - (\lambda_o/2b)^2}}$$

$$(4) \quad a_d \lambda_o = \frac{2\pi^3 (\epsilon_r - 1) (2a/\lambda_o)^2}{\epsilon_r^2 \sqrt{1 - (\lambda_o/2b)^2}} \tan \delta$$

$$(5) \quad a_b (\lambda_o)^{3/2} = \frac{1.8 (\epsilon_r - 1) (2a/\lambda_o)}{\sqrt{\sigma_w} \epsilon_r \sqrt{1 - (\lambda_o/2b)^2}}$$

where  $\lambda_o$  = the free space wavelength

$\epsilon_r$  = the dielectric constant of the dielectric strip

$\tan \delta$  = the dielectric loss tangent of the dielectric strip

$\sigma_w$  = the conductivity of the metal walls.

In the above equations, the attenuation is given in nepers per meter if  $a$ ,  $b$ , and  $\lambda_o$  are given in meters and  $\sigma_w$  is given in mhos per meter.

Some examples of the calculated losses of the trough guide  $PM_{11}$  mode are shown in Figures 9 through 14. These curves show the component attenuations ( $a_w$ ,  $a_d$ , and  $a_b$ ) and the total attenuation ( $a_T$ ) as functions of frequency for a number of values of the geometric parameters ( $a$  and  $b$ ). In all of these curves, the values of the normalized dielectric strip thickness ( $a/\lambda_o$ ) are sufficiently small so that the error introduced through the use of the approximate attenuation formulas of equations (3), (4), and (5) is negligible.

A number of general conclusions can be reached by comparing the various curves. In Figures 9, 10, and 11, the assumed parallel wall spacing ( $b$ ) is 1.0 millimeter and hence, the cutoff frequency is 150 Gc. These figures show that at the low frequency end of the band of interest, the attenuation due

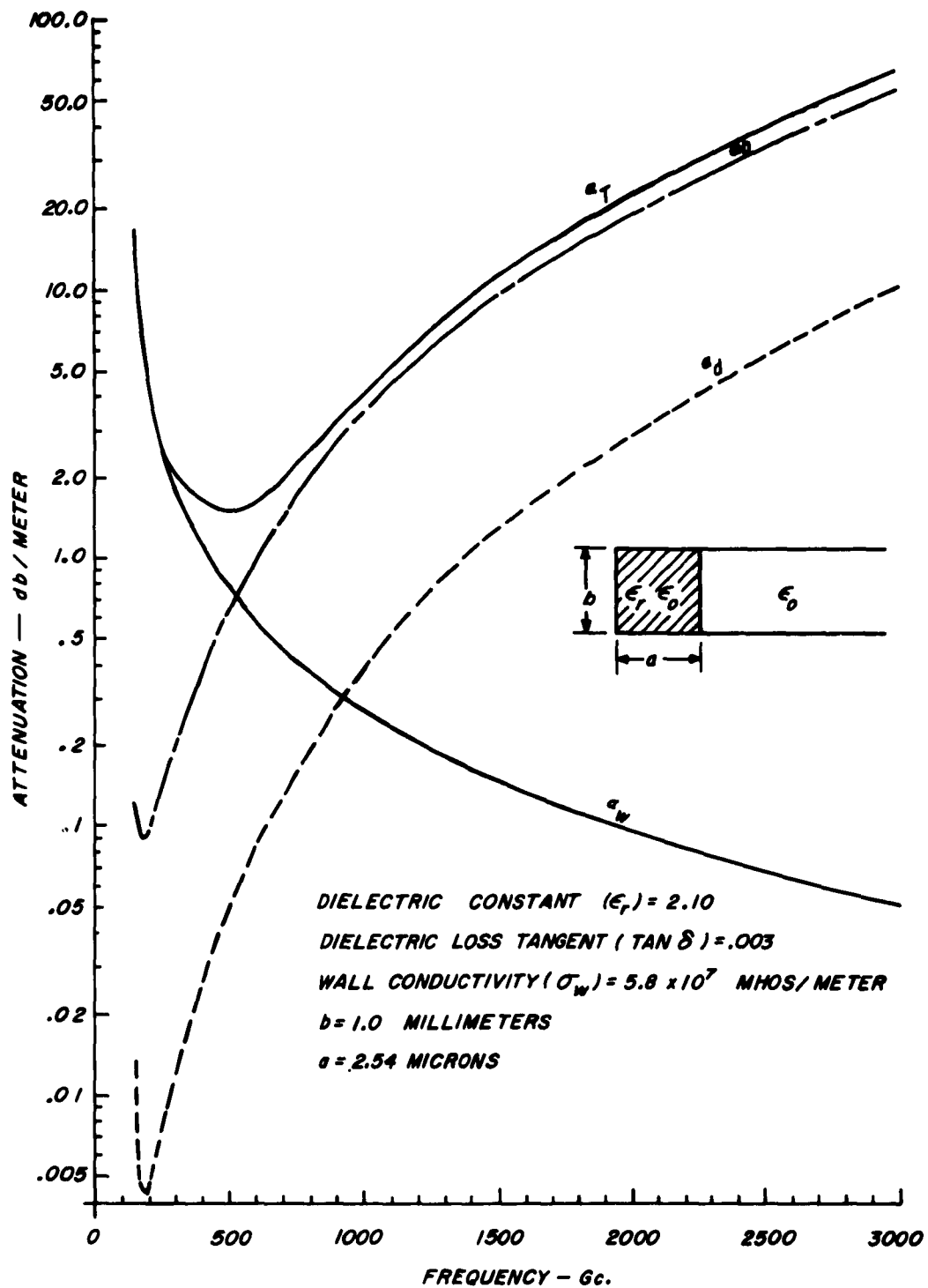


FIG. 9 - ATTENUATION OF THE  $PM_{11}$  MODE OF THE PARTIALLY DIELECTRIC LOADED TROUGH GUIDE VERSUS FREQUENCY

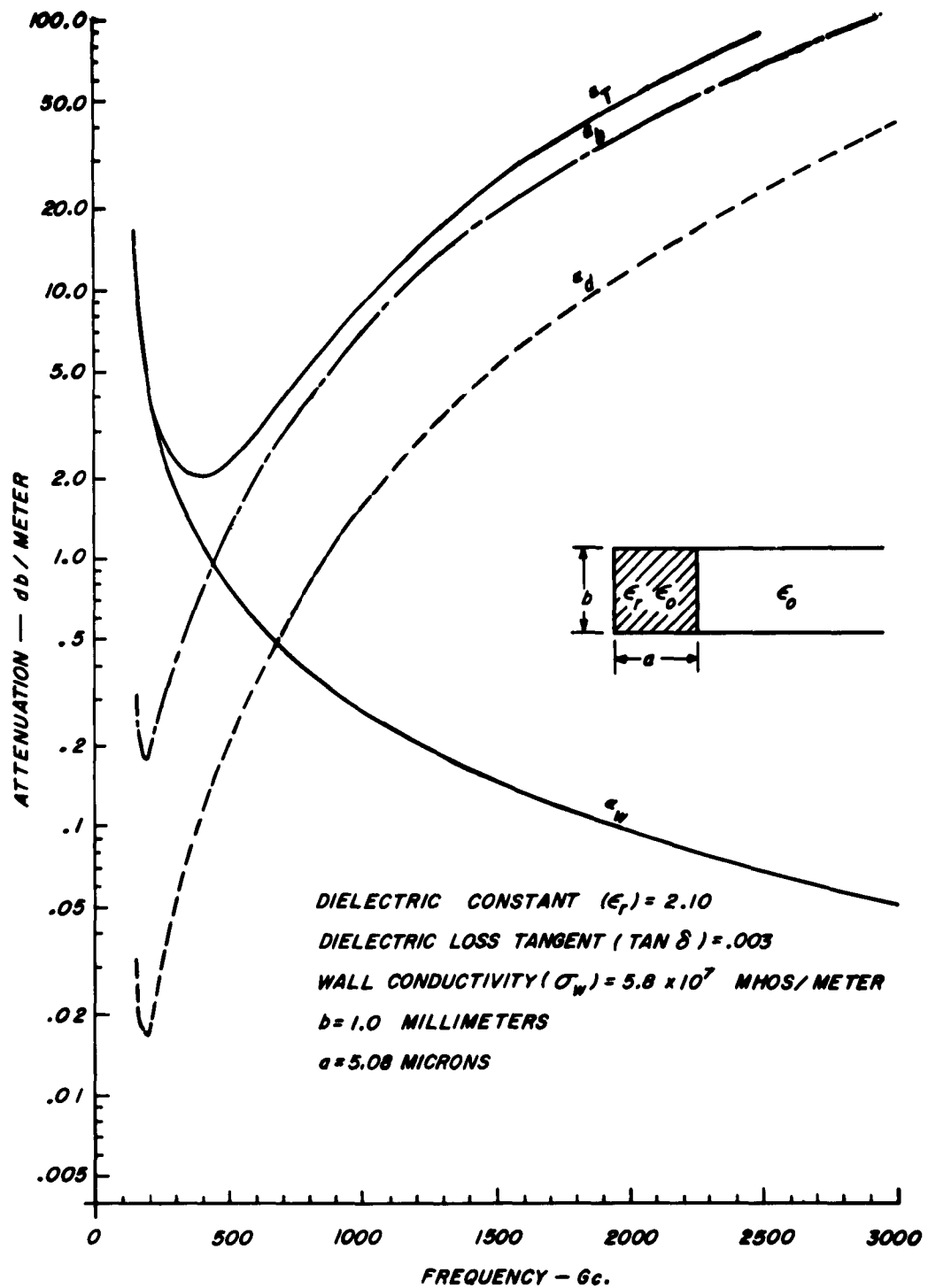


FIG. 10 - ATTENUATION OF THE  $PM_{11}$  MODE OF THE PARTIALLY DIELECTRIC LOADED TROUGH GUIDE VERSUS FREQUENCY

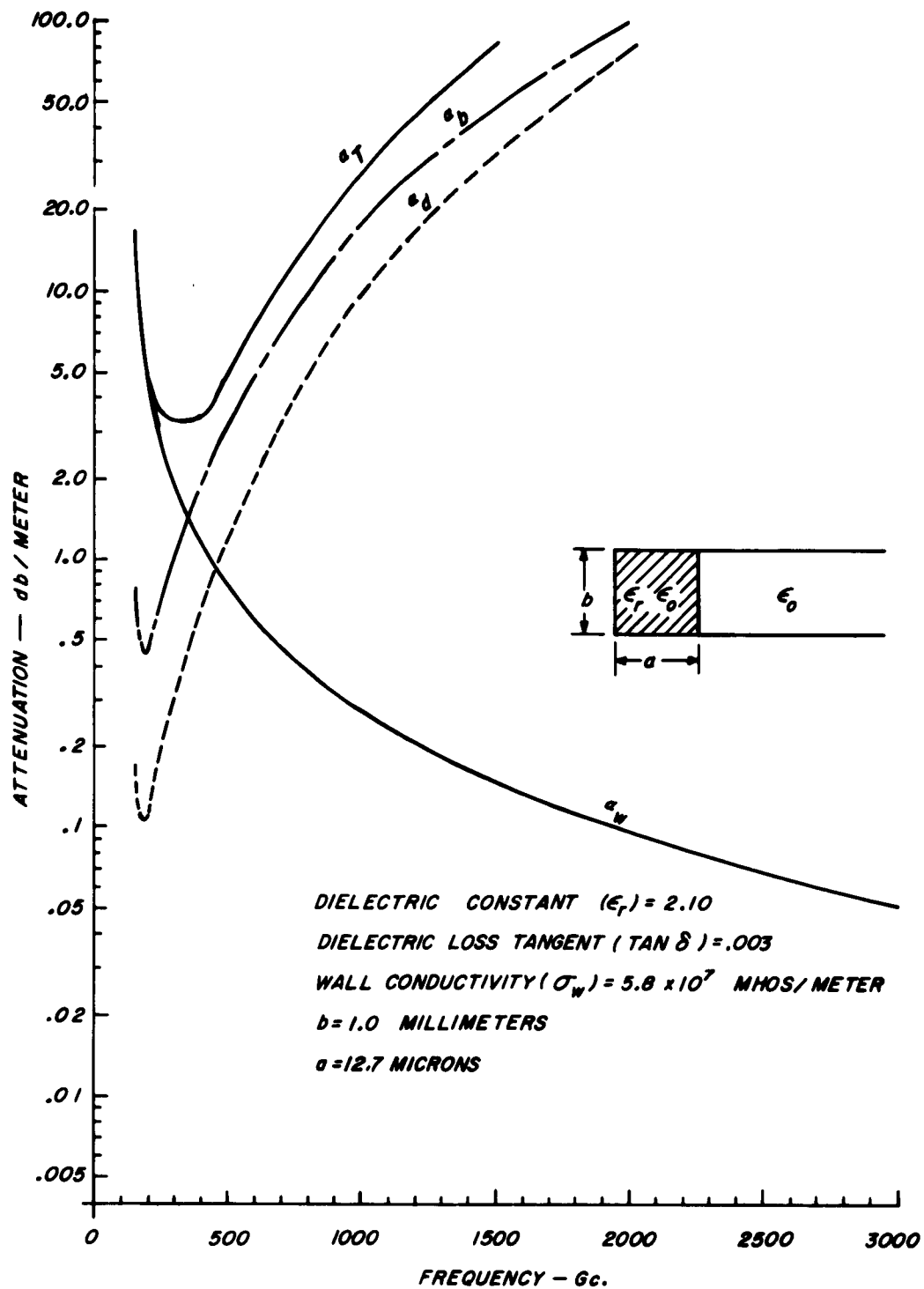


FIG. 11 - ATTENUATION OF THE  $PM_{11}$  MODE OF THE PARTIALLY DIELECTRIC LOADED TROUGH GUIDE VERSUS FREQUENCY

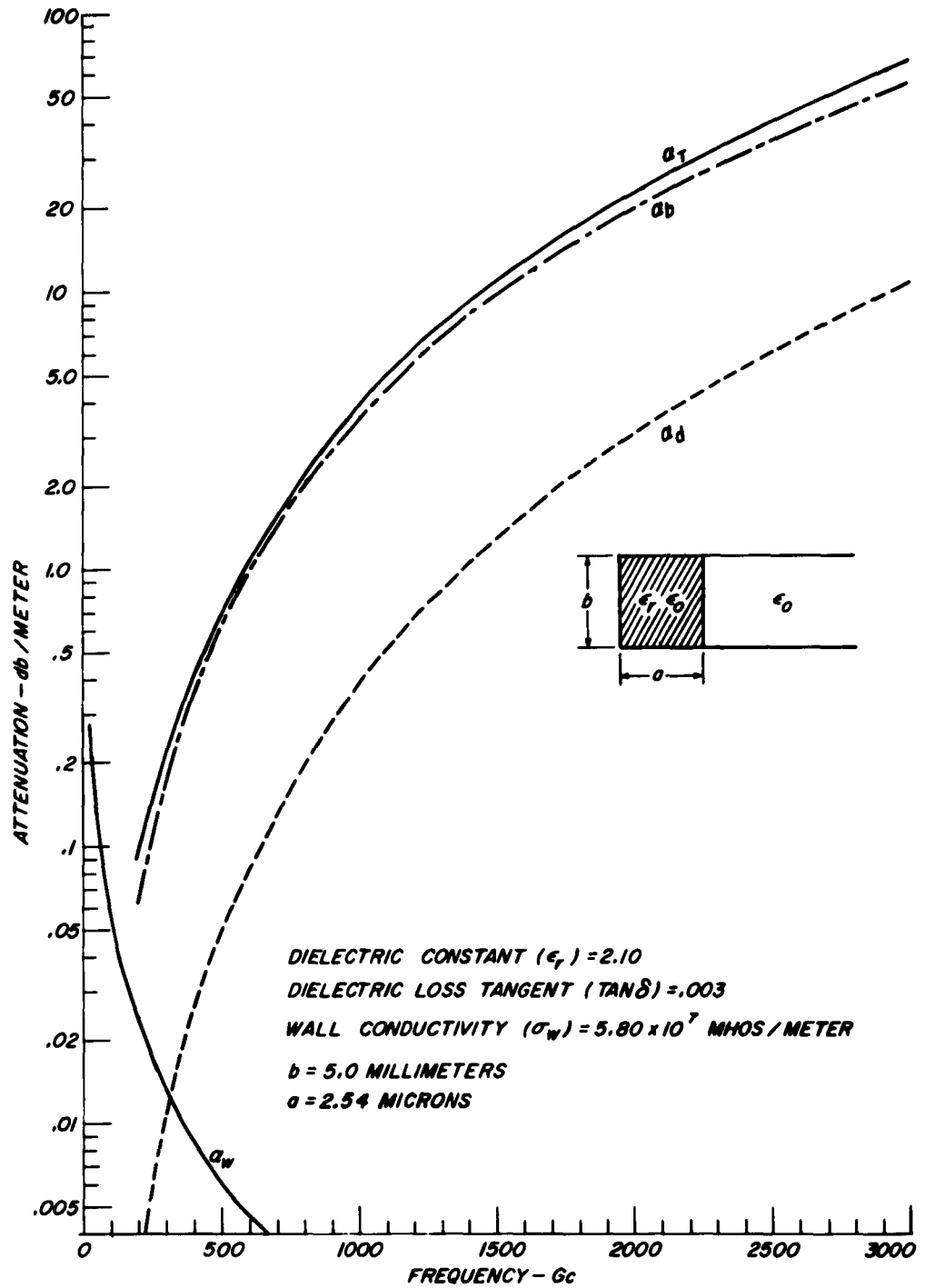


FIG. 12 - ATTENUATION OF THE  $PM_{11}$  MODE OF THE PARTIALLY DIELECTRIC LOADED TROUGH GUIDE VERSUS FREQUENCY

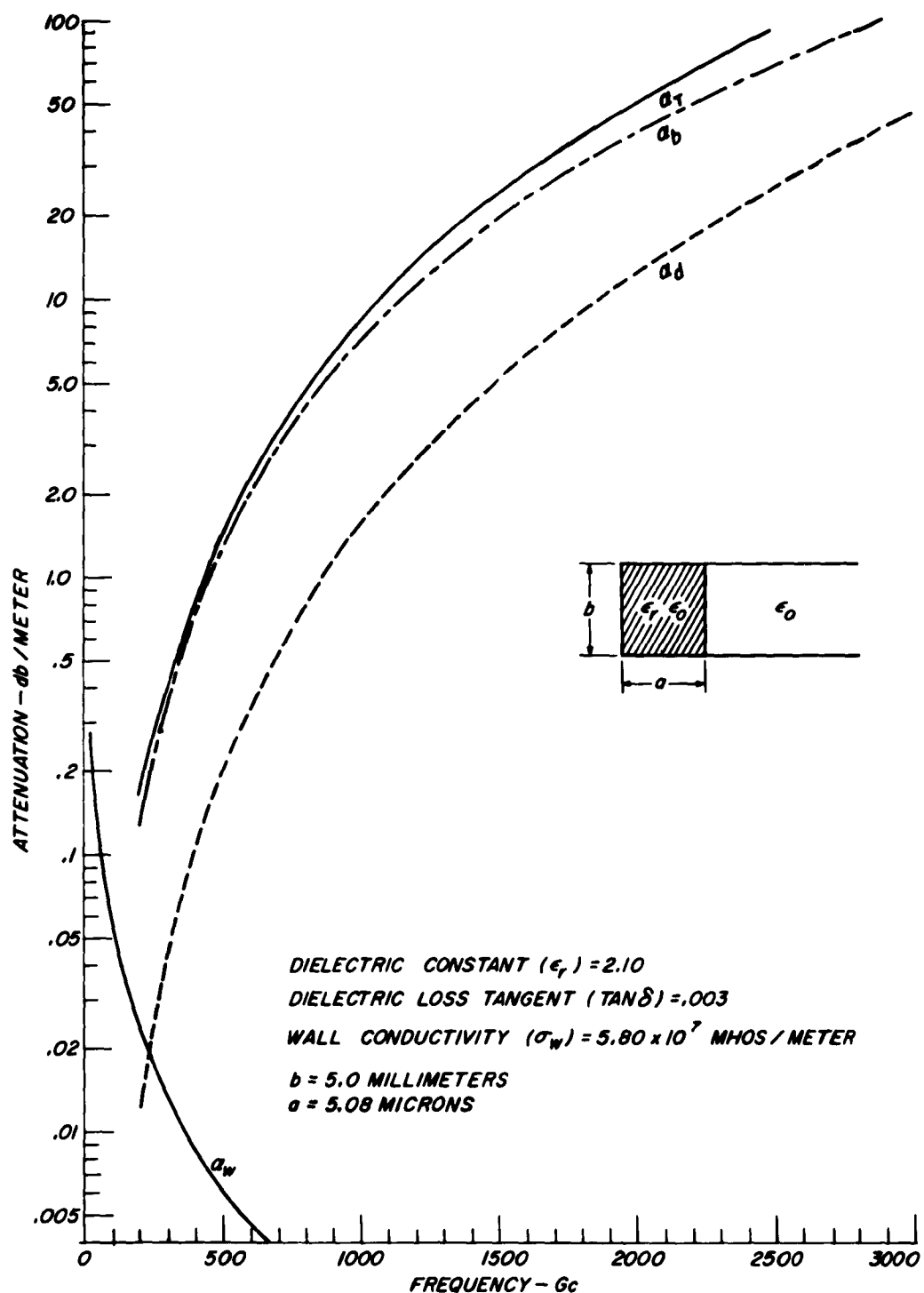


FIG. 13 - ATTENUATION OF THE  $PM_{11}$  MODE OF THE PARTIALLY DIELECTRIC LOADED TROUGH GUIDE VERSUS FREQUENCY

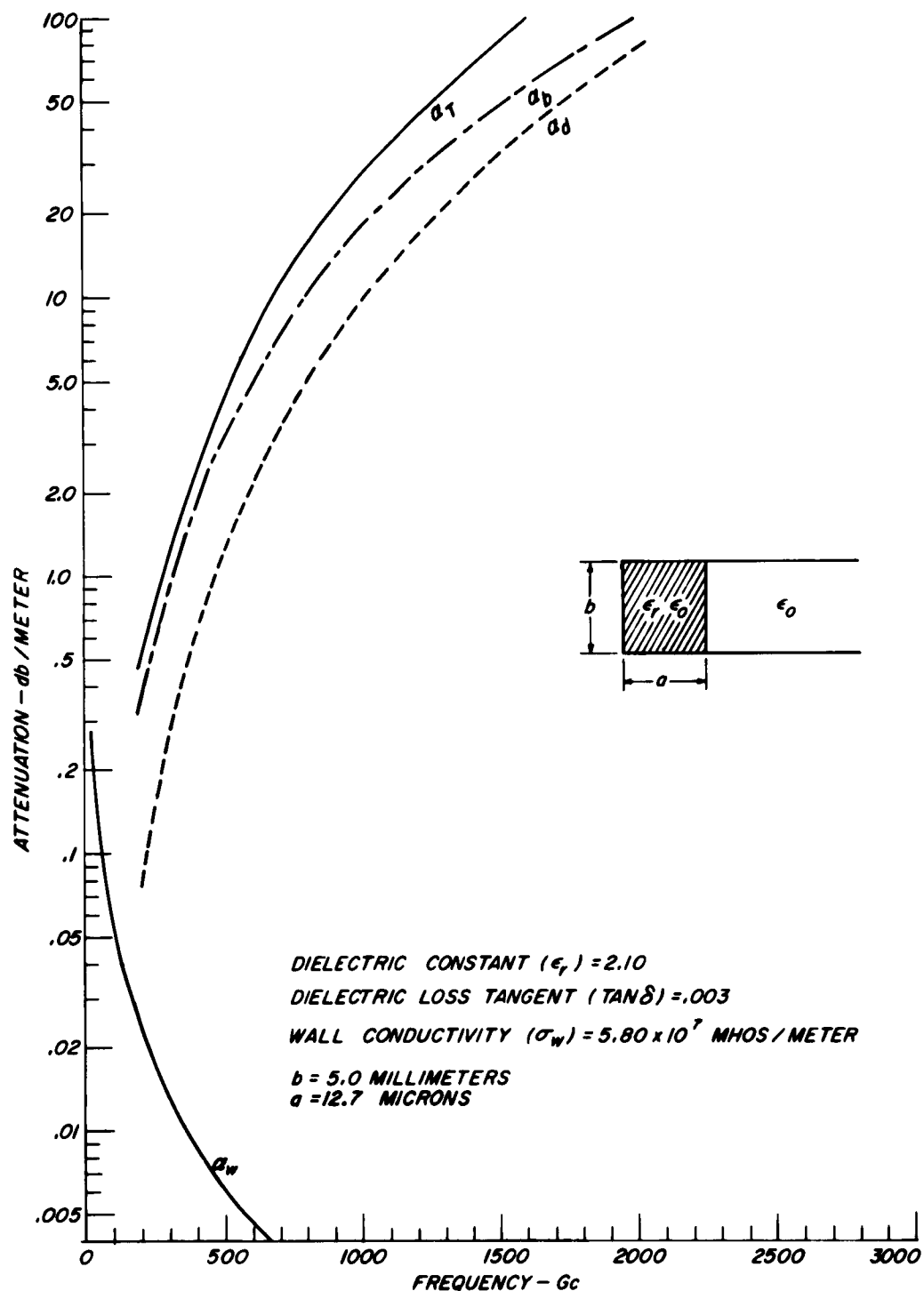


FIG. 14 - ATTENUATION OF THE  $PM_{11}$  MODE OF THE PARTIALLY DIELECTRIC LOADED TROUGH GUIDE VERSUS FREQUENCY

to parallel wall losses is the dominant term,  $\alpha_w$  is independent of  $a$  for small values of  $(a/\lambda_0)$ . At higher frequencies, the attenuation contributions due to bottom wall losses and dielectric losses are dominant and excessive unless very thin dielectric films are used. When very thin films are used, the higher frequency attenuation is almost entirely due to bottom wall losses. It is thus apparent that for sufficiently thin films, the loss tangent of the dielectric strip is not as important a parameter as it is for thicker films. In Figures 12, 13, and 14, the assumed parallel wall spacing ( $b$ ) is 5.0 millimeters and hence the cutoff frequency is 30 Gc. Comparison of Figures 9, 10, and 11 with Figures 12, 13, and 14 shows that extremely low values of attenuation are achievable at the low end of the frequency band of interest if large values of parallel wall spacing can be tolerated. For such large values of  $b$ , even thinner dielectric strips can be advantageously used and hence, the importance of the dielectric loss tangent would be even further lessened.

As shown in Figure 8, it is possible for higher order ( $n > 1$ )  $PM_{1n}$  modes to propagate on the trough guide if the wall spacing is greater than  $2b \approx \lambda_0$ . For example, at a frequency of 500 Gc, the trough guide of Figures 9, 10, and 11 can support two higher order modes ( $PM_{12}$  and  $PM_{13}$ ) in addition to the dominant  $PM_{11}$  mode. The structure of Figures 12, 13, and 14 can support fifteen higher order  $PM_{1n}$  modes ( $n = 2$  to 16). All of the even order modes ( $PM_{12}$ ,  $PM_{14}$ , etc.) can be suppressed by cutting a longitudinal slot along the center of the bottom conducting wall ( $x=0$ ,  $y=b/2$ ). The field configuration of the dominant mode and other odd order modes is such that wall currents associated with them are undisturbed by the slot, but wall currents of the even order modes are interrupted by it. The number of remaining higher order modes is considerably less than that

which can exist on equivalently oversize rectangular or circular waveguide. The remaining higher order modes would be attenuated more rapidly than the dominant mode. The greater attenuation of the undesired higher order modes reduces the probability of interference effects resulting from mode coupling at detectors or other obstacles along the trough guide. Similarly information distortion resulting from the different propagation velocities of the allowable modes is reduced. Nevertheless, launching of higher order modes should be avoided or minimized since any energy contained in these modes represents a loss of available energy from the source. A method of launching and collecting the  $PM_{11}$  mode, which discriminates against these higher order modes will be described in the next section.

The values of dielectric strip thickness (a) assumed in the computations of Figures 9 through 14 are less than can be obtained with tapes or conventional machining techniques. The required thin dielectric films will have to be applied by vapor deposition or equivalent techniques. As shown in Figure 7, the contemplated method of constructing the trough waveguide lends itself to deposition techniques. Controlled thickness films can be applied to the uppermost surface of the tee shaped bar which forms the bottom of the trough. After application of the film, two side walls can be attached.

Although trough guides, like those described above, were not constructed, the feasibility of doing so was investigated. Letters were sent to twenty-five companies to determine if they could apply specified dielectric films to conductors which we would supply. Replies from six of these companies stated sufficiently thin and uniform films of teflon can be applied to conductors which we would supply. These teflon films can be

applied in thicknesses from .001 microns ( $4 \times 10^{-8}$  inches). The tolerances quoted on uniformity of film thickness for lengths of many feet varied from  $\pm 1\%$  to  $\pm 10\%$ .

The prior discussion on the properties of the trough waveguide completely ignores the problem of launching and collecting the desired  $PM_{11}$  surface wave mode. If one is considering very long transmission paths, the launching and collecting losses may be insignificant compared to the transmission losses. For path lengths of a few meters, the launching and collecting losses may be comparable to or larger than the transmission loss, thus negating much of the advantage of a low loss surface wave system. In view of the above, the problem of launching and collecting the trough guide  $PM_{11}$  mode was investigated.

### 3.2 Excitation of the $PM_{11}$ Mode on the Partially Dielectric Loaded Trough Waveguide

A difficulty common to all forms of surface wave transmission is that of efficiently launching and collecting the wave. High launching and collecting losses cancel part of the advantage of using these low loss transmission lines. The radiation fields associated with inefficient launching also interfere with and hence reduce the accuracy of transmission measurements. For applications in which a number of surface wave lines are in proximity, the large radiation fields due to inefficient launching may cause the cross-talk level to be substantially different from that computed on the basis of the surface wave properties only.

#### 3.2.1 Boundary Value Problem

An analysis has been performed to determine the efficiency with which the  $PM_{11}$  mode of the trough line can be launched (and hence collected since reciprocity holds for surface wave launchers). Mathematically, the exciting source

consists of a transverse magnetic-current line source which is above and parallel to the dielectric-air interface. The magnitude of this line source varies through a half sinusoidal period over its length, i. e., it is a maximum at the center ( $y = b/2$ ) and zero at its end points ( $y = 0$  and  $y = b$ ). The required magnetic line source having the desired sinusoidal spatial variation is not just a mathematical concept, but can be realized physically through the use of a slot in a conducting end plate of the trough line. See Figure 7. This slot in turn is energized by a rectangular waveguide on the opposite side of the thin end plate. If the width of the rectangular waveguide and the length of the slot are both equal to the spacing between the parallel walls of the trough guide ( $b$ ), the magnetic field in the slot will have both the proper orientation and the required one half period of sinusoidal variation.

In the previously discussed oversize trough guide with a longitudinal slot centered in the bottom wall, the remaining higher order  $PM_{1n}$  modes ( $n = 3, 5, \text{etc.}$ ) would require  $y$ -direction sinusoidal variations of  $n$  half periods. By maintaining  $(b/\lambda_0)$  of the rectangular waveguide and trough guide between  $b_c$  and  $2b_c$  (as determined from Figure 8), only the  $PM_{11}$  mode can be launched and propagated. In order to obtain the previously cited low attenuation capability of the oversize trough guide, the spacing between the parallel walls can be increased via a taper section which begins a few wavelengths away from the launching slot.

The magnetic current line source  $\bar{K}$  as shown in an end view of the trough guide [ Figure 15(a) ] and in a side view [ Figure 15(b) ] is characterized by the following equation

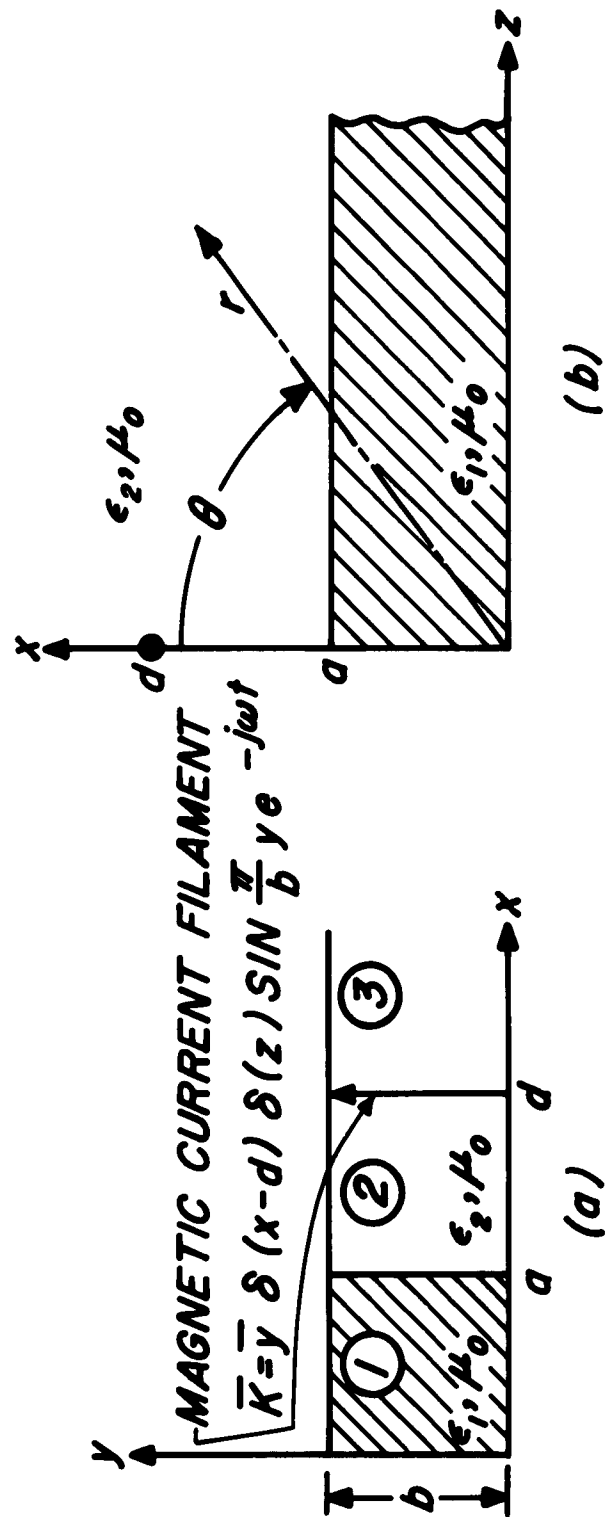


FIG. 15 - (a) END VIEW, AND (b) SIDE VIEW OF THE PARTIALLY DIELECTRIC LOADED TROUGH GUIDE EXCITED BY A MAGNETIC LINE SOURCE

$$(6) \quad \overline{K} = \overline{y} \delta(x-d) \delta(z) \sin \frac{\pi}{b} y e^{-j\omega t},$$

where

$\delta(x-d)$  and  $\delta(z)$  are Dirac delta functions

and  $\overline{y}$  is the unit vector in the  $y$ -direction.

In the remainder of this analysis an  $e^{-j\omega t}$  time dependence will be assumed for all of the field components. The magnetic line source is constrained to locations in the air space of the trough guide ( $d > a$ ). The trough guide geometry is such that the only mode which can propagate is the  $PM_{11}$  mode, i.e., equations (1) and (2) are satisfied.

The Maxwell curl equations, which include the magnetic line source term, and have the assumed time dependence are as follows:

$$(7) \quad \nabla \times \overline{E} = j\omega\mu\overline{H} - \overline{K}$$

$$(8) \quad \nabla \times \overline{H} = -j\omega\epsilon \overline{E}$$

The vector wave equation is thus

$$(9) \quad \nabla^2 \overline{H} + \omega^2 \mu\epsilon \overline{H} = -j\omega\epsilon \overline{y} \delta(x-d) \delta(z) \sin \frac{\pi}{b} y$$

Taking the  $y$  components of equation (9), the following nonhomogeneous scalar wave equation in  $H_y$  is obtained:

$$(10) \quad \nabla^2 H_y + \omega^2 \mu\epsilon H_y = -j\omega\epsilon \delta(x-d) \delta(z) \sin \frac{\pi}{b} y$$

Due to the restrictions on  $b$  and the prescribed  $y$ -dependence of the magnetic line source, the solutions of equation (10) will all be of the following form

$$(11) \quad H_y(x, y, z) = H'_y(x, z) \sin \frac{\pi}{b} y$$

Substituting (11) into (10) yields the following

$$(12) \left[ \frac{\partial^2}{\partial x^2} + \frac{\partial^2}{\partial z^2} + \omega^2 \mu \epsilon - \left( \frac{\pi}{b} \right)^2 \right] H'_y = -j\omega \epsilon \delta(x-d) \delta(z)$$

It should be noted that the above equation is that of a two dimensional problem in which  $\partial/\partial y = 0$ ; and  $\omega^2 \mu \epsilon$  is replaced by  $\omega^2 \mu \epsilon - (\pi/b)^2$ . This problem can thus be handled as though it were a two dimensional problem in which the actual permittivity  $\epsilon$  is replaced by  $\epsilon [1 - (\lambda_0/2b)^2]$ . Equation (12) will be solved by the method of Fourier Transforms.

$$(13) \quad \text{Let } H'_y(x, z) = \int_{-\infty}^{\infty} h(x, \zeta) e^{j\zeta z} d\zeta$$

The inverse Fourier Transform is

$$(14) \quad h(x, \zeta) = \frac{1}{2\pi} \int_{-\infty}^{\infty} H'_y(x, z) e^{-j\zeta z} dz$$

Substitute (13) into (12), multiply both sides by  $\frac{1}{2\pi} e^{-j\zeta z} dz$  and integrate from  $-\infty$  to  $+\infty$  to obtain:

$$(15) \quad \left[ \frac{d^2}{dx^2} - \zeta^2 + \omega^2 \mu \epsilon - \left( \frac{\pi}{b} \right)^2 \right] h(x, \zeta) = -j \frac{\omega \epsilon}{2\pi} \delta(x-d)$$

In region 1 ( $x \leq a$ ), equation (15) becomes

$$(16) \quad \frac{d^2 h_1}{dx^2} - \left[ \zeta^2 - \omega^2 \mu \epsilon_1 + \left( \frac{\pi}{b} \right)^2 \right] h_1 = 0$$

$$(17) \quad \therefore h_1 = A_1 \cosh k_1 x,$$

$$(18) \quad \text{where } k_1^2 = \zeta^2 - \omega^2 \mu \epsilon_1 + (\pi/b)^2$$

In region 2 ( $a \leq x \leq d$ ) and region 3 ( $x \geq d$ ) except at  $x = d, z = 0$ ; equation (15) becomes

$$(19) \quad \frac{d^2 h_2}{dx^2} - \left[ \zeta^2 - \omega^2 \mu \epsilon_2 + \left( \frac{\pi}{b} \right)^2 \right] h_2 = 0$$

$$(20) \quad \therefore h_2 = A_2 e^{k_2 x} + B_2 e^{-k_2 x}$$

and

$$(21) \quad h_3 = B_3 e^{-k_2 x}$$

where

$$(22) \quad k_2^2 = \zeta^2 - \omega^2 \mu \epsilon_2 + \left( \frac{\pi}{b} \right)^2$$

By expanding equation (8), remembering that in the equivalent two dimensional problem  $\partial/\partial y = 0$  and  $\epsilon$  becomes  $\epsilon [1 - (\lambda_0/2b)^2]$ , one obtains the following relationships:

$$(23) \quad E'_x = \frac{-j}{\omega \epsilon [1 - (\lambda_0/2b)^2]} \frac{\partial H'_y}{\partial z}$$

$$(24) \quad E'_y = \frac{j}{\omega \epsilon [1 - (\lambda_0/2b)^2]} \left( \frac{\partial H'_x}{\partial z} - \frac{\partial H'_z}{\partial x} \right)$$

$$(25) \quad E'_z = \frac{j}{\omega \epsilon [1 - (\lambda_0/2b)^2]} \frac{\partial H'_y}{\partial x}$$

The solutions to the wave equations in the three regions [equations (17), (20), and (21)] must satisfy the boundary conditions at  $x = a$  and  $x = d$ . At  $x=a$ ,  $H'_{y1} = H'_{y2}$  for all  $z$  and all  $\zeta$ .

$$(26) \quad \therefore h_1(a, \zeta) = h_2(a, \zeta)$$

$$(27) \quad \therefore A_1 \cosh k_1 a = A_2 e^{k_2 a} + B_2 e^{-k_2 a}$$

Similarly at  $x = a$ ,  $E'_{z1} = E'_{z2}$  for all  $z$  and all  $\zeta$ .

$$(28) \quad \therefore \epsilon_2 \frac{\partial h_1(a, \zeta)}{\partial x} = \epsilon_1 \frac{\partial h_2(a, \zeta)}{\partial x}$$

$$(29) \quad \therefore A_1 \epsilon_2 k_1 \sinh k_1 a = A_2 \epsilon_1 k_2 e^{k_2 a} - B_2 \epsilon_1 k_2 e^{-k_2 a}$$

At  $x = d$ ,  $H'_{y2} = H'_{y3}$  for all  $z$  and all  $\zeta$ .

$$(30) \quad \therefore h_2(d, \zeta) = h_3(d, \zeta)$$

$$(31) \quad \therefore A_2 e^{k_2 d} + B_2 e^{-k_2 d} = B_3 e^{-k_2 d}$$

The remaining boundary condition at  $x = d$  requires a different treatment. Multiply both sides of equation (15) by  $dx$  and integrate from  $d - \Delta x$  to  $d + \Delta x$  and let  $\Delta x$  approach zero, remembering that  $h$  is continuous at  $x = d$ .

$$(32) \quad \therefore \frac{\partial h_2(d, \zeta)}{\partial x} - \frac{\partial h_3(d, \zeta)}{\partial x} = j \frac{\omega \epsilon_2}{2\pi}$$

$$(33) \quad \therefore A_2 k_2 e^{k_2 d} - B_2 k_2 e^{-k_2 d} + B_3 k_2 e^{-k_2 d} = j \frac{\omega \epsilon_2}{2\pi}$$

Equations (27), (29), (31) and (33) can be solved to determine any of the four arbitrary constants ( $A_1, A_2, B_2$  and  $B_3$ ). Cramer's rule will be used to determine  $B_3$ . Let  $\Delta$  be the determinant of the left hand side of these equations. Solving for  $\Delta$  yields:

$$(34) \quad \Delta = -2k_2 e^{-k_2 a} (\epsilon_1 k_2 \cosh k_1 a + \epsilon_2 k_1 \sinh k_1 a)$$

It is interesting to note at this point, that if there were no magnetic line source, the four boundary value equations would be homogeneous. In that case the only non-trivial solution would require  $\Delta = 0$ . If  $\Delta$  is set equal to zero, the following equation is obtained.

$$(35) \quad k_2 = -\frac{\epsilon_2}{\epsilon_1} k_1 \tanh k_1 a$$

Equation (35) is the conditional or secular equation for the PM modes of the trough waveguide. See equation (43), page 27, of reference 8. Continuing with Cramer's Rule to solve for  $B_3$  and using equations (13) and (21), it is found that

$$(36) \quad H'_{y3}(x, z) =$$

$$\frac{j\omega\epsilon_2}{2\pi} \int_{-\infty}^{\infty} \frac{\epsilon_1 k_2 \cosh k_1 a \cosh k_2 (d-a) + \epsilon_2 k_1 \sinh k_1 a \sinh k_2 (d-a)}{k_2 [\epsilon_1 k_2 \cosh k_1 a + \epsilon_2 k_1 \sinh k_1 a]} e^{k_2 (a-x) + j\zeta z} d\zeta$$

### 3.2.2 Singularities of the Integrand

The real integral (36) is evaluated by considering it to be a contour integral in the complex  $\zeta$  plane and applying the Cauchy Residue Theorem. The integrand of (36) is multiple valued at  $k_1 = 0$  and  $k_2 = 0$ , but is an even function of  $k_1$ , and hence the only branch points occur at

$$(37) \quad \zeta = \zeta_b = \pm \sqrt{\omega^2 \mu \epsilon_2 - (\pi/b)^2} \quad (k_2 = 0)$$

If  $\omega^2 \mu \epsilon_2 > (\pi/b)^2$  then the branch point  $\zeta_b$  lies on the real  $\zeta$  axis. Let the branch cuts ( $\Gamma$ ) be along the line

$$\pm \zeta_b + \text{Im } \zeta.$$

The integrand of (36) has poles at  $\pm \zeta_p$  determined by

$$(38) \quad \epsilon_1 k_{2p} \cosh k_{1p} a + \epsilon_2 k_{1p} \sinh k_{1p} a = 0,$$

where  $k_{1p}$  and  $k_{2p}$  are respectively the values of the previously defined transverse wave numbers,  $k_1$  and  $k_2$  [see equations (18) and (22)] at the poles. A path of integration in the complex  $\zeta$ -plane which assures convergence of the integral is shown in Figure 16. Only the branch cut emanating from  $+\zeta_b$  will be considered since it represents radiation away from the magnetic line source. Similarly, only the pole at  $+\zeta_p$  is included in the contour of integration since it represents surface wave propagation away from the source.

### 3.2.3 Evaluation of the Contour Integral

$$(39) \quad \text{Let } H'_{y3}(x, z) = \int_{-\infty}^{\infty} U(\zeta) d\zeta$$

where

$$U(\zeta) \text{ is } -j \frac{\omega \epsilon}{2\pi} \text{ times the integrand of (36)}$$

In the limit as  $R$  approaches infinity, it can be shown that the contributions due to the integrals along the circular arcs  $R_1$  and  $R_2$  vanish.

$$(40) \quad \therefore H'_{y3}(x, z) = 2\pi j \text{ Residue } U(\zeta) \Big|_{\zeta=\zeta_p} - \int_{\Gamma} U(\zeta) d\zeta$$

### 3.2.4 Evaluation of the Branch Cut Integral (Radiation Field)

Instead of integrating along  $\Gamma$ , the path of integration is deformed from  $\Gamma$  to the path of steepest descent

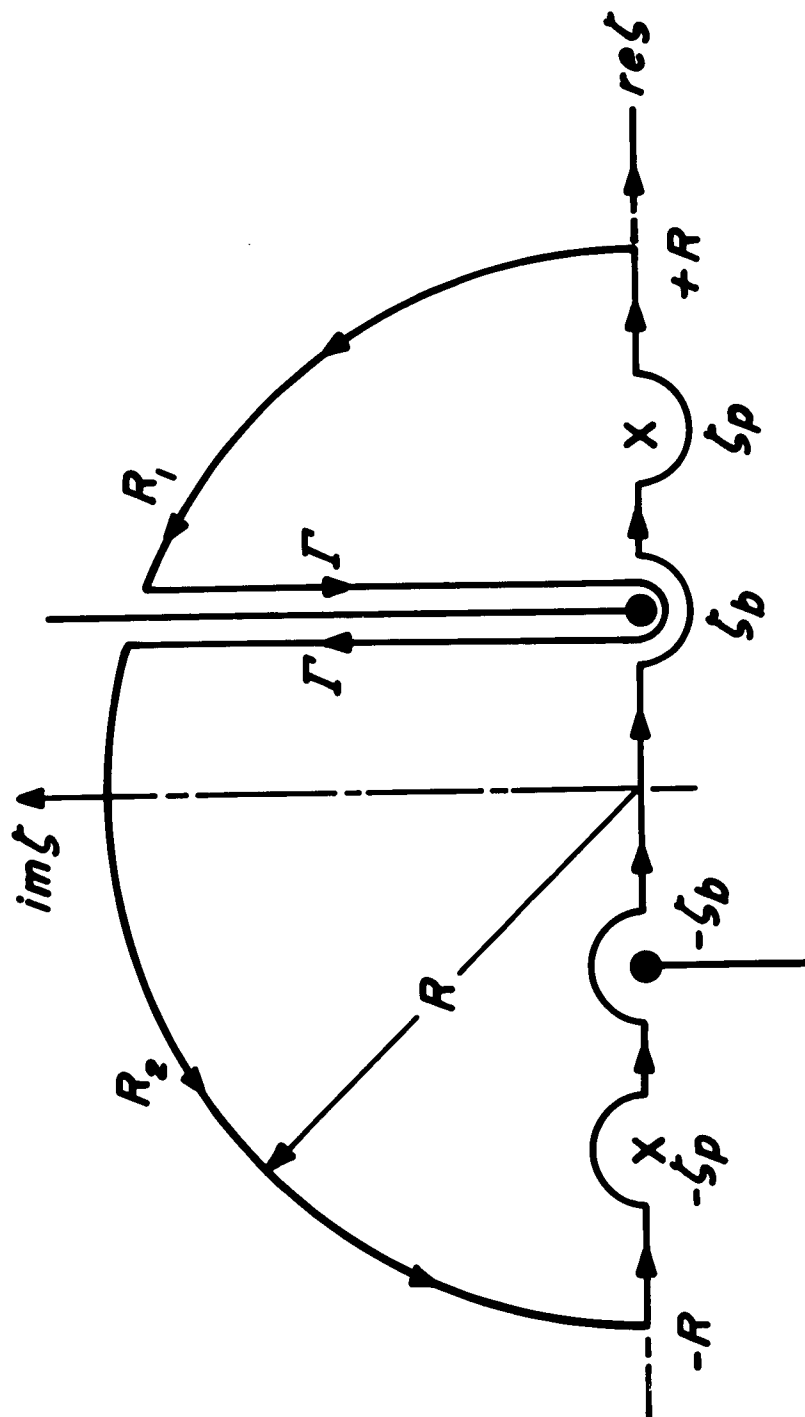


FIG. 16 - CONTOUR OF INTEGRATION IN THE  $\zeta$ -PLANE

$C_s$  through the saddle point of the integrand. The path  $C_s$  is in the opposite direction to  $\Gamma$ .

$$(41) \quad \therefore \int_{-\infty}^{\infty} U(\zeta) d\zeta = 2\pi j \text{Residue } U(\zeta) \Big|_{\zeta=\zeta_p} + \int_{C_s} U(\zeta) d\zeta$$

$$(42) \quad \text{Let } \zeta = \zeta_b \sin \tau, \text{ where } \tau = \psi + j \eta$$

The branch points at  $\zeta = \pm \zeta_b$  are transformed to the points  $\psi = \pm \pi/2, \eta = 0$  in the  $\tau$ -plane. The branch cuts at  $\text{Re}(\zeta) = \pm \zeta_b$  are transformed to the following curves in the  $\tau$ -plane.

$$(43) \quad \sin \psi \cosh \eta = \pm 1$$

The poles at  $\zeta = \pm \zeta_p$  are transformed as follows

$$(44) \quad \begin{cases} \zeta = + \zeta_p \longrightarrow \tau_p = \frac{\pi}{2} - j \cosh^{-1} \frac{\zeta_p}{\zeta_b} \\ \zeta = - \zeta_p \longrightarrow \tau_p = - \frac{\pi}{2} + j \cosh^{-1} \frac{\zeta_p}{\zeta_b} \end{cases}$$

The path of integration along the real axis of  $\zeta$ -plane is transformed to the following three straight line segments on the  $\tau$ -plane. See Figure 17.

$$(45) \quad \begin{cases} \zeta < - \zeta_b \longrightarrow \psi = - \frac{\pi}{2}, \eta > 0 \\ - \zeta_b < \zeta < \zeta_b \longrightarrow - \frac{\pi}{2} < \psi < \frac{\pi}{2}, \eta = 0 \\ \zeta > \zeta_b \longrightarrow \psi = \frac{\pi}{2}, \eta < 0 \end{cases}$$

Substitute equations (37) and (42) into equations (18) and (22).

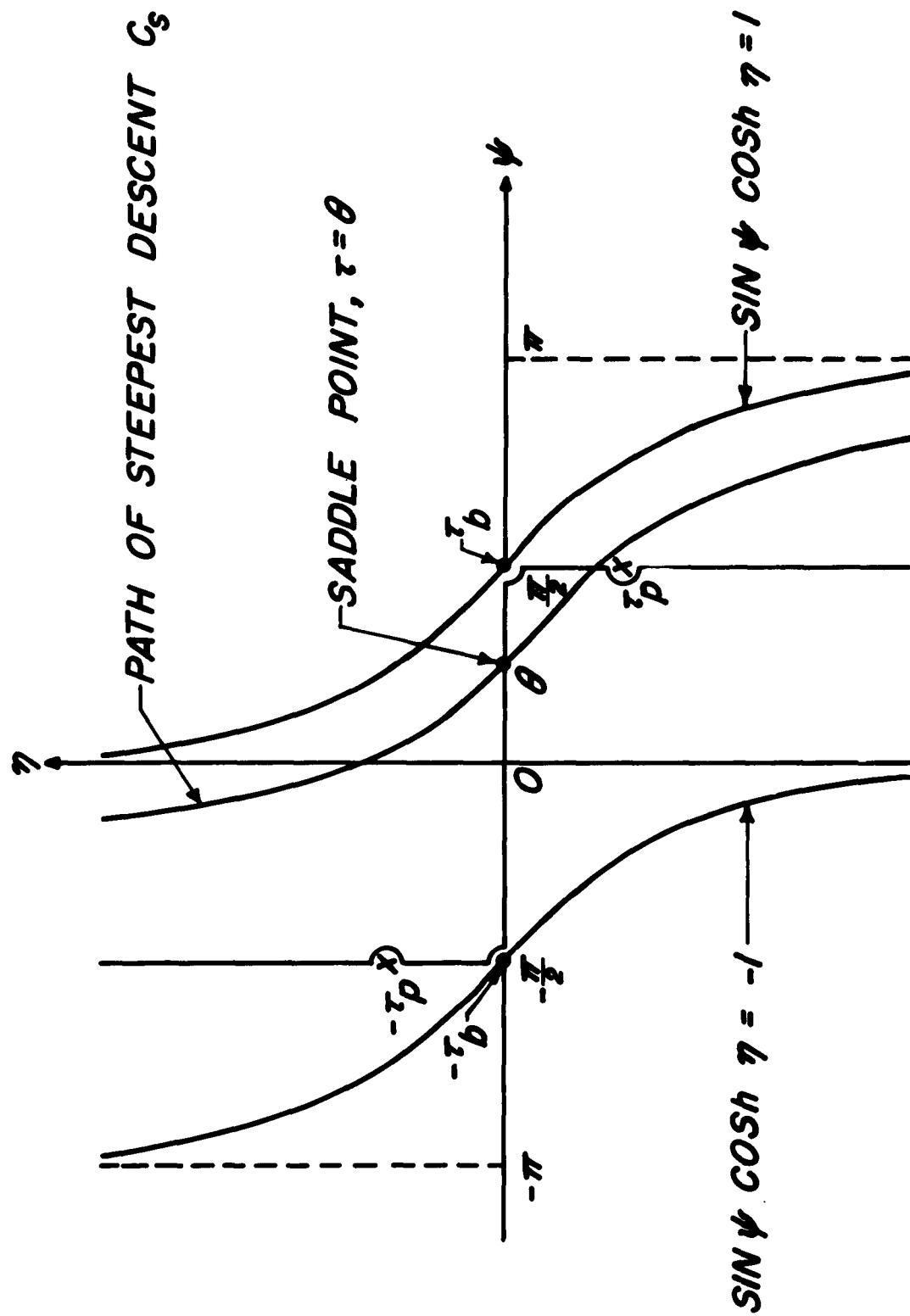


FIG. 17 - PATH OF INTEGRATION IN THE  $\tau$ -PLANE

$$(46) \quad k_1 = \pm j \sqrt{\zeta_b^2 \cos^2 \tau + \omega^2 \mu (\epsilon_1 - \epsilon_2)}$$

$$(47) \quad k_2 = -j \zeta_b \cos \tau$$

Substitute (46) and (47) into the transformed branch cut integral and change to polar coordinates as shown in Figure 15.

$$(48) \quad \int_{C_s} U(\zeta) = \frac{\omega \epsilon_2}{2\pi}$$

$$\int_{C_s} \frac{\epsilon_1 \zeta_b \cos \tau \cos Wa \cos [\zeta_b (d-a) \cos \tau] - \epsilon_2 W \sin Wa \sin [\zeta_b (d-a) \cos \tau]}{[\epsilon_1 \zeta_b \cos \tau \cos Wa - j \epsilon_2 W \sin Wa] e^{j \zeta_b a \cos \tau}} e^{j \zeta_b r \cos(\tau - \theta)} d\tau$$

$$(49) \quad \text{where} \quad W = \sqrt{\zeta_b^2 \cos^2 \tau + \omega^2 \mu (\epsilon_1 - \epsilon_2)}$$

The saddle point is defined by

$$(50) \quad \frac{d}{d\tau} [\cos(\tau - \theta)] = 0$$

$$(51) \quad \tau = \theta \text{ is the saddle point.}$$

The path of steepest descent through the saddle point is

$$(52) \quad \cos(\psi - \theta) \cosh \eta = 1$$

Let  $\mu = \mu_o$ ,  $\epsilon_2 = \epsilon_o$ , and  $\epsilon_1 = \epsilon_r \epsilon_o$

Evaluating (48) by the saddle point method and restoring the y-dependence, one obtains the following expression, which is valid for large r.

$$(53) \quad H_y^R(r, \theta, y) = \frac{\omega \epsilon_0}{\sqrt{2\pi \zeta_b r}} F(\theta) \sin \frac{\pi}{b} y e^{j(\zeta_b r - \pi/4)}$$

where

$$(54) \quad F(\theta) = \frac{\epsilon_r \zeta_b \cos \theta \cos Wa \cos [\zeta_b (d-a) \cos \theta] - W \sin Wa \sin [\zeta_b (d-a) \cos \theta]}{[\epsilon_r \zeta_b \cos \theta \cos Wa - jW \sin Wa] e^{j\zeta_b a \cos \theta}}$$

$$(55) \quad \text{and} \quad W = \sqrt{\zeta_b^2 \cos^2 \theta + \omega^2 \mu_0 \epsilon_0 (\epsilon_r - 1)}$$

The superscript R indicates a radiating field component. Equation (53) is recognized as a component of a radiating cylindrical wave front.  $F(\theta)$  is the radiation pattern of this wave.

In order to calculate the amount of power being radiated, only the relevant field components for large  $r$  are needed. For large  $r$ , the presence of the magnetic line source and the dielectric strip can be neglected. To an observer looking in the  $y$ -direction at a large  $r$ , the space between parallel conducting planes is a uniform homogeneous transmission line. Thus referenced to the  $y$ -direction, all modes are TE, TM, or TEM. Since an  $H_y$  component is present, the radiation fields must be transverse electric referred to the  $y$ -direction.

$$(56) \quad \therefore E_y^R(r, \theta, y) = 0$$

By expanding (8) in cylindrical coordinates, it is found that for large  $r$

$$(57) \quad E_\theta^R(r, \theta, y) = \frac{\omega \mu_0}{\zeta_b} H_y^R(r, \theta, y)$$

The total radiated power on the right hand side of the magnetic line source ( $z > 0$ ) is

$$(58) \quad P_R = \int_{y=0}^b \int_{\theta=0}^{\pi/2} 1/2 \operatorname{Re} [E_{\theta}^R \times H_y^{R*}] r d\theta dy$$

Substituting (53) and (57) into (58), the following normalized expression for the total far field radiated power is obtained

$$(59) \quad \frac{P_R \lambda_o}{b} = \frac{1}{960\pi [1 - (\lambda_o/2b)^2]} \int_0^{\pi/2} |F(\theta)|^2 d\theta$$

where

$$(60) \quad |F(\theta)|^2 = \frac{\left\{ \epsilon_r \sqrt{1 - (\frac{\lambda_o}{2b})^2} \cos \theta \cos [\zeta_b a (\frac{d}{a} - 1) \cos \theta] - \sqrt{\epsilon_r - 1 + \left[1 - (\frac{\lambda_o}{2b})^2\right] \cos^2 \theta} \tan Wa \sin [\zeta_b a (\frac{d}{a} - 1) \cos \theta] \right\}^2}{\left[1 - (\frac{\lambda_o}{2b})^2\right] \left[ \epsilon_r^2 + \tan^2 Wa \right] \cos^2 \theta + (\epsilon_r - 1) \tan^2 Wa}$$

$$(61) \quad \zeta_b a = \pi \left( \frac{2a}{\lambda_o} \right) \sqrt{1 - (\lambda_o/2b)^2},$$

and

$$(62) \quad Wa = \pi \left( \frac{2a}{\lambda_o} \right) \sqrt{\epsilon_r - 1 + \left[1 - (\lambda_o/2b)^2\right] \cos^2 \theta}$$

A few sample plots of  $|F(\theta)|^2$ , the power radiation pattern are shown in Figures 18 and 19. The plots of  $|F(\theta)|^2$  shown in Figure 19 are for a condition which results in high launching efficiency.

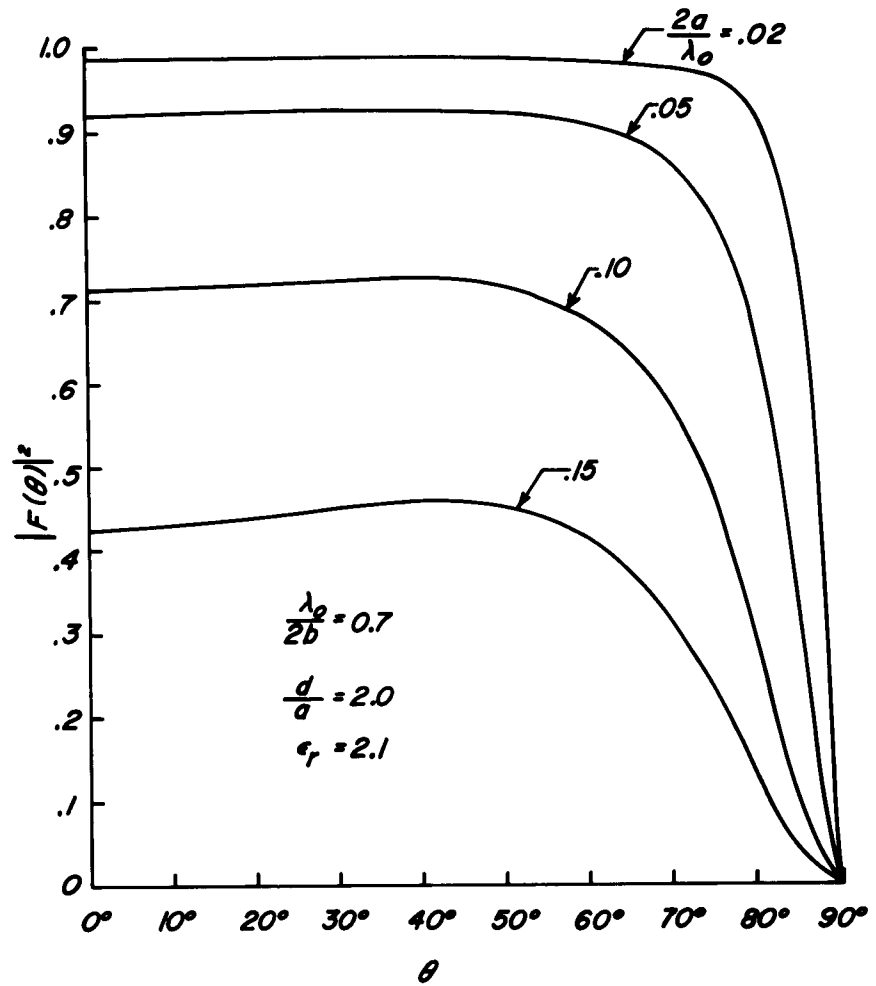


FIG. 18 - POWER RADIATION PATTERNS DUE TO A MAGNETIC LINE SOURCE LOCATED ABOVE THE DIELECTRIC STRIP OF A DIELECTRIC LOADED TROUGH GUIDE

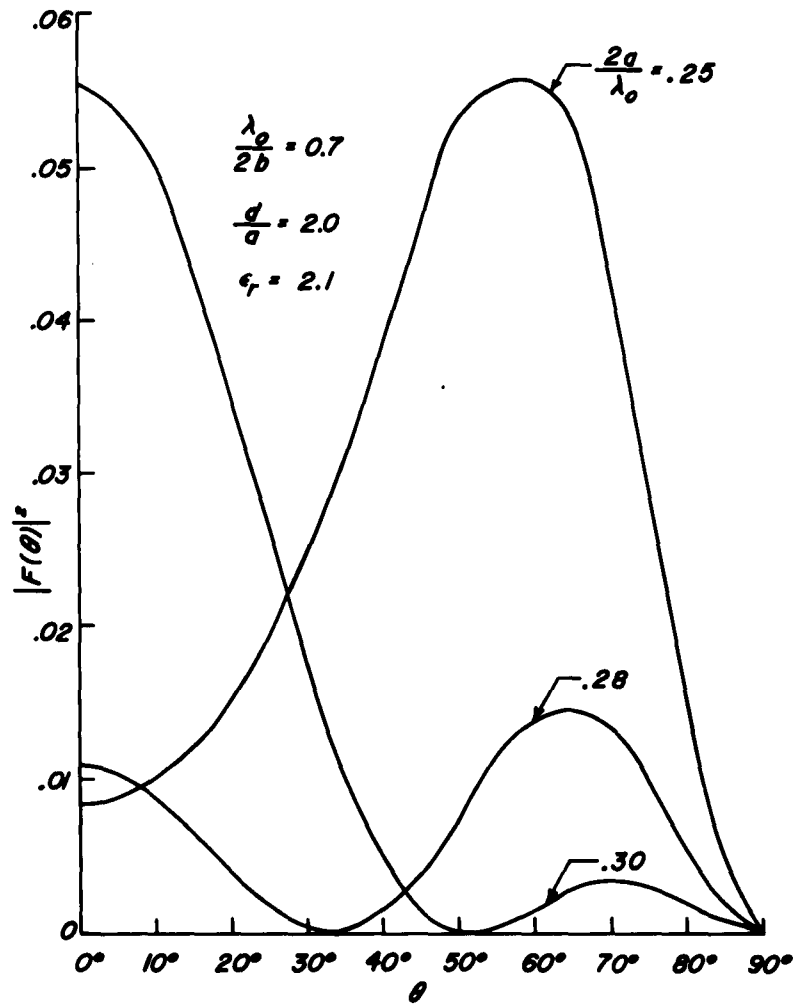


FIG. 19 - POWER RADIATION PATTERNS DUE TO A MAGNETIC  
 LINE SOURCE LOCATED ABOVE THE DIELECTRIC STRIP OF A  
 DIELECTRIC LOADED TROUGH GUIDE

### 3.2.5 Evaluation of the Pole Residue (Surface Wave Field)

When the contour integral is evaluated, the residue contribution from the pole will be in the form

$$(63) \quad C e^{k_{2p}(a-x) + j \zeta_p z}$$

For this term to represent a surface wave propagating in the + z direction on a dissipationless line,  $\zeta_p$  must be real. From equations (18) and (22), we obtain the following relations between the longitudinal wave number ( $\zeta_p$ ) and the transverse wave numbers ( $k_{1p}$  and  $k_{2p}$ ) of the surface wave.

$$(64) \quad k_{1p}^2 = \zeta_p^2 - \omega^2 \mu_o \epsilon_o \epsilon_r + (\pi/b)^2$$

$$(65) \quad k_{2p}^2 = \zeta_p^2 - \omega^2 \mu_o \epsilon_o + (\pi/b)^2$$

All of the terms on the right hand sides of (64) and (65) are real. Therefore, both  $k_{1p}$  and  $k_{2p}$  are either pure real or pure imaginary quantities. In order to satisfy the radiation condition as  $x \rightarrow 0$ ,  $k_{2p}$  must be real and positive. It can be shown from equation (38) that if  $k_{2p}$  is real and positive, then  $k_{1p}$  must be an imaginary quantity, and ( $k_{1p} a$ ) is restricted to certain intervals.

$$(66) \quad \text{Let } k_{1p} = jk_d,$$

where the subscript d refers to the dielectric region (region 1).

Equation (38) then has the following form

$$(67) \quad k_{2p} = \frac{1}{\epsilon_r} k_d \tan k_d a,$$

where ( $k_d a$ ) must be in an odd quadrant. From (64), (65), and (66) the following is obtained

$$(68) \quad (k_{2p}a)^2 + (k_d a)^2 = \pi^2 \left(\frac{2a}{\lambda_o}\right)^2 (\epsilon_r - 1)$$

From (67) and (68), the following is obtained

$$(69) \quad (k_d a)^2 \left[ 1 + \frac{\tan^2 k_d a}{\epsilon_r^2} \right] = \pi^2 \left(\frac{2a}{\lambda_o}\right)^2 (\epsilon_r - 1)$$

Values of  $(k_d a)$  of the  $PM_{1n}$  modes as a function of  $(2a/\lambda_o)$  and  $\epsilon_r$ , are available in graphical form. See Figure 9, page 55 of reference 8. These values of  $(k_d a)$  are necessary to compute the total surface wave power ( $P_s$ ) of the  $PM_{11}$  mode. Performing the residue integration and restoring the  $y$ -dependence, one obtains

$$(70) \quad H_{y3}^s(x, y, z) = \frac{\omega \epsilon_o \epsilon_r}{\zeta_p} \frac{k_d \sin k_d a \cos k_d a e^{-k_{2p}(d-2a+x)}}{(k_d a) \tan k_d a + \sin^2 k_d a + \epsilon_r^2 \cos^2 k_d a} \sin \frac{\pi}{b} y e^{j \zeta_p z}$$

The superscript "s" stands for the surface wave fields. Far from the magnetic line source (large  $z$ ), one can readily compute  $H_y^s$  for regions 1 and 2. Similarly  $E_x^s$  can be computed for all three regions. Using these results, the following normalized expression for the total surface wave power ( $P_s$ ) flowing in the positive  $z$ -direction is obtained.

$$(71) \quad \frac{P_s \lambda_o}{b} = \frac{\epsilon_r \left[ \pi^2 \left( \frac{2a}{\lambda_o} \right)^2 \epsilon_r - (k_d a)^2 \right]}{480 \left\{ \pi^2 \left( \frac{2a}{\lambda_o} \right)^2 [\epsilon_r - (\lambda_o/2b)^2] - (k_d a)^2 \right\}^{3/2}} \cdot \left\{ \frac{(k_d a) \sin k_d a \cos k_d a e^{-2k_{2p} a \left( \frac{d}{a} - 1 \right)}}{(k_d a) \tan k_d a + \sin^2 k_d a + \epsilon_r^2 \cos^2 k_d a} \right\}$$

### 3.2.6 Calculation of the $PM_{11}$ Mode Launching Efficiency

The launching efficiency ( $\eta_L$ ) is defined as the ratio of the surface wave power to the total power incident on the slot which forms the magnetic line source. Since the surface wave and radiation fields are orthogonal, the total incident power is the sum of the surface wave and radiated power.

$$(72) \quad \eta_L = \frac{P_s}{P_s + P_r} = \frac{(P_s \lambda_o / b)}{(P_s \lambda_o / b) + (P_r \lambda_o / b)}$$

The surface wave power is easily computed using equation (71). The computations of the radiated power, using equations (59) through (62), were performed on an electronic computer. These computations have been performed for a range of values of the normalized dielectric strip thickness ( $2a/\lambda_o$ ), normalized parallel wall spacing ( $\lambda_o/2b$ ), normalized magnetic line source location ( $d/a$ ) and a particular value of the dielectric constant ( $\epsilon_r = 2.1$ ). A number of families of curves of the computed launching efficiency as a function of the above normalized parameters are shown in Figures 20 through 31. These curves show that the  $PM_{11}$  mode can be very efficiently launched onto the trough waveguide from a properly located and energized slot in an end plate of the trough.

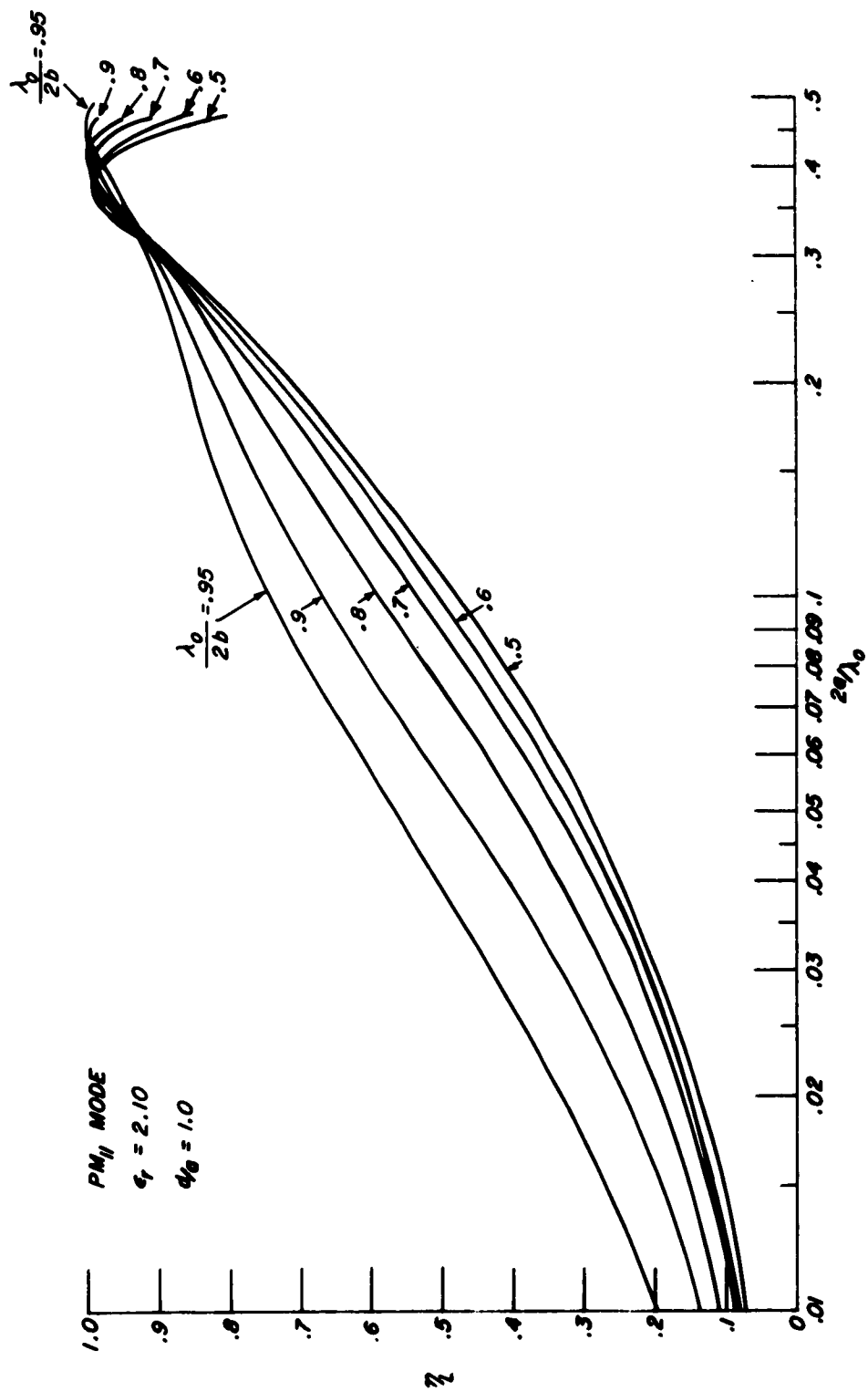


FIG 20 - LAUNCHING EFFICIENCY ( $\eta_L$ ) VERSUS NORMALIZED DIELECTRIC STRIP THICKNESS ( $2a/\lambda_0$ ),  $\psi_0 = 1.0$

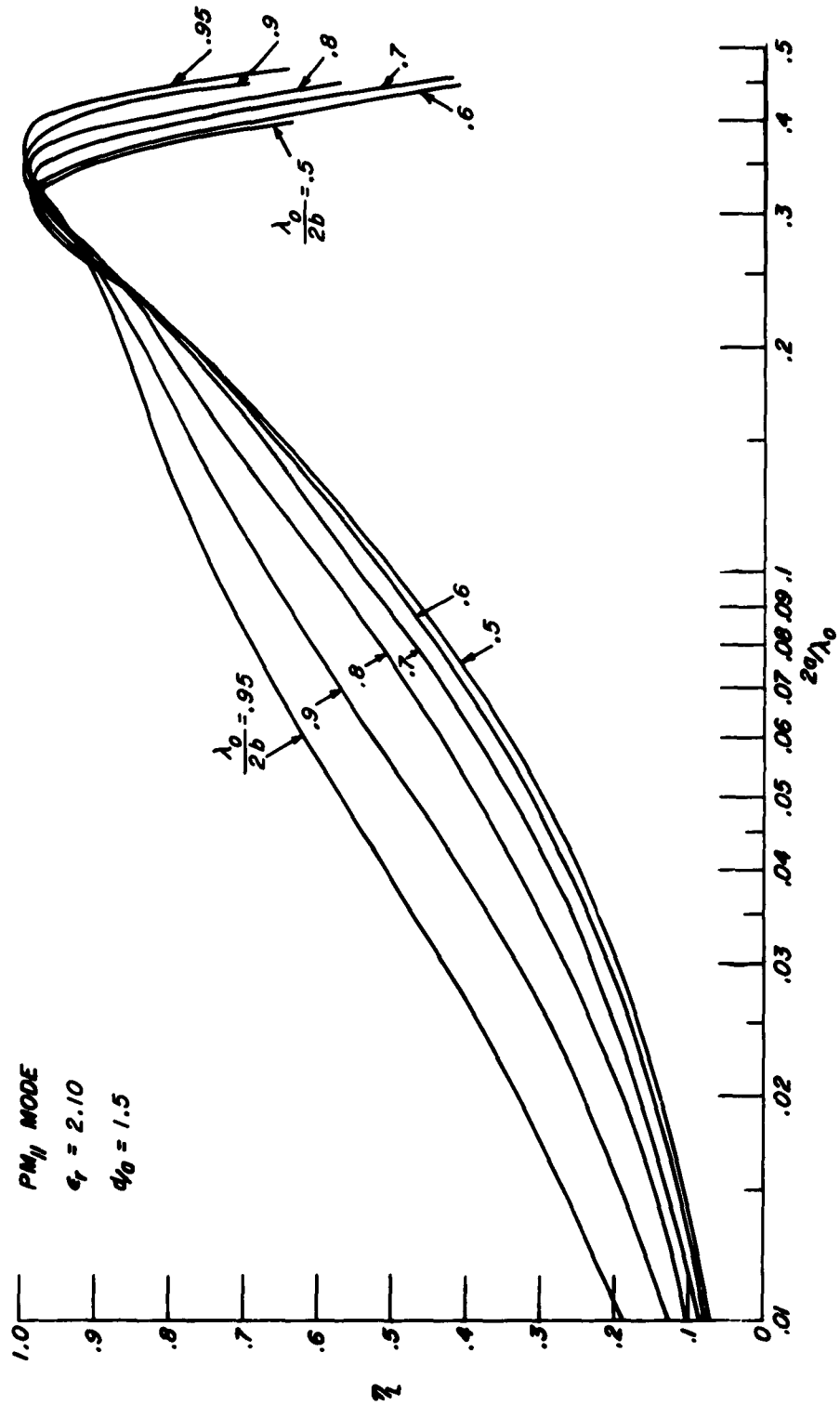


FIG. 21 - LAUNCHING EFFICIENCY ( $\eta_L$ ) VERSUS NORMALIZED DIELECTRIC STRIP THICKNESS ( $2a/\lambda_0$ ),  $d_0 = 1.5$

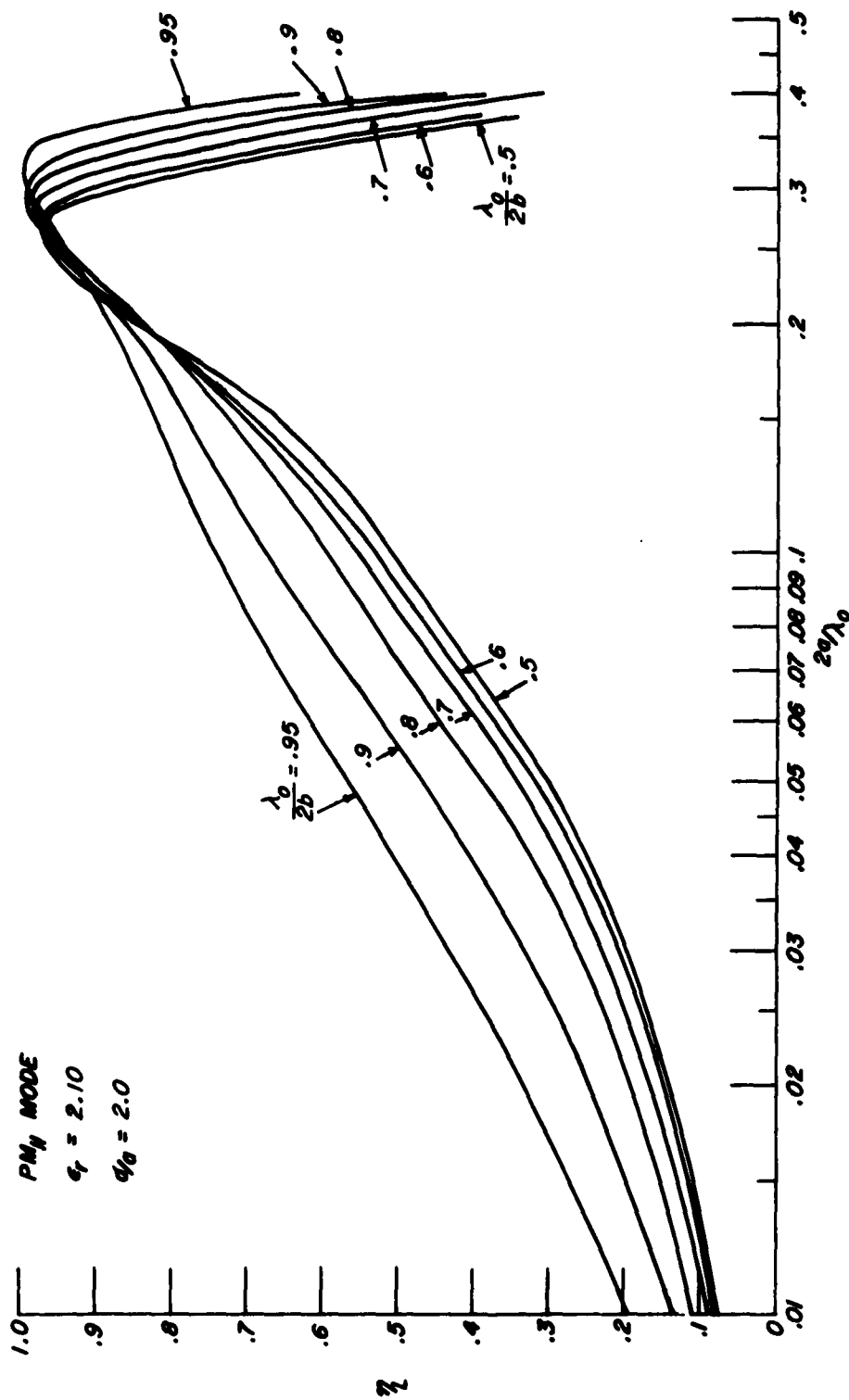


FIG. 22 - LAUNCHING EFFICIENCY ( $\eta_L$ ) VERSUS NORMALIZED DIELECTRIC STRIP THICKNESS ( $2a/\lambda_0$ ),  $\epsilon_0 = 2.0$

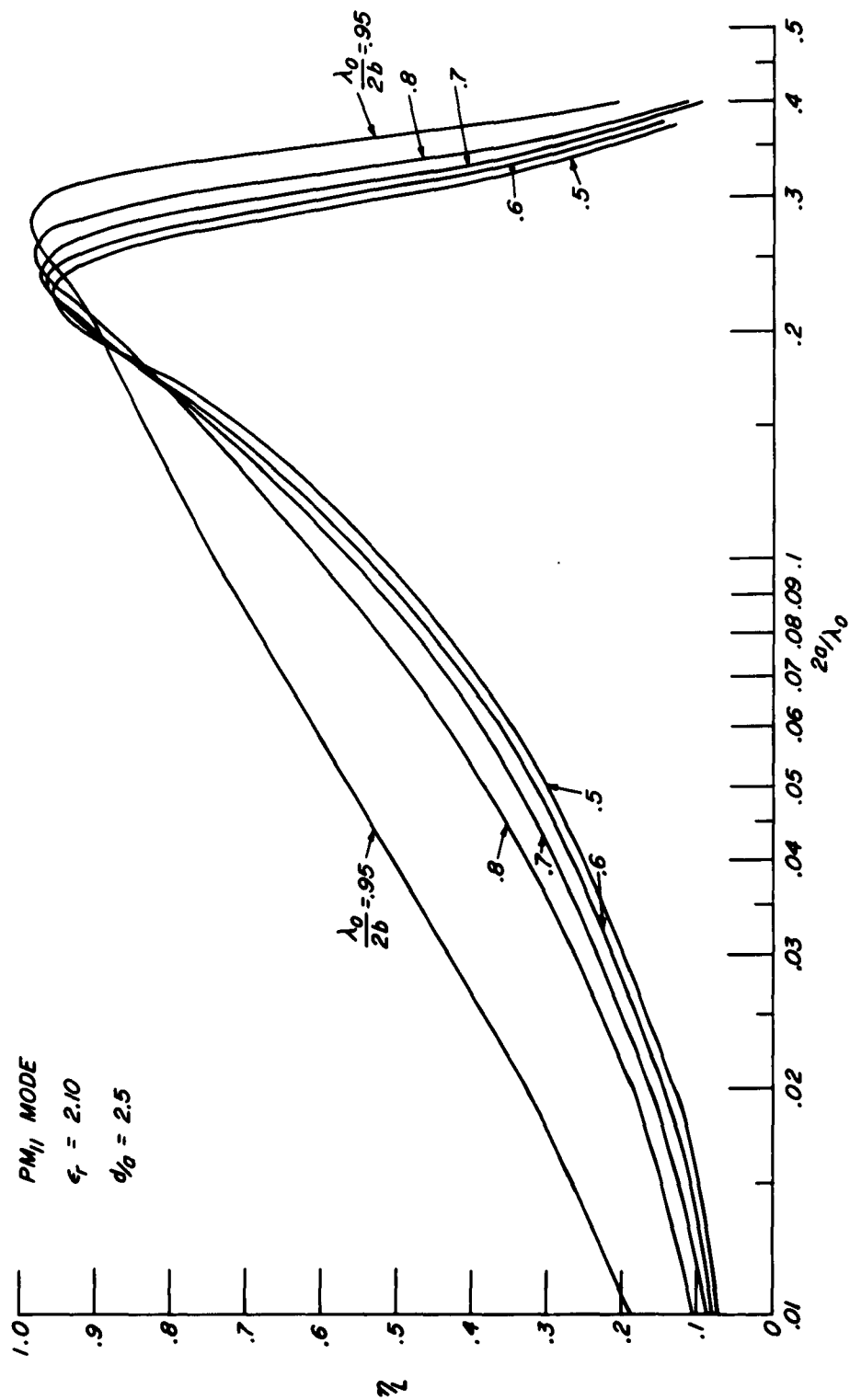


FIG. 23 - LAUNCHING EFFICIENCY ( $\eta_L$ ) VERSUS NORMALIZED DIELECTRIC STRIP THICKNESS ( $2a/\lambda_0$ ),  $\epsilon_r = 2.10$ ,  $d_0 = 2.5$

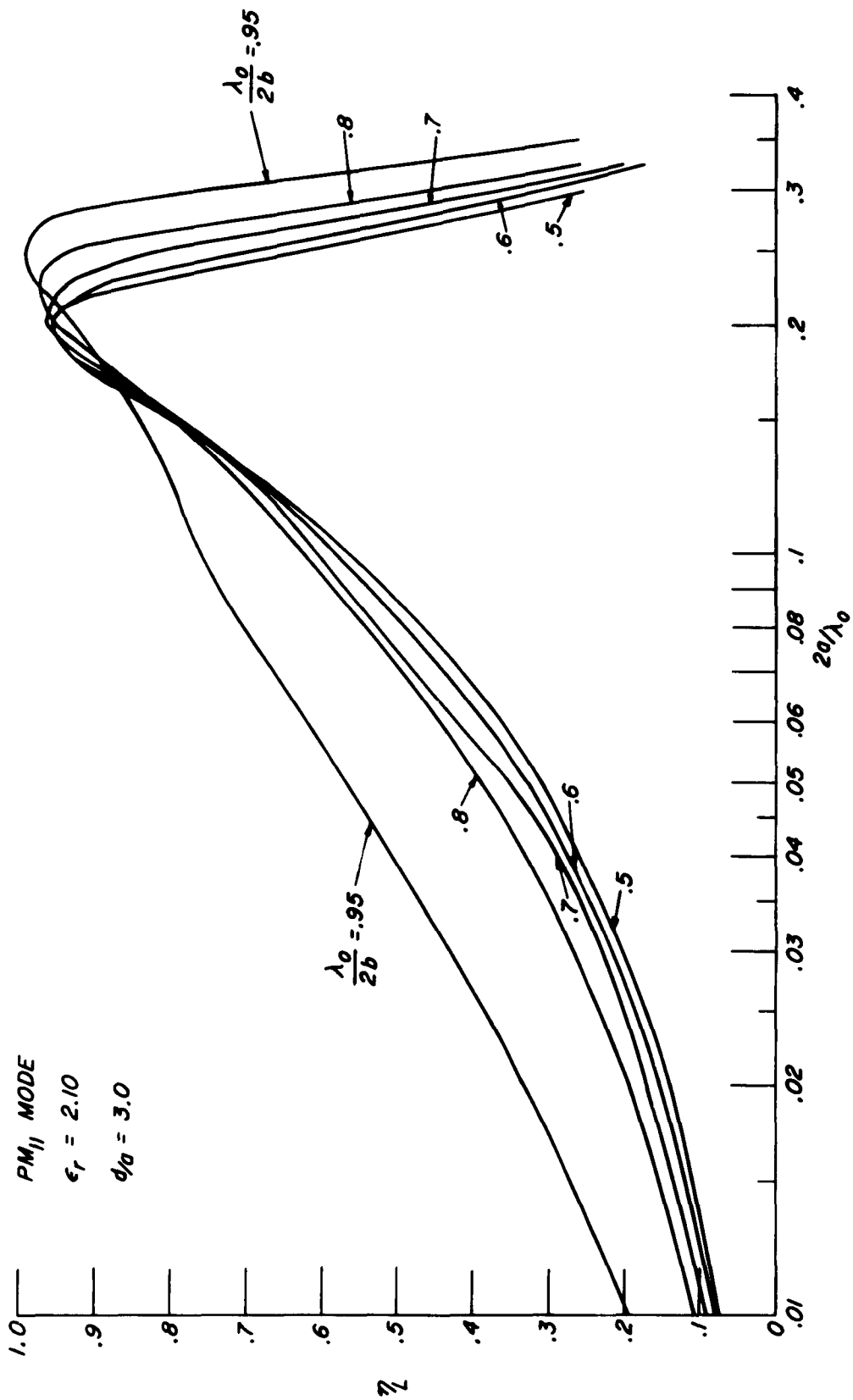


FIG. 24 - LAUNCHING EFFICIENCY ( $\eta_L$ ) VERSUS NORMALIZED DIELECTRIC STRIP THICKNESS ( $2a/\lambda_0$ ),  $d/a = 3.0$

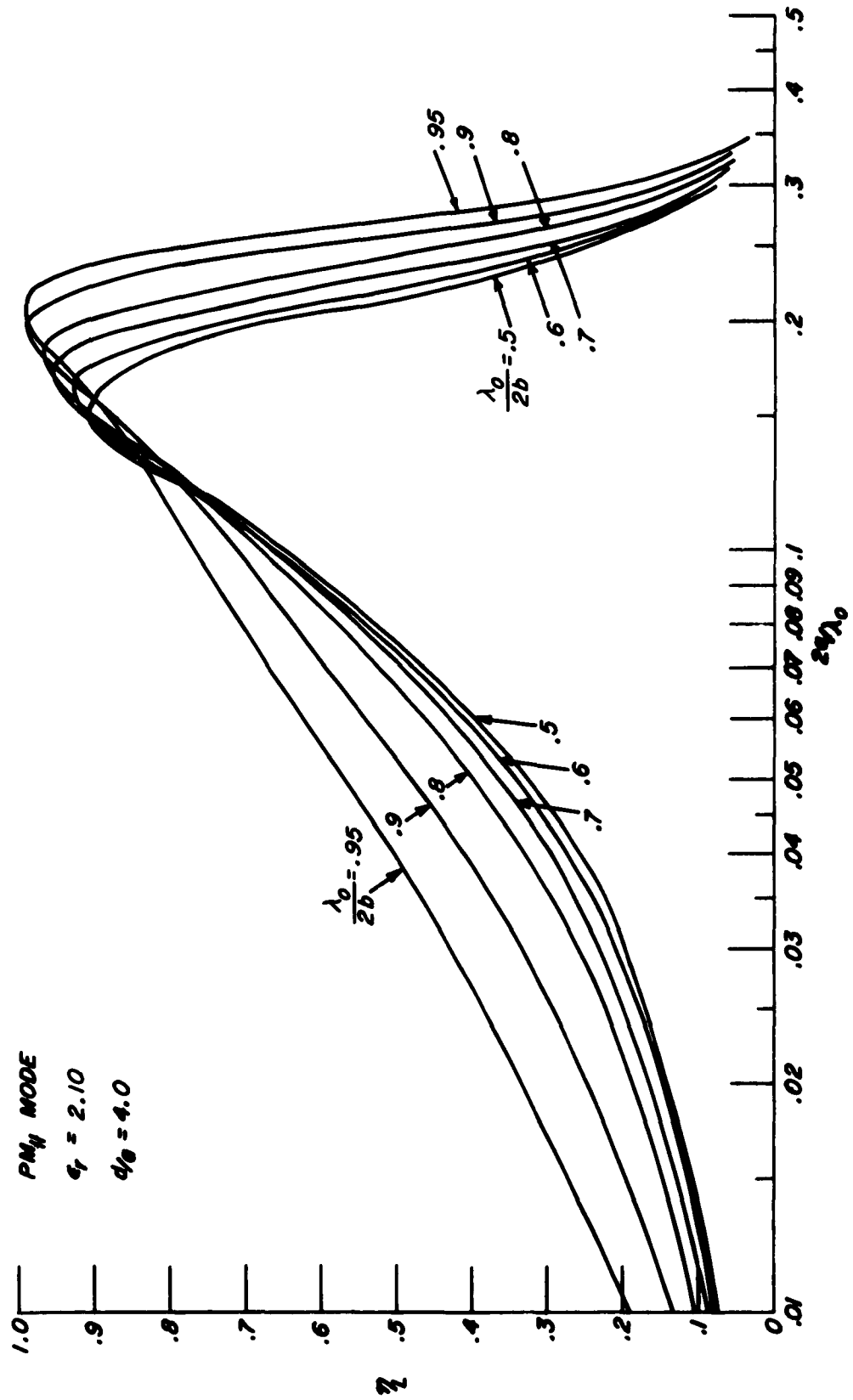


FIG 25 - LAUNCHING EFFICIENCY ( $\eta_L$ ) VERSUS NORMALIZED DIELECTRIC STRIP THICKNESS ( $2d/\lambda_0$ ),  $d/b = 4.0$

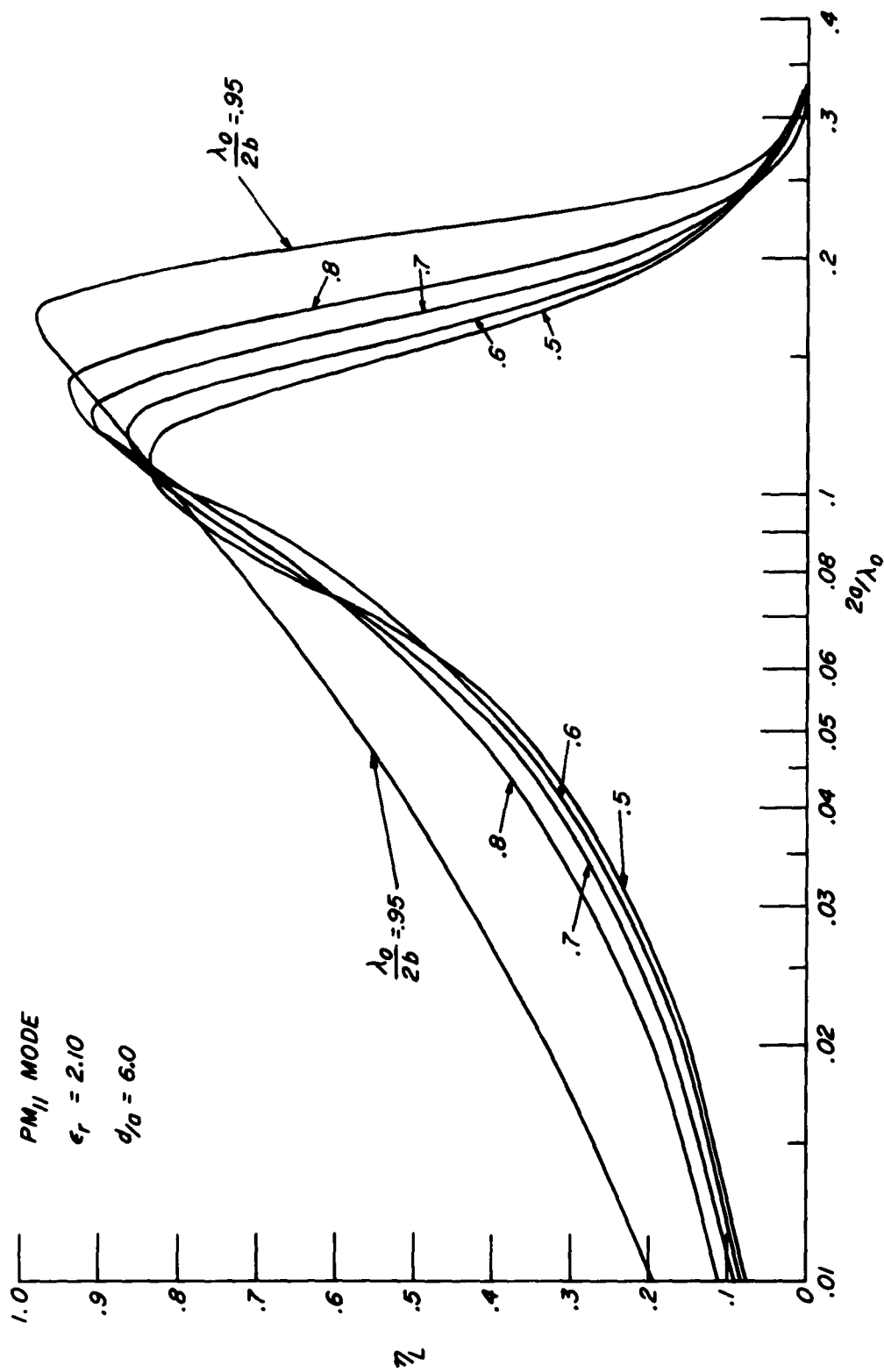


FIG. 26 - LAUNCHING EFFICIENCY ( $\eta_L$ ) VERSUS NORMALIZED DIELECTRIC STRIP THICKNESS ( $2a/\lambda_0$ ),  $d_0 = 6.0$



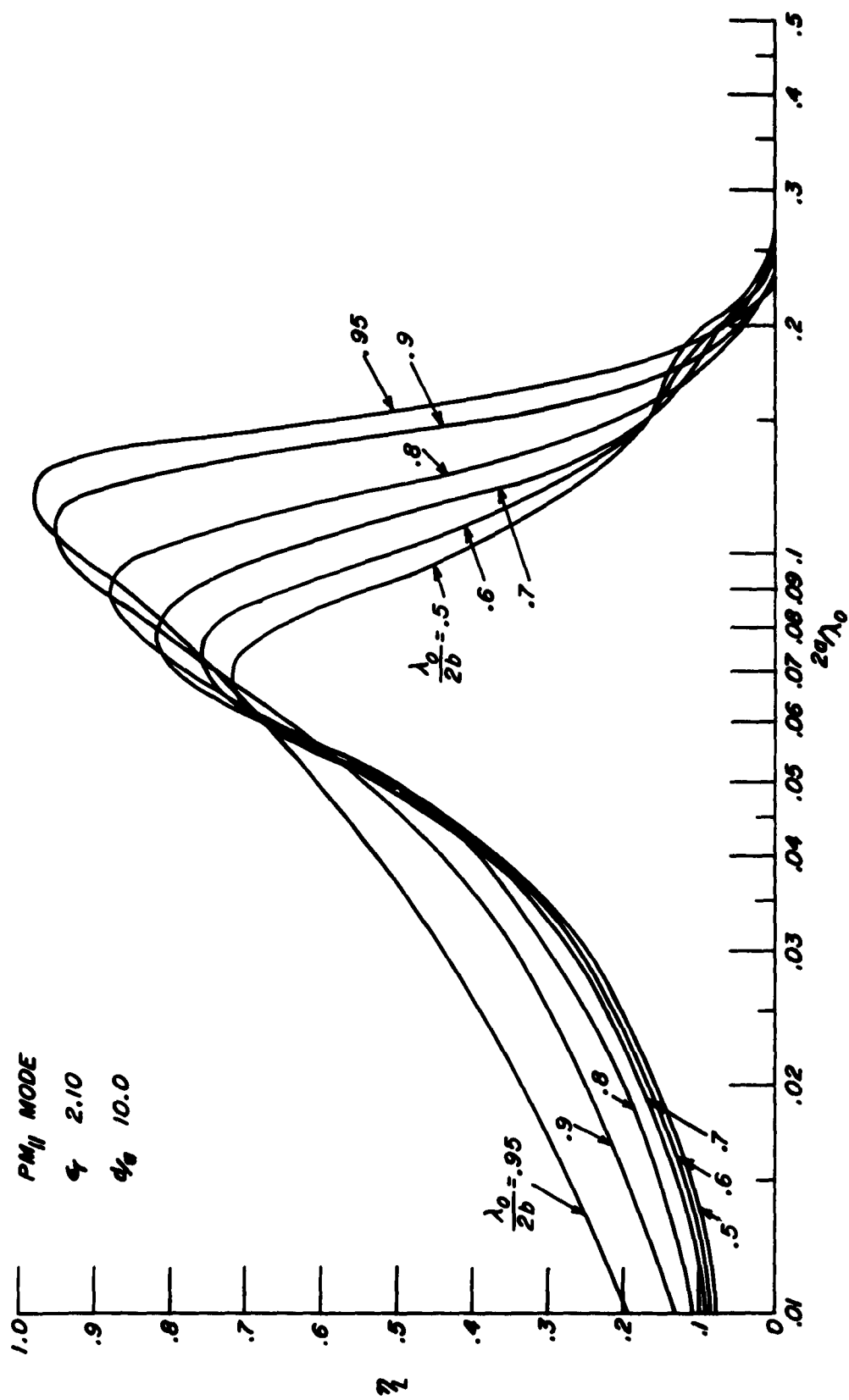


FIG. 28 - LAUNCHING EFFICIENCY ( $\eta$ ) VERSUS NORMALIZED DIELECTRIC STRIP THICKNESS ( $2a/\lambda_0$ ),  $\epsilon_r = 10.0$

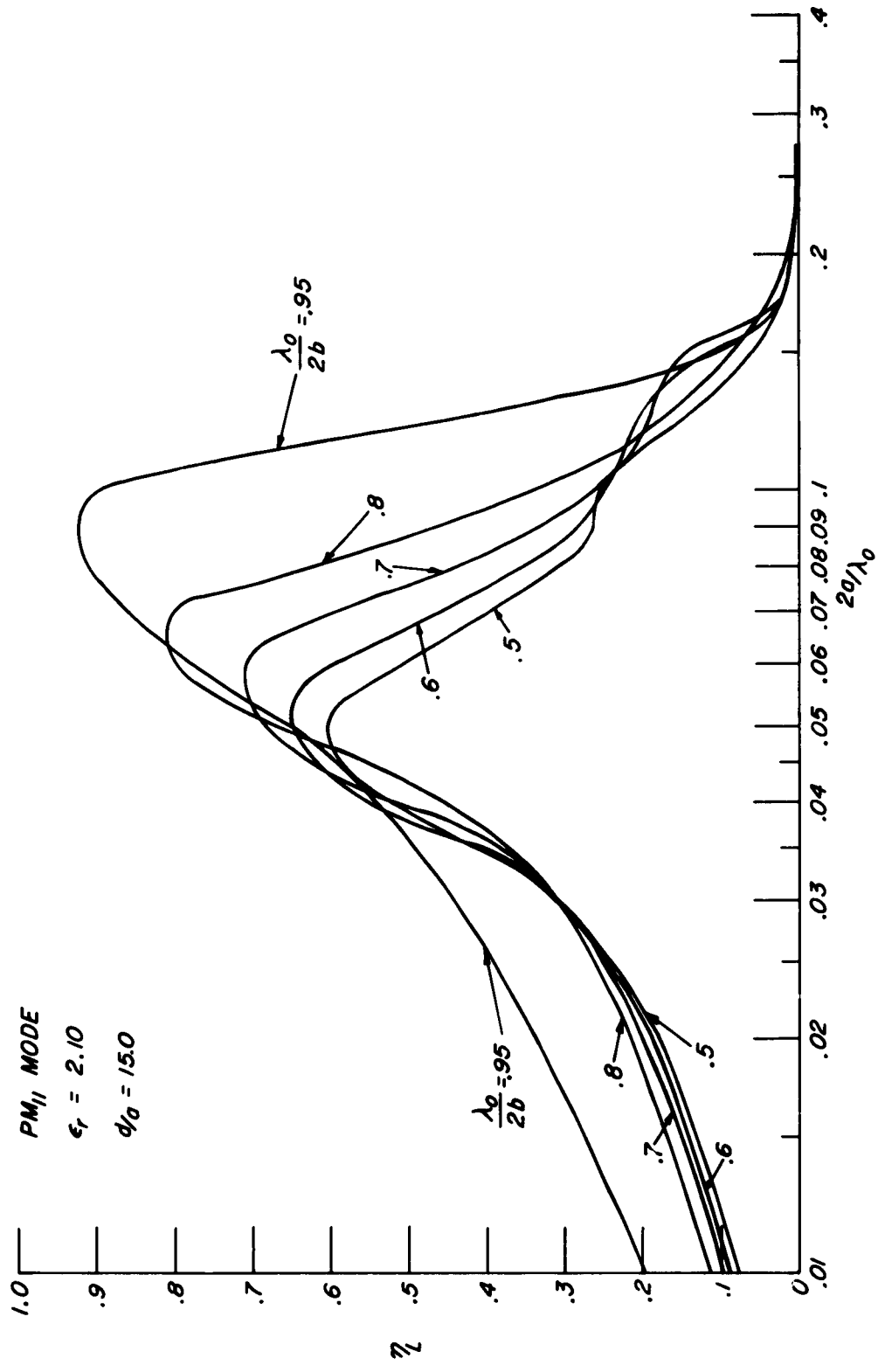


FIG. 29 - LAUNCHING EFFICIENCY ( $\eta_L$ ) VERSUS NORMALIZED DIELECTRIC STRIP THICKNESS ( $2a/\lambda_0$ ),  $d/\lambda_0 = 15.0$



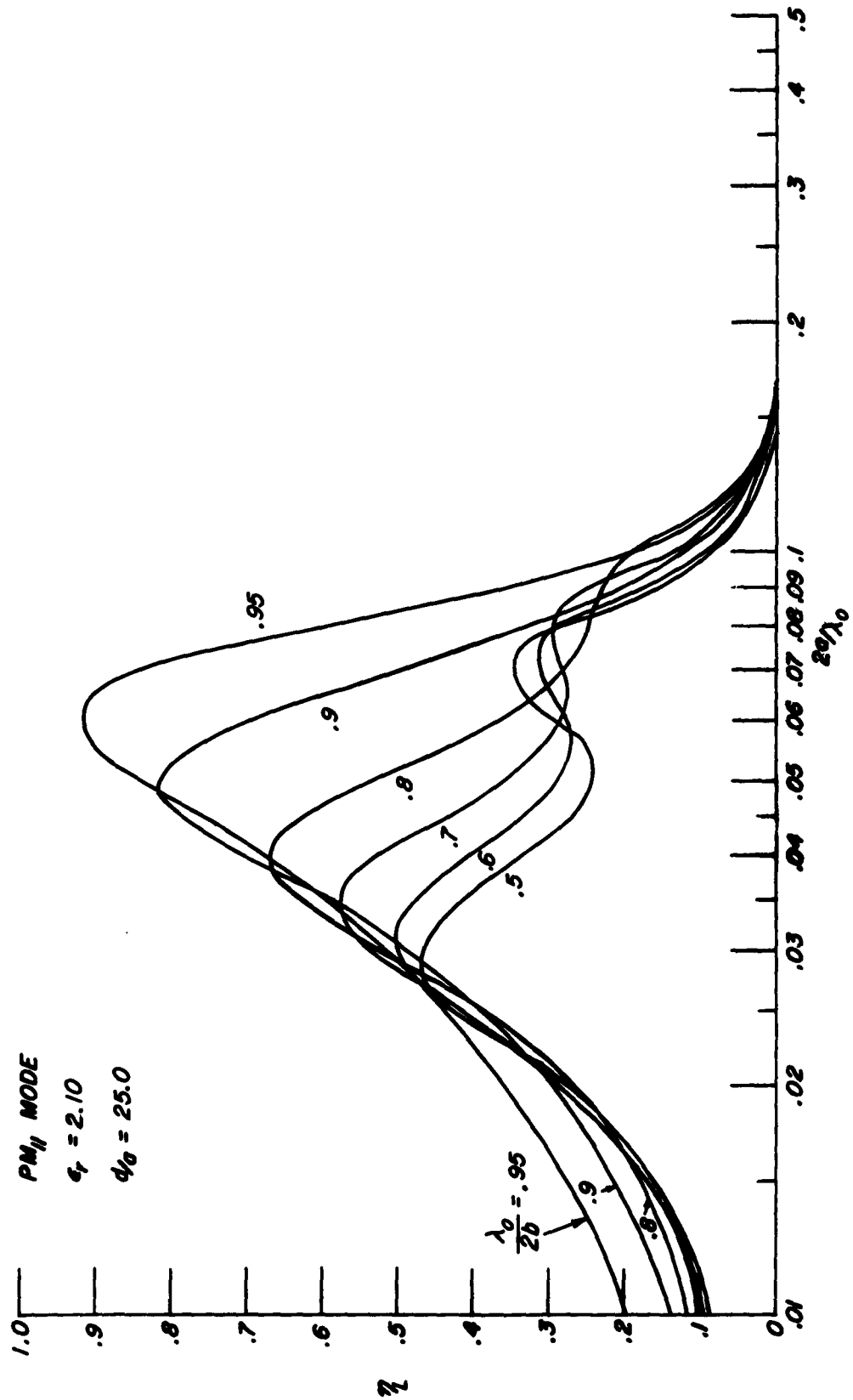


FIG. 31 - LAUNCHING EFFICIENCY ( $\eta$ ) VERSUS NORMALIZED DIELECTRIC STRIP THICKNESS ( $2a/\lambda_0$ ),  $\epsilon_r = 2.10$

### 3.2.7 Launching Efficiency Measurements

In view of the complexity of the surface wave launching analysis, it is desirable to obtain experimental verification of the predicted launching efficiencies. The most accurate means of determining the launching efficiency is to treat the trough waveguide with its input launching slot and output collecting slot as a lossy two port device. Measurements must be made of the input impedance as a function of known output impedances. To perform these measurements in the submillimeter wavelength region, precision impedance measuring equipment would have to be developed. Since the results of the excitation analysis are valid in any frequency range, it was decided to perform the measurements on a frequency scaled trough guide at frequencies in the vicinity of 30 Gc.

Preliminary launching efficiency measurements were made on a six foot long trough waveguide obtained on loan (later purchased) from the Johns Hopkins University. More precise measurements were made on a one meter long trough waveguide constructed on a different contract<sup>9</sup> in order to investigate the feasibility of a trough guide excited slot array antenna. The latter trough guide was specified by the following parameters:  $a = .0761 \text{ cm}$ ,  $b = .711 \text{ cm}$ , and  $\epsilon_r = 2.1$ . The side walls extend about 20 cm above the dielectric slab; a height more than sufficient to assure that the surface wave fields have decayed to a negligible magnitude. Special non-reflecting loads were placed at the top opening of the trough to insure against any radiated power being reflected back into the trough. The launching and collecting slots were each located on movable end plates so that the slot height ( $d$ ) above the bottom conducting plate could be varied. The slot length, trough guide parallel wall spacing, and width of the RG-96/U rectangular waveguide which illuminates the launching slot were all equal ( $b = 0.711 \text{ cm}$ ). The width of the slot was 1.0 mm.

The launching efficiency is determined from insertion loss measurements on the trough guide. The insertion loss in turn is measured via a method described by Tomiyasu.<sup>10</sup> This technique allows the intrinsic insertion loss of a two port device to be measured independently of the impedance mismatch effects which may exist at either port. The technique consists of moving a short circuit at one of the ports to successive positions which produce a maximum VSWR ( $S_{\max}$ ) and a minimum VSWR ( $S_{\min}$ ) at the other port. The total insertion loss (I. L.) between the location of the short circuit and the location of the slotted line probe is given by the following formula.

$$(73) \quad \text{I. L. (db)} = 8.686 \coth^{-1} (S_{\max}/S_{\min})^{1/2}$$

A movable rectangular waveguide short circuit was located after the slot used for collecting the surface wave. The slotted line was located ahead of the launching slot. The movable short circuit was adjusted to positions which successively maximize and minimize the output observed at a directional coupler located so as to sample the wave reflected from the launching slot. At each of these positions the VSWR is measured. Independently determined dissipative losses within both the trough guide and the rectangular waveguide are subtracted from the overall loss as determined from equation (73). The remaining loss equals double the launching loss of one slot.

After the geometric parameters of a trough guide (a and b) are specified: universal curves, like those of Figures 20 through 31 can be used to plot curves  $\eta_L$  versus frequency for various launching slot heights (d). Such a set of curves, for the trough guide used in the launching efficiency measurements (a = .0761 cm, b = .711 cm) is shown in Figure 32. These curves show that by a proper selection of launching

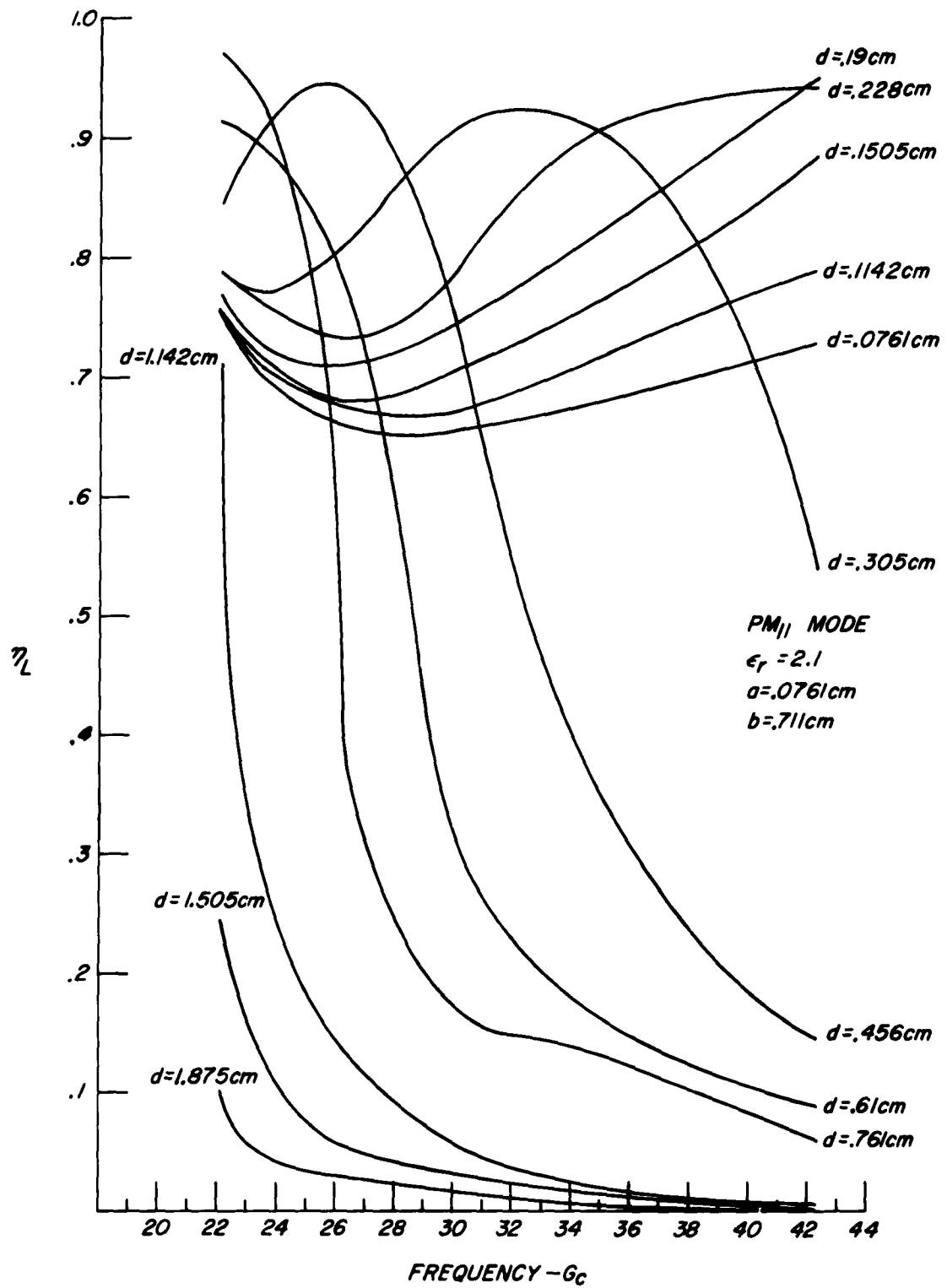


FIG. 32 -LAUNCHING EFFICIENCY VERSUS FREQUENCY AND HEIGHT OF LAUNCHING SLOT.

slot locations, very efficient launching should be achievable over a broad frequency range. Using the above Figure, curves of  $\eta_L$  versus  $d$  for frequencies of 29 Gc and 35 Gc were plotted and are shown in Figures 33 and 34 respectively. On each of these curves, the measured launching efficiency is shown for comparison. The measured points, when corrected for system dissipative losses are in excellent agreement with the theoretically predicted launching losses.

### 3.3 Recommendations and Conclusions Concerning the Trough Guide

Calculations of the expected attenuation of the  $PM_{11}$  mode on the trough guide show that low loss transmission is feasible at the lower end of the submillimeter wavelength region (300-1000 Gc). It is likely that considerable experimentation will be required to fabricate lengths of trough guide with the necessary thin dielectric films. Oversize trough guide, like oversize circular and rectangular waveguides, yield substantially lower attenuations. The oversize trough, however, offers the additional advantage of supporting substantially fewer higher order modes, all of which are polarized in the same direction as the desired dominant mode.

The theoretical analysis of achievable launching efficiency has been verified experimentally. This analysis has shown that except for the case of a very loosely bound wave, extremely efficient launching can be achieved with a simple slot launcher. Since it is the very loosely bound wave condition which results in low losses, it is recommended that further work be done on the problem of launching onto such a low loss structure. A possible approach is that of using more than one launching slot on the end plate. These slots might be energized in phase and with an amplitude distribution that more closely matches the

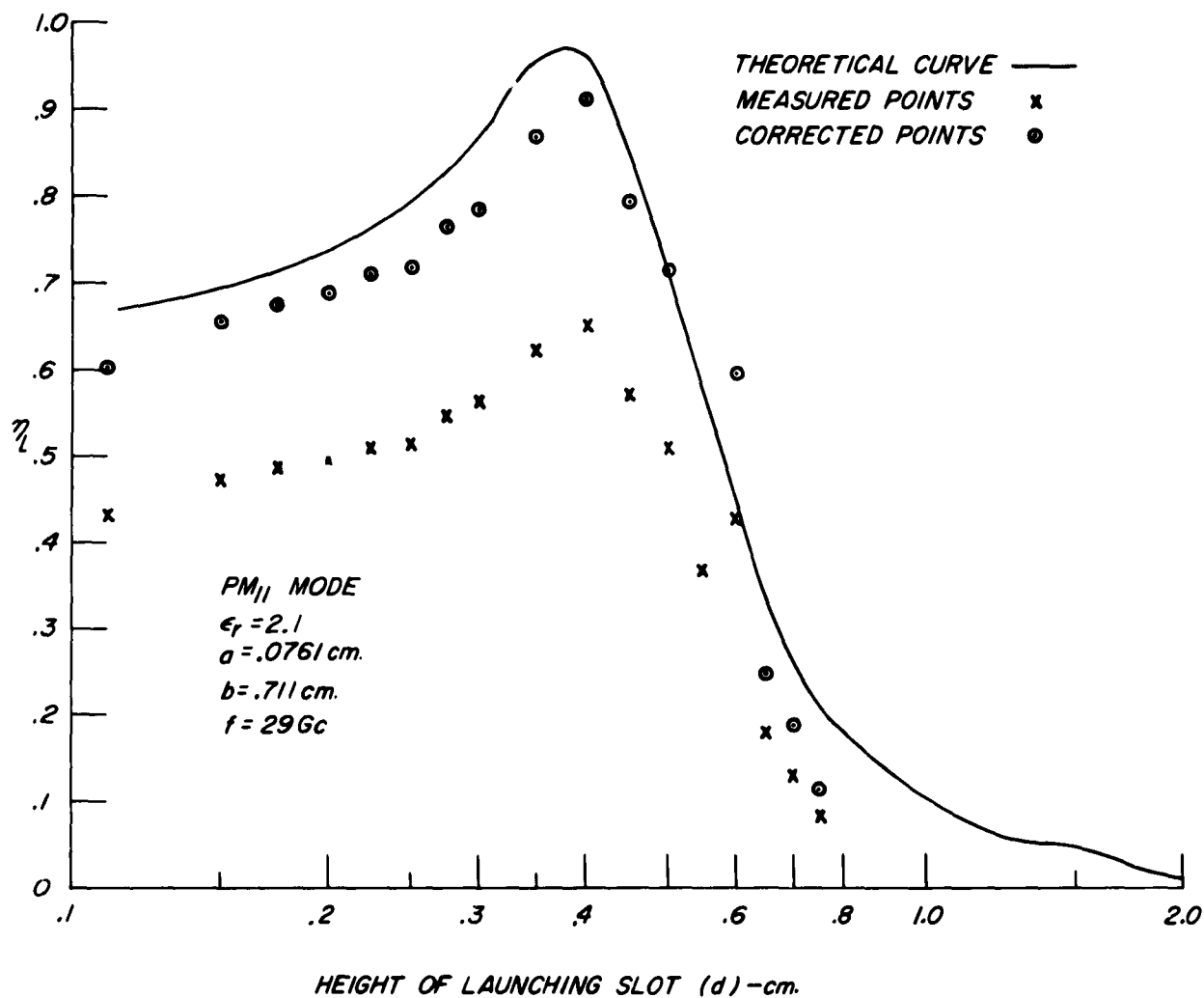


FIG.33 - MEASURED AND CALCULATED LAUNCHING EFFICIENCY VERSUS HEIGHT OF LAUNCHING SLOT.

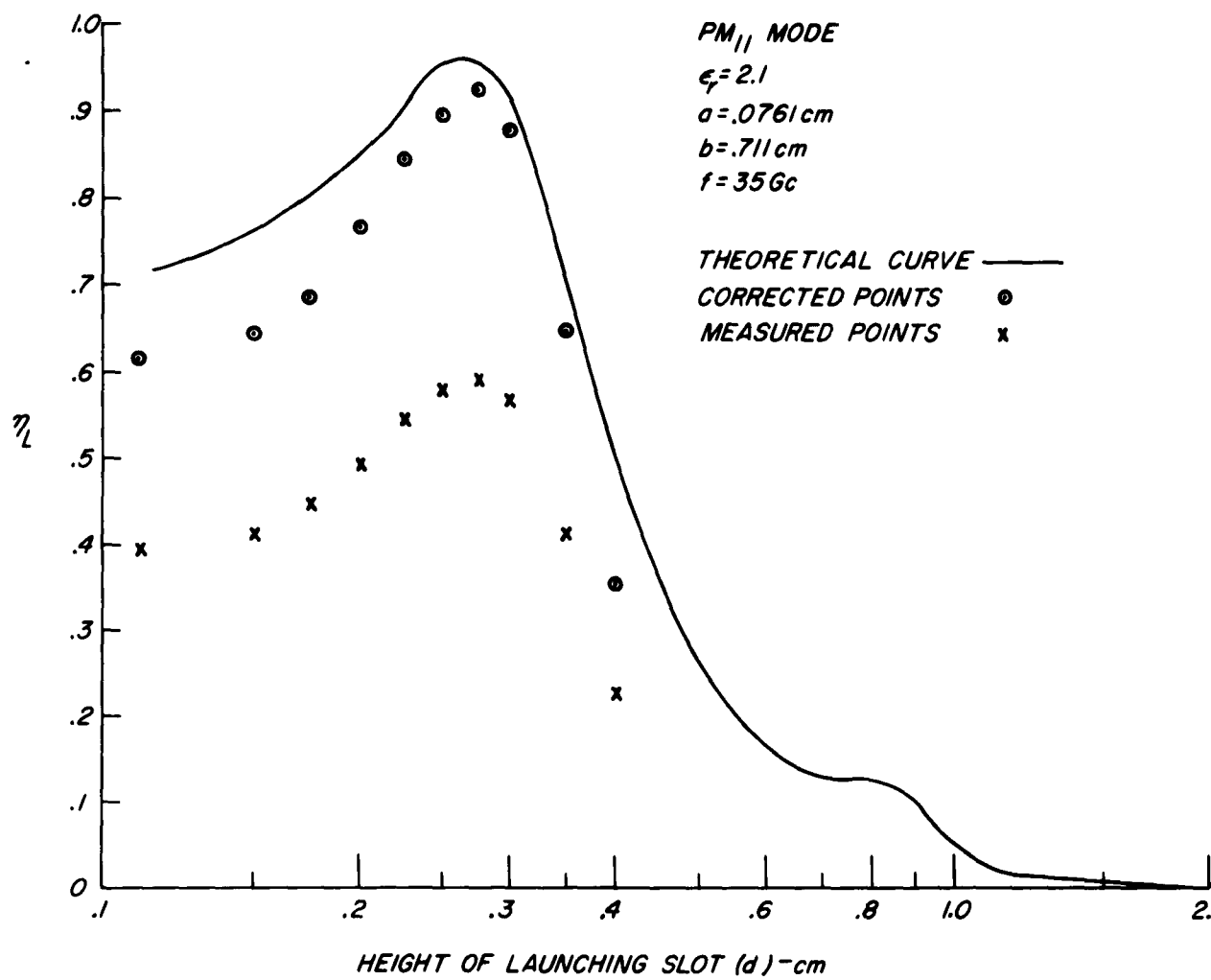


FIG. 34 - MEASURED AND CALCULATED LAUNCHING EFFICIENCY VERSUS HEIGHT OF LAUNCHING SLOT.

x-direction field distribution of a loosely bound wave. A second approach is to use a tapered dielectric slab between the tightly bound region where initial launching is performed and the thin film where low loss transmission is possible. The latter approach is currently being investigated for the aforementioned slot array antenna application.<sup>9</sup> Thus far a 70% launching efficiency has been achieved at 35 Gc with a 17 cm long linear taper between teflon slabs whose thickness is .0761 cm and .00761 cm. Scaling these results to a 350 Gc system, results in a 1.7 cm long taper between teflon slabs whose thickness is 76.1 microns and 7.61 microns. Note that the latter thickness is in the range of values for which low attenuation of the  $PM_{11}$  mode was calculated. See Figures 9 through 14.

One may speculate about the properties of various components built in a trough waveguide. Unless one bears in mind that the trough guide is a surface wave structure, in which any discontinuity will produce radiation in addition to a reflected wave, much of the speculation will be found to be utter nonsense. The high launching efficiencies, which have been demonstrated to be achievable, make it feasible to use conventional components in short sections of rectangular waveguide located between sections of trough guide. Due to very small size of rectangular waveguide, such schemes are only possible at the extreme lower frequency end of the submillimeter wavelength region.

The construction of true trough guide components will be plagued by the same problems as are inherent in constructing components for oversize enclosed waveguide or optical systems, e.g., alteration of the modal distribution and scattering. Even such mundane transmission line components as bends and tees will require an extensive development program.

The design of such components as multi-hole or multi-slot directional couplers can be shown to be related to the surface wave launching problem. Two trough guides joined by a common wall containing properly arranged coupling apertures will undoubtedly provide some directivity. The directivity however, will only be a measure of how the surface wave energy in the secondary guide divides between the forward and backward directions. In general a sizeable fraction of the energy coupled into the secondary guide will also radiate. In the case of two trough guides joined by a common bottom wall, the prior launching efficiency analysis may be of some value. It would be a relatively simple problem to perform the companion excitation analysis for a magnetic line source or slot located within the dielectric slab ( $d/a \leq 1$ ). A special case of such an analysis would be for the condition in which the slot were located in the bottom conducting plate ( $d = 0$ ). The results of such an analysis would tell how much of the energy coupled into the secondary guide would be launched as the desired  $PM_{11}$  mode.

In the air space of the trough guide, the surface wave fields decay exponentially with increasing distance from the dielectric-air interface. Advantage can be taken of this to design variable attenuators and phase shifters. Lowering a dielectric material into the region of higher field intensity would increase the phase shift experienced by a wave traversing that part of the trough guide. A simple mechanism to achieve the phase shift would be an eccentrically mounted dielectric wheel, rotation of which would vary the depth of insertion. Similarly, a lossy material could be used to achieve a variable attenuator. In both of these devices, the critical point to be examined is that of radiation resulting from the introduction of the dielectric or lossy material.

A component which is particularly attractive is a trough guide antenna. Many types of antenna patterns can be synthesized by properly locating and energizing an array of slots cut in one of the side walls of the trough. The same thin dielectric slab condition, necessary for low loss transmission, also provides a field distribution which extends a large distance above the dielectric-air interface. It is thus possible to illuminate a large array. In essence, the feed line and antenna are one integral unit.

## 4. FRESNEL ZONE PLATES

### 4.1 Operating Principle of Zone Plates

The simplest form of the Fresnel zone plate, consisting of a plane array of alternately opaque and transparent concentric circular rings, acts upon a normally incident plane wave, transforming it into a converging wave and concentrating the radiation in a small region about a point on the axis. This point has the characteristics usually associated with the focal point of a lens. The zone plate is thus an image forming device, but the mechanism involved for this simple screen is not refraction at the boundary between different dielectric media, but diffraction at the series of annular apertures and subsequent interference of the diffracted radiation.

Because of the short wavelengths involved, zone plates for the optical spectrum are restricted to rather small diameters and long focal lengths; that is, they are optically "slow" components. Furthermore, because of the difficulty in fabricating annular regions each of which introduces a specified phase change, zone plates for the visible spectrum are generally of the simplest form, rather than the phase-correcting type. However, these limitations are largely removed if radiation in the millimeter wavelength region is used.

In the diagram of Figure 35, the line segment W represents a portion of a plane wave of radiation having a wavelength of  $\lambda_0$  and moving to the right. When the wave front reaches the plane U, which contains the annular openings, we may consider each point on the wave front to be a secondary source. That is, radiation is considered to be emitted in all forward directions from each elemental portion of the wave front (Huygens-Fresnel principle).

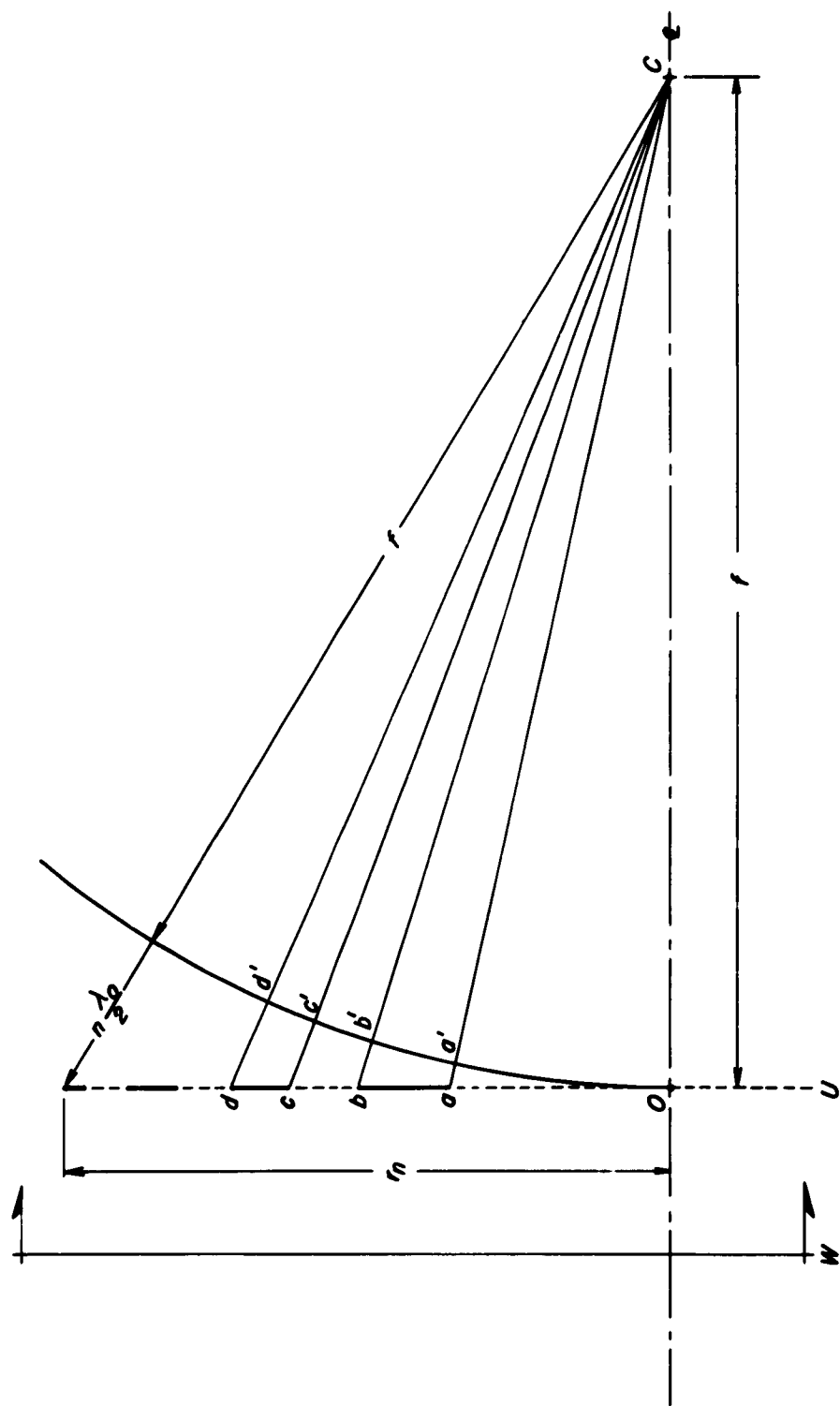


FIG. 35 - RAY GEOMETRY OF ZONE PLATE

Radiation from the axial point O travels a distance  $f$  to the focus at C. The distance to C from all other points in the plane U is greater than  $f$ , and obviously depends on their radial distances from O. The point a on the diagram is at the distance  $f + \frac{\lambda_0}{2}$ ; the point b at a distance  $f + \lambda_0$ ; c is at  $f + \frac{3\lambda_0}{2}$ , and so on. That is, the sizes of the intervals  $aa'$ ,  $bb'$ ,  $cc'$ ,  $dd'$ , etc. are respectively  $\lambda_0/2$ ,  $\lambda_0$ ,  $3\lambda_0/2$ ,  $2\lambda_0$ , etc. The outer radius of the  $n^{\text{th}}$  annular region is given by

$$(1) \quad r_n = \sqrt{nf\lambda_0 + \frac{n^2\lambda_0^2}{4}}.$$

Thus, the path length for radiation arriving at C from any point within a single annular region does not vary by more than  $\lambda_0/2$ , and the phase variation is not more than  $\pi$  radians\*. On the other hand, the phase of the net contribution from one zone is just opposite that of the contribution from an immediately adjacent zone. The destructive interference at C of such pairs of contributions can be prevented by screening out the radiation from alternate zones. In this manner, the remaining open areas of the screen transmit radiation all portions of which arrive at the point C with phases not differing by more than  $\pi$  radians; that is, constructive interference results. The superposition of these portions of the original plane wave results in an intensity at the focal point C which is much greater (if a large number of zones are used) than that which would result from the unobstructed wave.

If alternate zones of the screen are modified so as to reverse the phase of the radiation passing through them, the total amplitude transmitted by the entire array is doubled, and

---

\* Each such annular region is known as a Fresnel half-period zone.

the intensity at the focus is increased four-fold. This phase reversal can be accomplished by preparing a zone plate from a sheet of low loss dielectric material in which adjacent zones are made to differ in thickness by an amount which introduces a phase change of  $\pi$  radians. (It is clearly feasible to construct zones for which the total phase variation of radiation at the focus is  $\pi/2$  radians or any arbitrary fraction of a full period )

If the focal length and diameter of a zone plate are held constant but the phase increment per subzone,  $2\phi$ , is made smaller, the intensity,  $I$ , at the focus of the plate increases toward a limiting value,  $I_0$ , which is the intensity that would be produced by the use of a vanishingly small phase increment. This relation is given by

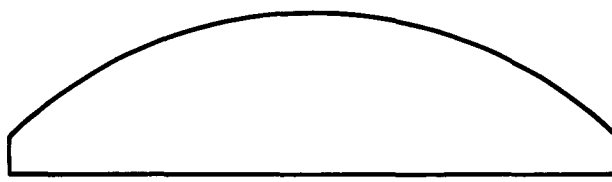
$$(2) \quad \frac{I}{I_0} = \left( \frac{\sin \phi}{\phi} \right)^2,$$

so that for a half-period zone plate,  $2\phi = \pi$ , and  $I = 0.40 I_0$ ; for a quarter-period plate,  $2\phi = \frac{\pi}{2}$ , and  $I = 0.81 I_0$ .

As the subzones are made indefinitely smaller, the face of the zone plate becomes a series of concentric rings each of which has a smoothly curved surface and occupies two Fresnel half-period zones. Thus, in the limit, the zone plate takes on the shape of a Fresnel lens. The schematic cross sectional views shown in Figure 36 suggest the relation between zone plates and conventional dielectric lenses.

#### 4.2 Intensity at the Focal Point

It is most convenient to treat the case of a normally incident plane wave front and obtain an expression for the radiation intensity at the focus of the Fresnel zone plate. It is assumed at the start of the analysis that the zones have been constructed



*SIMPLE LENS*



*FRESNEL LENS*



*QUARTER - PERIOD  
ZONE PLATE*



*PHASE - REVERSING  
ZONE PLATE*



*SIMPLE  
ZONE PLATE*

*FIG. 36 - RELATION BETWEEN LENSES AND ZONE PLATES*

to coincide with the half-period Fresnel zones for a particular wavelength,  $\lambda_0$ . A similar analysis could of course be carried out for phase-correcting plates with other subzone divisions.

#### 4.2.1 General Procedure

In Figure 37 an infinite and uniform plane wave moving to the right is momentarily coincident with the plane U, which is one face of a half-period (or phase-reversing) Fresnel zone plate. The zone plate is constructed so as to have a focal length  $f$  for radiation of wavelength  $\lambda_0$ , and it is fabricated from a dielectric material which is assumed to be lossless and to have a relative magnetic permeability of unity. Thus, if the dielectric constant is  $\epsilon_0$  at the frequency corresponding to the wavelength  $\lambda_0$ , then the refractive index  $\eta_0$ , is given by  $\eta_0 = \sqrt{\epsilon_0}$ .

The amplitude of the electric field vector at the focus of the zone plate may be found by superimposing the contributions from the individual zones, taking into account the relative phase of each such contribution.

#### 4.2.2 Contribution from the $n^{\text{th}}$ Zone

In order to determine the contribution (at the focus) from each zone, it is necessary to integrate over the area of the zone the differential associated with each element of the wavefront. If the contribution of the  $n^{\text{th}}$  zone is denoted by  $E_n$ , then

$$(3) \quad E_n = \int_{n^{\text{th}} \text{ zone}} dE_n$$

Now, using the Fresnel-Kirchhoff diffraction formula,<sup>11</sup> the differential  $dE_n$  may be written as

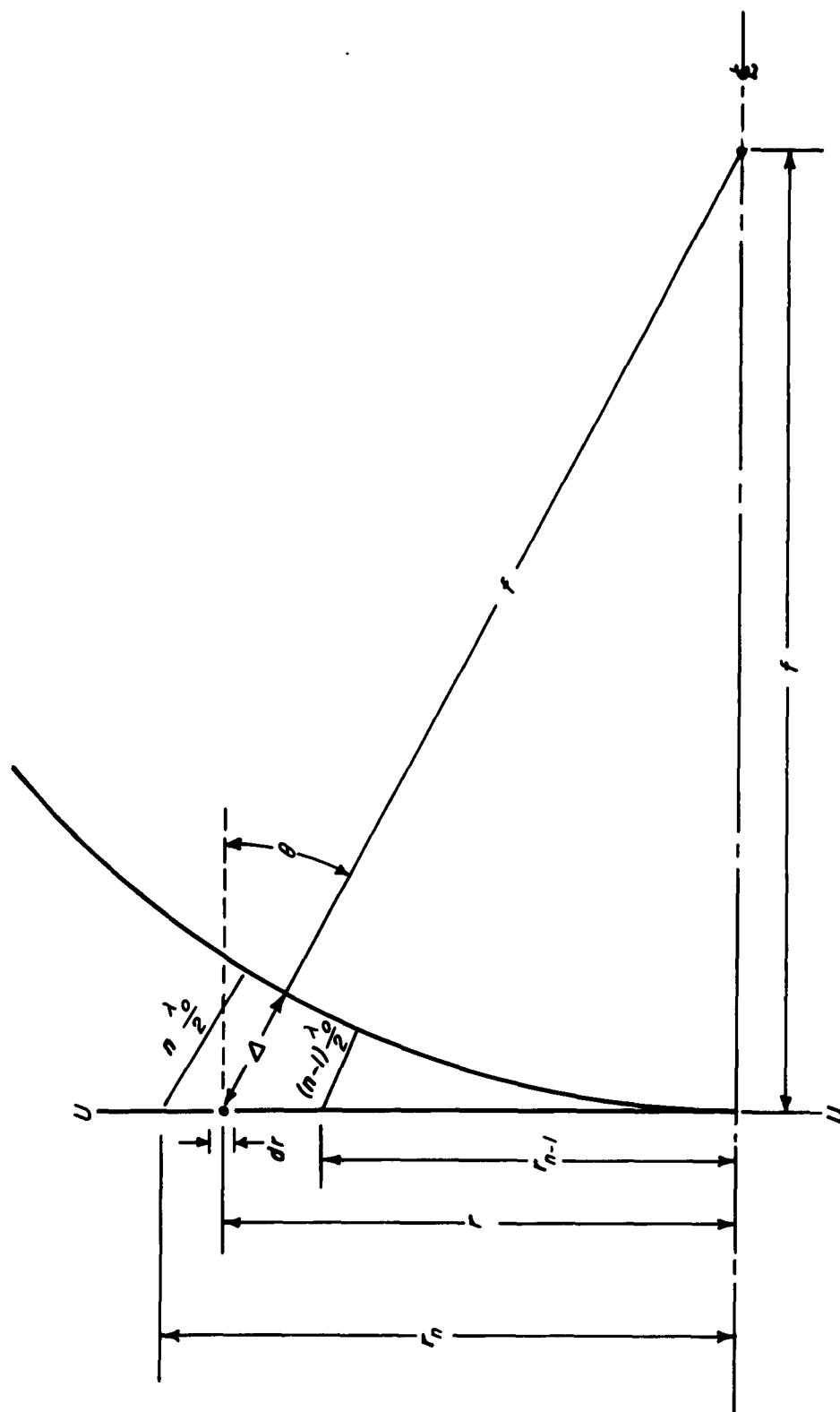


FIG. 37 - GEOMETRY OF THE  $n^{\text{th}}$  ZONE

$$(4) \quad dE_n = \frac{iE_\lambda}{2\lambda\rho} (1 + \cos \theta) e^{i \frac{2\pi}{\lambda} \rho} dS$$

in which

$\lambda$  = the wavelength of the radiation

$E_\lambda$  = the electric field at the plane wave front

$dS$  = the element of area at the plane wave front

$\rho$  = the distance from  $dS$  to the point, say  $C$ , at which the field is to be determined

and  $\theta$  = the angle between the normal to the wave front and the direction to the point  $C$ .

For this derivation, we let

$$(5) \quad E_\lambda = E_o e^{i \frac{2\pi ct}{\lambda}} e^{-i\delta_n}$$

in which  $E_o$  is the magnitude of the electric field vector at the plane  $U$  (see Figure 37),  $2\pi ct/\lambda$  determines the time variation of the field (velocity of light =  $c$ , time =  $t$ ), and  $\delta_n$  is the phase change in the incident radiation brought about by the thickness of the dielectric plate in the  $n^{\text{th}}$  zone.

The material of the zone plate has a refractive index  $\eta = \sqrt{\epsilon}$  for radiation of wavelength  $\lambda$ , and grooves of depth  $d$  are cut into alternate half-period zones. Therefore, the phase retardation for the  $n^{\text{th}}$  zone is given by

$$(6) \quad \delta_n = \frac{2\pi}{\lambda} (\eta - 1) d.$$

This retardation is measured relative to the phase of the radiation which has traversed the full thickness of the dielectric plate. The groove depth,  $d$ , is so chosen as to make the value of  $\delta_n$  for the

design wavelength  $\lambda_o$  exactly equal to  $\pi$  for each even-numbered zone, and equal to zero for the odd-numbered zones. That is,

$$(7) \quad d = \frac{\lambda_o}{2(\eta_o - 1)} g(n) ,$$

in which  $g(n) = 0$  for  $n = 1, 3, 5, 7, \dots$

and  $g(n) = 1$  for  $n = 2, 4, 6, 8, \dots$

Using relations derived from Figure 37, and introducing a simplifying approximation, it can be shown<sup>12</sup> that the contribution, at the focus, of the  $n^{\text{th}}$  zone of the half-period Fresnel zone plate is given by

$$(8) \quad E_n = E_o A(n) e^{\frac{i2\pi}{\lambda} (ct+f)} e^{\frac{i\pi\lambda_o}{\lambda} \left[ n - \frac{\eta-1}{\eta_o-1} g(n) \right]} e^{-\frac{i\pi\lambda_o}{\lambda}} .$$

in which

$$(9) \quad A(n) = \frac{8f/\lambda_o + 2n-1}{8f/\lambda_o + 2(2n-1)} .$$

Equation (8) can be simplified by assuming  $\eta = \eta_o$  and noting that the quantity  $n - g(n)$  satisfies the relations

$$(10) \quad n - g(n) = n, \text{ for } n \text{ odd}$$

$$\text{and} \quad n - g(n) = n-1, \text{ for } n \text{ even}$$

A convenient way of expressing this dependence on the integer  $n$  is to make use of a notation called the greatest integer value, abbreviated as GIV. The GIV of any variable, say  $z$ , is written  $\text{GIV}(z)$  and is defined as the largest integer which is less than  $z$  or exactly equal to  $z$ . Hence, we may write

$$(11) \quad n - g(n) = 2 \text{ GIV} \left( \frac{n-1}{2} \right) + 1 ,$$

and equation (8) becomes

$$(12) \quad E_n = E_o A(n) e^{i \frac{2\pi}{\lambda} (ct+f)} \left\{ e^{i \frac{\pi\lambda}{\lambda} [2 \text{GIV}(\frac{n-1}{2}) + 1]} - e^{-i \frac{\pi\lambda}{\lambda} [2 \text{GIV}(\frac{n-1}{2})]} \right\}.$$

#### 4.2.3 Intensity Ratio for N Half-Period Zones

The separate contribution arriving at the focus of the zone plate from the  $n^{\text{th}}$  half-period zone is given by equation (12). These contributions can now be superposed to determine the amplitude (of the electric field) at the focus which results from the action of a total of N half-period zones. Calling the resultant electric field  $E(N)$ ,

$$(13) \quad E(N) = E_o e^{i \frac{2\pi}{\lambda} (ct+f)} \sum_{n=1}^N A(n) \left\{ e^{i \pi \frac{\lambda}{\lambda} [2 \text{GIV}(\frac{n-1}{2}) + 1]} - e^{-i \pi \frac{\lambda}{\lambda} [2 \text{GIV}(\frac{n-1}{2})]} \right\}.$$

Using Euler's equation and rearranging terms,

$$(14) \quad E(N) = E_o e^{i \frac{2\pi}{\lambda} (ct+f)} \sum_{n=1}^N A(n) \left\{ \cos \frac{\pi\lambda}{\lambda} [2 \text{GIV}(\frac{n-1}{2}) + 1] - \cos \frac{\pi\lambda}{\lambda} [2 \text{GIV}(\frac{n-1}{2})] \right. \\ \left. + i \sin \frac{\pi\lambda}{\lambda} [2 \text{GIV}(\frac{n-1}{2}) + 1] - i \sin \frac{\pi\lambda}{\lambda} [2 \text{GIV}(\frac{n-1}{2})] \right\}.$$

The intensity of the radiation at the focus is given by the square of the modulus of  $E(N)$ . If we denote by  $R(N)$  the ratio of  $|E(N)|^2$ , the focused intensity produced by the Fresnel zone plate, to  $E_o^2$ , the intensity in the absence of the plate, then we may write

$$R(N) = \left[ \sum_{n=1}^N A(n) \left\{ \cos \pi \frac{\omega}{\omega_0} \left[ 2 \text{GIV}\left(\frac{n-1}{2}\right) + 1 \right] - \cos \pi \frac{\omega}{\omega_0} \left[ 2 \text{GIV}\left(\frac{n-1}{2}\right) \right] \right\} \right]^2$$

(15)

$$+ \left[ \sum_{n=1}^N A(n) \left\{ \sin \pi \frac{\omega}{\omega_0} \left[ 2 \text{GIV}\left(\frac{n-1}{2}\right) + 1 \right] - \sin \pi \frac{\omega}{\omega_0} \left[ 2 \text{GIV}\left(\frac{n-1}{2}\right) \right] \right\} \right]^2.$$

In this equation,  $\lambda_0/\lambda$  has been replaced by  $\omega/\omega_0$ , the ratio of the frequency of the incident wave to the design frequency of the zone plate.

The intensity ratio  $R(N)$  is symmetrical about all integer values of  $\omega/\omega_0$  (i.e., the harmonics of the design frequency). At the even harmonics ( $\omega/\omega_0 = 0, 2, 4, 6, \dots$ ),  $R(N) = 0$ . When  $\omega/\omega_0$  takes on odd integer values,  $R(N)$  reaches its maximum value,

$$(16) \quad R(N)_{\max} = 4 \left[ \sum_{n=1}^N A(n) \right]^2 = 4 \left[ \sum_{n=1}^N \frac{8f/\lambda_0 + 2n-1}{8f/\lambda_0 + 2(2n-1)} \right]^2$$

If the quantity  $f/\lambda_0$  is large relative to  $N$ , then  $A(n)$  is nearly equal to unity for each value of  $n$ , and the intensity ratio for  $\omega/\omega_0 = 1, 3, 5, 7, \dots$  reduces to this simple approximation:

$$(17) \quad R(N)_{\max} \approx 4N^2 \text{ for } f/\lambda_0 \gg N.$$

#### 4.2.4 Intensity Ratio for $N$ Quarter-Period Zones

For a quarter-period phase correcting Fresnel zone plate, the intensity ratio can be shown<sup>12</sup> to be

$$\begin{aligned}
(18) \quad R(N') = & \left[ \sum_{n=1}^{N'} A'(n) \left\{ \cos \frac{\pi}{2} \frac{\omega}{\omega_0} \left[ 4 \text{GIV}\left(\frac{n-1}{4}\right) + 1 \right] - \cos \frac{\pi}{2} \frac{\omega}{\omega_0} \left[ 4 \text{GIV}\left(\frac{n-1}{4}\right) \right] \right\} \right]^2 \\
& + \left[ \sum_{n=1}^{N'} A'(n) \left\{ \sin \frac{\pi}{2} \frac{\omega}{\omega_0} \left[ 4 \text{GIV}\left(\frac{n-1}{4}\right) + 1 \right] - \sin \frac{\pi}{2} \frac{\omega}{\omega_0} \left[ 4 \text{GIV}\left(\frac{n-1}{4}\right) \right] \right\} \right]^2,
\end{aligned}$$

in which  $N'$  is the number of quarter-period zones (based on  $\lambda_0$ ) which are included in the zone plate. The coefficients  $A'(n)$  are given by

$$(19) \quad A'(n) = \frac{16f/\lambda_0 + 2n-1}{16f/\lambda_0 + 2(2n-1)}.$$

The function  $R(N')$  has a period of  $4\omega_0$  and is symmetric about all even harmonics of the design frequency. Equation (18) reduces to simpler forms for certain values of  $\omega/\omega_0$ , as follows:

$$(20) \quad \begin{cases} R(N') = 2 \left[ \sum_{n=1}^{N'} A'(n) \right]^2 & \text{for } \omega/\omega_0 = 1, 3, 5, 7, \dots \\ R(N') = 0 & \text{for } \omega/\omega_0 = 0, 4, 8, 12, \dots \\ R(N') = 4 \left[ \sum_{n=1}^{N'} A'(n) \right]^2 & \text{for } \omega/\omega_0 = 2, 6, 10, 14, \dots \end{cases}$$

As the last equation shows, a quarter-period plate designed for the frequency  $\omega_0$  acts as a half-period plate at the second harmonic,  $2\omega_0$ .

In Figure 38, the calculated intensity ratio in decibels is plotted against the normalized frequency,  $\omega/\omega_0$ , for two Fresnel zone plates. One plate has 24 quarter-period zones (solid curve) and a focal length of  $50\lambda_0$ . The second plate has

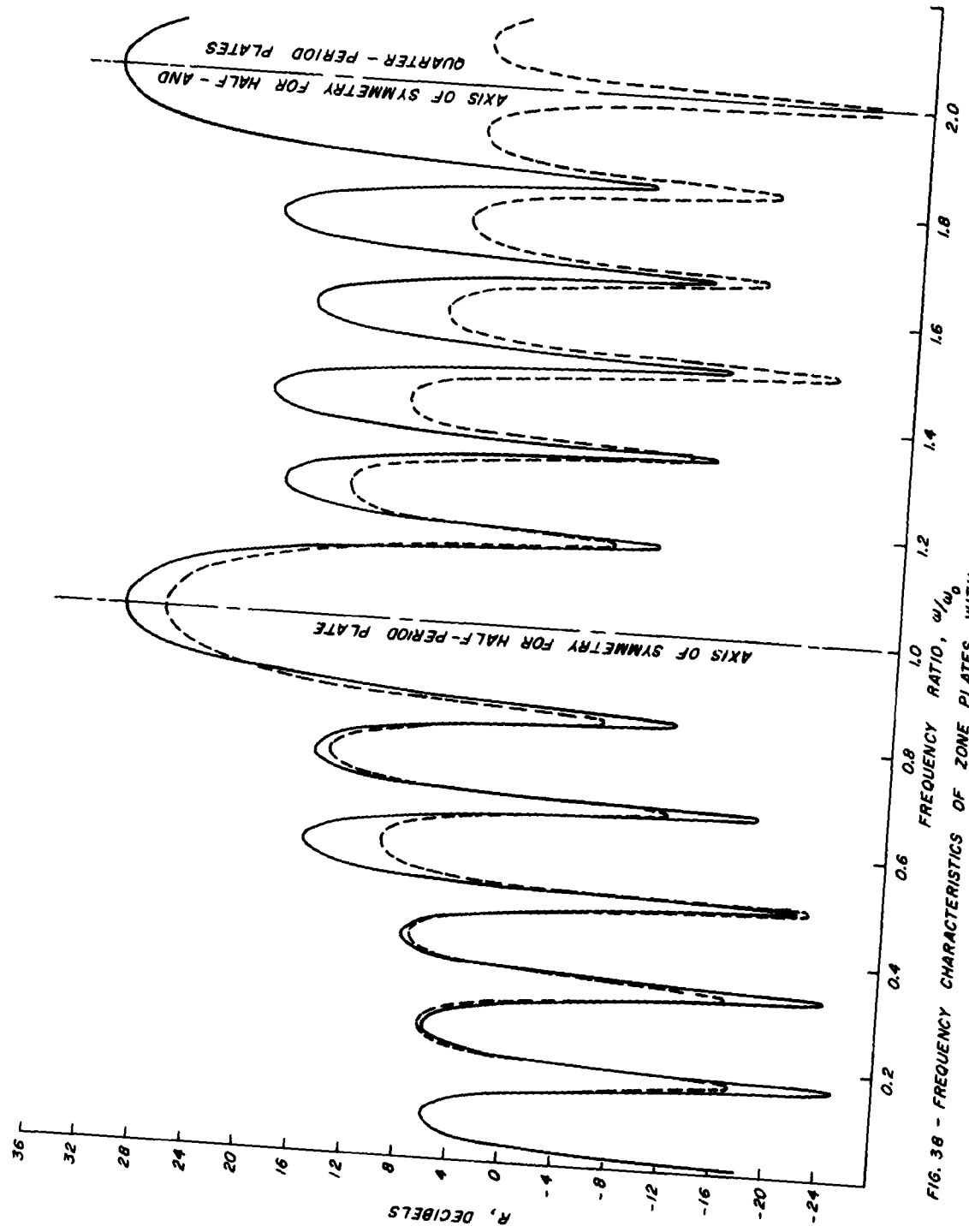


FIG. 38 - FREQUENCY CHARACTERISTICS OF ZONE PLATES WITH  $f = 50 \lambda$ . QUARTER-PERIOD PLATE OF 24 ZONES, HALF-PERIOD PLATE OF 12 ZONES.

the same diameter and focal length, but contains 12 half-period zones (dashed curve).

#### 4.2.5 Intensity Ratio for M Open Zones

As has been pointed out, the simplest form of half-period zone plate contains alternate opaque zones. Such a construction results in an intensity ratio given by

$$(21) \quad R(M) = \left[ \sum_{m=1}^M A(m) \left\{ \cos \pi \frac{\omega}{\omega_0} (2m-1) - \cos \pi \frac{\omega}{\omega_0} (2m-2) \right\} \right]^2 + \left[ \sum_{m=1}^M A(m) \left\{ \sin \pi \frac{\omega}{\omega_0} (2m-1) - \sin \pi \frac{\omega}{\omega_0} (2m-2) \right\} \right]^2 ,$$

in which M is the total number of open half-period zones. If the center zone is a transparent one, then

$$(22) \quad A(m) = \frac{8f/\lambda_0 + 4m-3}{8f/\lambda_0 + 2(4m-3)} ,$$

and if the center zone is opaque, then

$$(23) \quad A(m) = \frac{8f/\lambda_0 + 4m-1}{8f/\lambda_0 + 2(4m-1)} .$$

The function R(M) has symmetry properties like those of R(N) and reaches its maximum value

$$(24) \quad R(M)_{\max} = 4 \left[ \sum_{m=1}^M A(m) \right]^2 \quad \text{for } \omega/\omega_0 = 1, 3, 5, 7, \dots$$

Similar results for plates with opaque zones have been reported by Van Buskirk and Hendrix.<sup>13</sup>

#### 4.3 Fresnel Zone Plates as Frequency Filters

The marked minima in the frequency characteristics shown in Figure 38 suggest the use of Fresnel zone plates as frequency filters in the millimeter wave spectrum. Such devices

should be of special interest at frequencies above 300 Gc, where more conventional filter techniques such as the use of squeeze-section waveguides may be impractical.

It would be of interest to determine theoretically the locations of the relative maxima and minima in the intensity ratio of any zone plate. An exact analysis of this nature has not been carried out, but approximate results have been obtained<sup>14</sup> for certain simpler cases and are presented here.

For a half-period zone plate containing an even number of zones we can write  $N = 2W$ . The integer  $W$  is thus the number of whole period zones in the plate. The minima of  $R(N)$  then occur at the normalized frequencies given by  $\omega/\omega_0 = P/W$ , in which  $P$  is any integer satisfying  $P \neq W, 3W, 5W, \dots$ . For a quarter period zone plate with  $N'$  equal to any multiple of 4, we write  $N' = 4W$  and the minima are at  $\omega/\omega_0 = P'/W$ , in which  $P' \neq W, 3W, 5W, 7W, \dots$  and  $P' \neq 2W, 6W, 10W, 14W, \dots$ .

With regard to the 3 db bandwidth of zone plates, again no theoretical equation for the general case has been derived. However, an empirical relation was obtained from calculated curves for half-period zone plates with  $f = 50\lambda_0$  and  $N = 1, 2, 3, \dots, 21$ . If the frequency interval between the half-power points is denoted by  $\Delta\omega_0$ , then the bandwidth, centered at the design frequency  $\omega_0$ , is given approximately by

$$(25) \quad \Delta\omega_0/\omega_0 \approx 1.8/N.$$

The approximation is better for even values of  $N$  than for odd and improves rapidly as  $N$  increases.

#### 4.4 Zone Plates as Antennas

A phase correcting Fresnel zone plate with a properly designed feed horn at its focal point constitutes an antenna. The functions  $R(N)$  and  $R(N')$  are not identical with the gain,  $G$ ,

(on the central axis) as it is usually defined for an antenna of a given aperture. However, the quantitative relation between R and G is readily obtained.

The usual calculation of G assumes that all the radiated power passes outward through the aperture of the antenna. Thus, for example, if the antenna is composed of a parabolic reflector fed by a horn at its focus, it is assumed that all the power radiated by the horn feed falls on the paraboloid. The quantity G is then corrected if there is any spillover. On the other hand, the calculation of the intensity ratio R for zone plates was carried out in a manner equivalent to the assumption of an isotropic feed, and under this assumption only a certain fraction of the power radiated from the focus falls on the zone plate. This fraction is equal to  $\Omega_z/\Omega_t$ , in which  $\Omega_z$  is the solid angle subtended by the zone plate as viewed from the focal point and  $\Omega_t$  is the total solid angle surrounding the focal point. The latter quantity is identically  $4\pi$  steradians, and  $\Omega_z$  is related to the diameter, D, and the focal length, f, of the zone plate as follows:

$$(26) \quad \Omega_z = 2\pi \left( 1 - \frac{2f}{\sqrt{4f^2 + D^2}} \right) .$$

Consequently, the gain as ordinarily defined is given by

$$(27) \quad G = \frac{4\pi}{\Omega_z} \cdot R = \frac{2 \sqrt{4f^2 + D^2}}{\sqrt{4f^2 + D^2} - 2f} \cdot R ,$$

in which R is the intensity ratio for the zone plate. If we denote by W the number of whole period zones in the plate, i. e.,  $W = N/2$  for a half-period plate,  $W = N'/4$  for a quarter-period plate, and  $W = M$  for a plate with alternate opaque zones, then the equation for gain takes on the simpler form

$$(28) \quad G = \frac{2 (f/\lambda_o + W) R}{W} .$$

It is also of importance to know the characteristics of the radiation pattern of such an antenna, that is, the locations and magnitude of side lobes (and back lobes), and the shape of the main lobe of the antenna in the forward direction. The Kirchhoff scalar diffraction theory, applied to a plane circular aperture of diameter  $D$  illuminated by a plane wave of uniform amplitude, indicates that the first zero in the diffraction pattern lies at the angle  $\theta_0$  away from the central axis, where  $\sin \theta_0 = 1.220\lambda/D$ . (This is the angular half-diameter of the first dark ring or Airy disk). The theory predicts that the radiation intensity reaches one half the value which it has on axis in the direction  $\theta_{1/2} = 0.515\lambda/D$ . These analytical results<sup>11</sup> are confirmed quite well by tests made on a half-period zone plate with a diameter of 20 cm, designed for use at 140 Gc.

The positions and intensities of side lobes in the radiation pattern of a zone plate are not readily calculated a priori. However, it seems reasonable to predict that the pattern of a plate having numerous zones (and therefore numerous discontinuities in its surface) may possess a rather large number of sidelobes, symmetrically disposed about the central axis and probably of small magnitude. If no attempt is made to construct the zone plate for minimum reflection<sup>16</sup> a back lobe may be expected, still much smaller than the main forward lobe, but of greater magnitude than the side lobes. These qualitative predictions are also borne out; the angular radiation patterns of the 20 cm 140 Gc half-period zone plate showed about 45 side lobes, all at least 30 db down from the main lobe.

#### 4.5 Some Comments on Quasi-Optical Components

Quasi-optical and optical techniques can be readily applied to the design of components for use with millimeter waves. By using well-collimated beams of radiation (usually well within

the Fresnel region of the apertures), the components may be designed to operate on very nearly plane wave fronts. Collimation is readily effected by means of simple dielectric lenses (e.g., fused quartz or polystyrene) or phase-correcting Fresnel zone plates.<sup>17</sup>

The introduction of a controlled (and calculable) phase shift in a plane wave may be accomplished by permitting the radiation to pass through a parallel slab of low-loss dielectric material of adjustable thickness. A pair of identical prisms of relatively small apex angle, in sliding contact along the hypotenuse dimension, would provide such adjustability. Since the flux density would remain low, the power capacity of such a phase shifter would probably be quite high.

Directional couplers or beam-splitters can be devised in a number of ways. One simple component would be a thin partially reflecting metallic film. By evaporation in a vacuum, uniform layers of gold or aluminum can be deposited on a dielectric base in thicknesses of a fraction of a micron. If the supporting dielectric is sufficiently thin (e.g., Mylar .001") it will contribute very little to absorption and the radiation reflected from its internal and external face will interfere destructively. Thus, only the reflection from the metallic film needs to be considered. Such a beam-splitter should, like its optical counterpart, be broad-banded.

Another form of coupler would consist of a plane parallel slab of low loss dielectric uncoated with any metallic film. In this case, the thickness of the slab is selected so that for a convenient incidence angle,  $i$ , the relative phase of the wave fronts reflected from the two surfaces is such as to produce the desired amplitude division of the incident wave. The amplitude coefficients (or Fresnel coefficients<sup>18</sup>), involve the

angle  $i$  and the refractive index,  $\eta$ , which for a low loss dielectric with unit permeability is given by  $\eta = \sqrt{\epsilon}$ , in which  $\epsilon$  is the dielectric constant. It is obvious that because of the thickness of the dielectric, the degree of coupling is dependent on the wavelength.

A variable beam splitter (and simultaneously a variable attenuator) can be formed by making use of the evanescent waves external to a dielectric in which "total" internal reflection takes place. The experimental arrangement for observation of the effect is illustrated in Figure 39, for a plane wave incident from the left. The two congruent prisms are fabricated from a low loss dielectric. Equations for the transmitted and the reflected power are given by Fellers<sup>19</sup> and involve the prism angle, the dielectric constant, the wavelength, and the separation of the prism faces. For  $45^\circ$  prisms with  $\epsilon = 2.45$ , a separation of two wavelengths results in an attenuation of about 40 db.

A polarization selective transmitting / reflecting structure for millimeter wavelengths might be constructed from a set of uniformly spaced conducting slats. The spacing is so chosen that each pair of conducting strips acts like a waveguide which is well below cut-off at the desired operating frequency. Hence, a wave polarized parallel to the slats is almost totally reflected; a wave polarized perpendicular to them is almost wholly transmitted. The construction might be carried out by stacking alternate sheets of dielectric and metal foil, bonding the layers, and slicing through the stack to prepare the desired set of rather narrow strips. Such an ensemble could be made rather broad-banded by using a spacing between conducting planes equal to less than a half wavelength at the highest frequency required, but the small spacings necessary would result in rather high

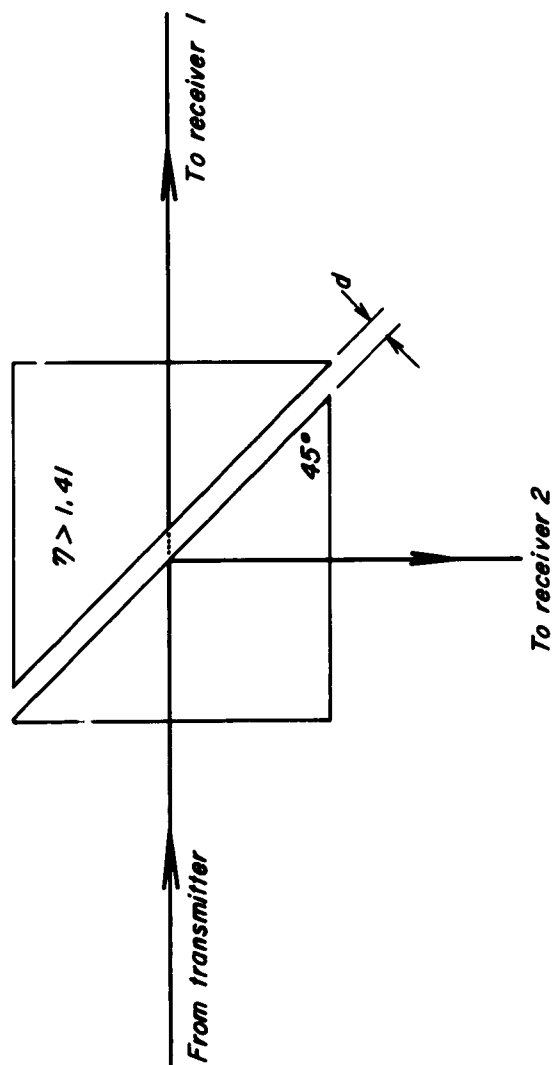


FIG. 39 - DOUBLE PRISM COUPLER (AND ATTENUATOR)

transmission loss.

A set of conducting strips with spacing greater than a half wavelength and with appropriate width will act on an incident plane polarized wave converting it to a circularly polarized wave. A duplexer which makes use of polarization selective reflectors and circular polarizers for 35 Gc has been described elsewhere.<sup>20</sup>

## 5. OVERSIZED ENCLOSED WAVEGUIDE

The high attenuation which characterizes dominant-mode, hollow metal waveguide can be substantially reduced if the cross-sectional dimensions of the guide are increased sufficiently. (It is assumed that a high-conductivity metal, such as silver or copper, is used in either case.) The wall losses are lower for such a guide, but as a result of the increase in size, the number of possible modes propagating with low loss may be large. The application of the familiar low loss  $TE_{01}$  mode in circular guide is an example of a case where an overmoded structure is frequently used; however, in this case, the size is ordinarily chosen so that only a moderate number (perhaps a few tens) of additional modes could propagate, and high purity of the  $TE_{01}$  mode is preserved by means of careful launching methods, accurate control of waveguide dimensions, and extensive use of mode suppressors. Mention has already been made of the extreme difficulty of maintaining the dimensional tolerances necessary in such a system as one goes to submillimeter wavelengths. We therefore desire to have a simpler method for utilizing the overmoded enclosed waveguide, but before describing such a method, the work recently reported by others is summarized below because of its relevance to the problem.

Lewin has considered six types of propagation at millimeter wavelengths,<sup>21</sup> depending on whether single, multiple, or an infinite number of modes exist in the perpendicular directions defining the cross section of the structure. Taking into account problems of diffraction and aperture reflection for the various types of waveguides, he suggests that single mode oversize waveguide is the most promising, and in particular, the rectangular ( $TE_{10}$  - mode) or circular ( $TE_{11}$  - mode) guide. A number of methods for feeding the guide are considered and

suggestions are made for some components. He points out that the circular or square guide gives the added advantage of symmetry, permitting the use of perpendicular polarization for a second channel, which may be of value for components like hybrid-tees.

Transmission by the  $TE_{10}$  mode in a large rectangular guide has been considered by Garnham,<sup>22</sup> who suggests that the square cross section makes the system unnecessarily bulky, and that the dimension parallel to the electric field may be reduced without affecting the symmetry of the mode. Such a reduction does affect the attenuation, however. If a compromise 2:1 ratio of dimensions is chosen as in most conventional waveguide, the attenuation for silver (conductivity  $6.2 \times 10^7$  mhos per meter) may be calculated from

$$\alpha = \frac{5.60 \times 10^{-9} \sqrt{f}}{b} \quad \text{db/meter}$$

where  $b$  is the dimension parallel to the electric field and the effects of surface roughness are neglected. A comparison of the loss for large guides to the loss for conventional silver waveguide is made, showing the first to be much smaller than the second. For example, the calculated attenuation at 300 Gc for RG-139/U waveguide is 12 db per meter, whereas for silver guide 0.90 inch by 0.40 inch I.D. the calculated loss is 0.3 db per meter (this number also neglects mode conversion losses).

Karbowiak has performed an approximate analysis of electromagnetic wave propagation in metallic waveguides for wavelengths in the submillimetric region.<sup>23</sup> The analysis is carried out for two types of waveguides; a planar, parallel-plate waveguide in which one plate is a perfect conductor and the other imperfect, and the circular metallic waveguide of imperfect conductivity. Karbowiak concludes that in the case of  $TE_0$  modes

for both waveguides the attenuation is proportional to (frequency)<sup>-3/2</sup>. In addition, he concludes that transverse magnetic (TM) waves, which are proportional to (frequency)<sup>-1/2</sup> at moderately high frequencies, become proportional to (frequency)<sup>-5/2</sup> at sufficiently high frequencies. In a later article by Martin,<sup>24</sup> however, it is demonstrated that this is not the case for certain TM modes. An exact analysis is performed showing that the attenuation continues to increase with frequency for the TEM and TM<sub>01</sub> waves in the more practical case of a planar waveguide consisting of two parallel plates of imperfect conductivity. It is also indicated that the attenuation of the TM<sub>01</sub> wave in the circular guide increases with frequency. Other TM modes are considered in both cases and do have decreasing attenuations at high enough frequencies. Karbowiak, in reply to Martin,<sup>25</sup> implies that the inconsistency in results for the planar case is due to the different mathematical models, and he does not comment on the inconsistent results for the TM<sub>01</sub> wave in the circular guide. It appears however, that Karbowiak made an approximation to the cut-off coefficient which may not be valid at extremely high frequencies. Mr. Martin has agreed in private communication that the effect of the imperfectly conducting walls on the cut-off coefficient is more complicated at these frequencies than Karbowiak has allowed and that the difference in results is due to more than just the different models.

It should be mentioned that some of the usual approximations for the attenuation of the various modes in closed metal waveguides are not valid as the frequency increases indefinitely. An example is Ramo and Whinnery's<sup>26</sup> treatment of TM or TE waves propagating between two parallel conducting plates. The cutoff coefficient is written as  $K^2 = \gamma^2 + k^2$  where  $\gamma$  is the propagation constant ( $\gamma = \alpha + j\beta$ ), and  $k^2 = \omega^2 \mu \epsilon (1 - \frac{j\sigma}{\omega \epsilon})$ . If the plates

are perfectly conducting, it is found from applying the boundary condition  $E_z = 0$  that  $K = n\pi/a$ , where  $a$  is the separation of the plates. The attenuation constant is calculated for the case of finite conductivity by a perturbation technique, assuming  $K$  is still very close to  $n\pi/a$ . This approximation will be valid as long as  $E_z$  is very close to zero at the boundary. At high enough frequencies, however, the approximation  $E_z \approx 0$  at the metal boundary is not valid and the cutoff coefficient  $K$  can no longer be approximated by  $n\pi/a$ . This was taken into consideration by Karbowiak and Martin. Martin assumes the metal remains perfectly smooth, but retains exact equations, solving them by a numerical method of successive approximations.

The question is: at what frequency does the usual approximation (cf., Ramo and Whinnery<sup>26</sup>) break down? The answer depends on the size and material (i. e., the conductivity) of the waveguide. The larger the guide the sooner the "turning point" in the attenuation is reached. (At frequencies above the vicinity of the turning point the attenuation begins to decrease with increasing frequency, whereas at frequencies below the turning point the attenuation increases as frequency increases.) Lowering the conductivity has a similar effect. Martin's results were used and some sample calculations were carried out for the  $TM_{02}$  mode propagating in a parallel plate waveguide. The walls were assumed to be perfectly smooth and the conductivity was taken to be that of copper. For a plate separation of 1 cm, the attenuation began to decrease after reaching a frequency of about 7700 Gc (around 3 db/m); for 10 cm separation, the turning point was on the order of 1700 Gc (0.16 db/m); and for 100 cm, the frequency was about 360 Gc (0.007 db/m). To get some idea of the effect of surface roughness, a decrease in conductivity by a pessimistic factor of 9 was assumed. The effect was to lower

the turning point, but increase the attenuation. For instance, for a separation of 1 cm, the turning point was about 3700 Gc (7 db/m) and for 10 cm, it was about 800 Gc (0.3 db/m). For practical size waveguides, however, these values of the turning point frequencies are higher than the frequency range under consideration, and the usual approximation for the TM or TE modes (Ramo and Whinnery) should be valid.

For the TEM modes (electric field component normal to plates) propagating between parallel conducting plates, Ramo and Whinnery develop an approximation which is valid if  $\sigma_1/\omega\epsilon_1 \ll 1$  and  $\omega\epsilon_2/\sigma_2 \ll 1$ , where  $\sigma_1$  and  $\epsilon_1$  are the conductivity and permittivity of the dielectric and  $\sigma_2$  and  $\epsilon_2$  are the same quantities for the metal. If the plates are good conductors, e.g., silver or copper, and if surface roughness is neglected, the restriction  $\omega\epsilon_2/\sigma_2 \ll 1$  is satisfied up through the visible wavelength region. Since surface roughness in effect decreases the conductivity of the metal ( $\sigma_2$ ), the approximation will not really be valid to such short wavelengths, but certainly should be valid down to wavelengths near 0.1 millimeter.

Wave propagation through a hollow steel pipe at optical wavelengths has recently been considered by Eaglesfield.<sup>27</sup> He concludes that low-loss transmission may be possible in this type of guide, the inner surface of which has a mirror finish.\*

Because the ratio of diameter to wavelength is very large in the optical case, many modes will propagate and individual treatment of modes is not considered. Instead, waves are classified as transverse electric (TE) or transverse magnetic (TM) according to their polarization. In the case studied by Eaglesfield, the TM-mode attenuation is much greater than that for TE modes,

---

\* According to Eaglesfield a suitable pipe has a bore of 1 in. diameter to a tolerance of  $\pm 3$  mil with a silver surface.

and both decrease with frequency.

In summary, the foregoing studies have generally proposed the use of the dominant mode in an oversize waveguide in order to reduce attenuation. In the frequency range up to at least 1000 Gc attenuation still increases with frequency for guides of reasonable size (moderate transverse dimensions on the order of a few inches). This proposed method appears to have the simplicity desired, but this could be partly illusory because questions relating to problems with higher order modes have been left begging. The assumption has simply been made that the particular dominant mode (say the  $TE_{10}$  mode in oversize rectangular guide) would be launched carefully and efficiently and that "quasi-optical" components would be used which would introduce a minimum amount of conversion of energy to higher-order modes.

Ordinarily, when many modes may propagate, there are at least two important disadvantages. Since the various modes do not all propagate with the same velocity, the information content of a signal may be distorted as the wave travels down the guide. It may also be difficult to build components which can recover, transfer, or otherwise act on all the modes efficiently. If, however, the waveguide is considerably oversize, so that a very large number of modes (perhaps several thousand) may propagate, and if the energy transfer down the guide is shared among many mode configurations, then the two problems cited above are not so important. In such a highly over-moded guide many of the modes travel at a velocity near that of a wave in free space, so distortion can be small unless very short pulse lengths or long path lengths are to be used. In other words, phase distortion of the signal can be small even if many modes propagate, just as long as the energy is carried in those modes

that are far from cut-off and hence have group velocities that are nearly equal. Components may be constructed using quasi-optical techniques, such as gratings, prisms, semi-reflecting coatings, thin dielectric sheet beam-splitters, and the double prism (evanescent wave) attenuator.

For a specified amount of phase distortion we can make an estimate of the magnitudes of the system parameters. In order to travel a given distance  $d$  with a phase error not greater than, say, one-tenth of the period of the modulation signal ( $0.1 \tau_m$ ), the energy must be concentrated within some group of modes whose cutoffs lie within a certain range of frequencies. The difference between the reciprocals of the group velocities of the two modes with the highest and the lowest cutoff frequencies must not exceed  $0.1 \tau_m / d$ , or

$$(1) \quad \left( \frac{1}{v_{gh}} - \frac{1}{v_{gd}} \right) = \frac{0.1 \tau_m}{d}, \quad v_g = c \sqrt{1 - \left( \frac{f_c}{f} \right)^2}$$

where

$v_{gh}$  = group velocity of mode having highest allowable cutoff frequency

$v_{gd}$  = group velocity of dominant mode

$c = 3 \times 10^8$  meters per second

$f_c$  = cutoff frequency of specified mode

$f$  = operating frequency

The oversize guide would presumably be excited from a conventional dominant-mode waveguide, hence in the oversize guide there would tend to be preferential excitation of the low-order modes (i. e., a Fourier-type analysis of the propagating wave in the oversize guide would contain mainly low-order terms). Measurements to be described in a later section were made on such an oversize waveguide system at frequencies near 300 Gc;

in this case the oversize guide was excited by means of a horn and lens combination fed from RG-139/U rectangular guide (TE<sub>10</sub> mode).

Rearranging Equation (1) above gives the following expression for the cutoff frequency ( $f_{cn}$ ) of the highest order mode having no more than the permitted phase error in the given distance (d):

$$(2) \quad f_{cn} = f \left[ 1 - \frac{1}{\left[ \frac{c\tau_m}{10d} + \frac{1}{\sqrt{1 - \left(\frac{f_{cd}}{f}\right)^2}} \right]^2} \right]^{1/2}$$

where  $f_{cd}$  is the cutoff frequency of the dominant mode. Values calculated from this equation are given in the accompanying table. The waveguide size chosen corresponds to conventional S-band rectangular guide, and operating frequencies of 300 and 600 Gc were assumed. At 300 Gc, for example, this guide will support more than 16,000 modes, and for modulation frequencies up to a megacycle the calculations show that propagation over distances as large as 100 meters can occur with low phase distortion even if the signal is propagated in thousands of modes. Obviously, by carefully exciting only the lowest few tens of modes, low distortion signals could be propagated over distances of several tens of kilometers.

The conclusion reached above can also be obtained by means of a somewhat different analysis. Suppose we assume that the input signal to the oversize waveguide excites a "direct ray" which travels down the axis and an indirect ray which enters at an angle  $\theta$  with the guide axis (see Figure 40). Suppose further that the travel time for these two rays is to differ by only  $0.1 \tau_m$  seconds after traveling a given axial distance "d" down

TABLE IV

Calculated Values for Multimode Rectangular Waveguide (1.340 x 2.840 inches; cutoff frequency for TE<sub>10</sub> mode =  $f_{cd} = 2.08$  Gc.)

Operating frequency (f)	Modulating frequency (f <sub>m</sub> )	Length of waveguide in meters (d)	Cutoff frequency for specified phase error (f <sub>cn</sub> )		No. of TE modes below f <sub>cn</sub>	No. of TM modes below f <sub>cn</sub>	Total No. of modes below f <sub>cn</sub>	No. of possible modes at operating frequency	Angle $\theta$ $\cos \theta = \left(\frac{0.1c}{f d} + 1\right)^{-1}$
			$\frac{f_{cn}}{f}$	$\frac{f_{cn}}{f_{cd}}$					
300 Gc	1 Mc	190,000	.019	2.75	5	2	7	16338	$\sim 1^\circ$
		12,000	.071	10.23	49	34	83		$\sim 4^\circ$
		100	.60	86.6	3007	2878	5885		$\sim 40^\circ$
		12	.96	138	7582	7375	14957		$\sim 73.5^\circ$
		100	.023	3.4	6	2	8		$\sim 1.5^\circ$
		12	.071	10.23	49	34	83		$\sim 4^\circ$
600 Gc	1 Mc	190,000	.019	5.51	16	8	24	65352	$\sim 1^\circ$
		12,000	.071	20.5	180	150	330		$\sim 4^\circ$
		100	.60	173	11933	11673	23606		$\sim 40^\circ$
		12	.96	277	30330	29915	60245		$\sim 73.5^\circ$
		100	.023	6.76	23	13	26		$\sim 1.5^\circ$
		12	.071	20.5	180	150	330		$\sim 4^\circ$

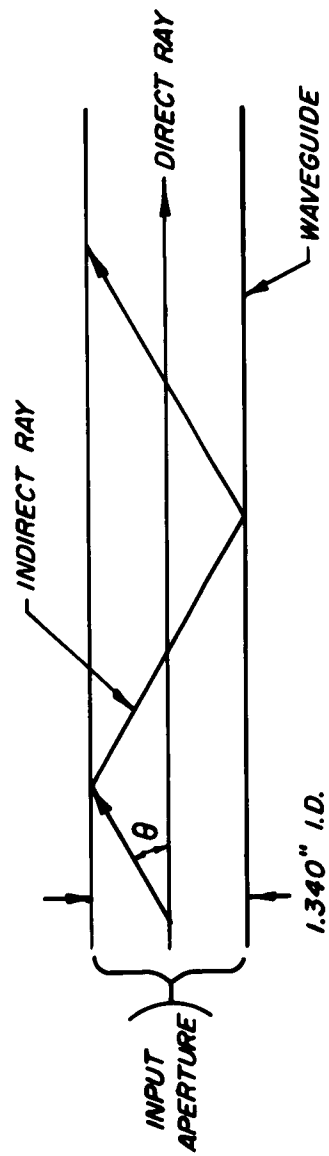


FIG. 40 - GEOMETRY FOR DIRECT AND IN DIRECT RAYS IN OVERSIZE WAVEGUIDE  
(SIDE VIEW OF S-BAND WAVEGUIDE)

the guide. Such a calculation for  $\theta$  gives the values shown in the final column of the accompanying table.

The values of  $\theta$  given in the table may be compared with the calculated far-field beamwidths for an aperture 1.340 inches in width. (In this dimension of the waveguide the illumination of the entrance aperture is nearly uniform, whereas in the orthogonal transverse direction the illumination is tapered. Nonetheless, the E-plane dimension is so much less than the 2.840 inch-dimension in the H-plane that the calculated far-field beamwidth is less in the E-plane than in the H-plane.) Taking the E-plane far-field beamwidth as a pessimistic (larger) value, we find that the far-field 3 db half-beamwidth for such an aperture is less than a degree. The first pattern null occurs at an angle of about two degrees, and the second null occurs at about four degrees. As a rough rule of thumb for a narrow beam antenna, about half of the radiated power is concentrated in the half-power beamwidth. Hence, in the accompanying table, whenever  $\theta$  exceeds about one degree, the majority of the power radiated from an aperture 1.340 inches by 2.840 inches is included in the range of angles for which phase distortion is low out to a distance "d". In most cases  $\theta$  is much greater than a degree, indicating the (optimistic) result that most of the power goes into the desired lower-order modes which give low phase distortion.

## 6. MEASUREMENT SYSTEM

A measurement system for use in the submillimeter region was proposed and assembled in the contract period. A block diagram of the system is shown in Figure 41. Since existing sources which have fundamental power at 300 Gc or above were prohibitive in cost, the design specified harmonic generation from a lower fundamental transmitter power.

One of the drawbacks generally associated with harmonically generated signals, namely the identification and separation of the harmonics, was eliminated with this design by utilizing harmonic mixing. As indicated in the diagram, when the primary power source and the local oscillator are maintained at nearly the same fundamental frequency, but separated by a fixed difference frequency  $f_d$ , then the frequencies generated in the mixer will result from the sum and difference terms of  $nf$ , and  $nf + nf_d$ . The resulting IF frequency can then be chosen as  $nf_d$  and will be unique for each harmonic.

The details of the components of the system will be discussed individually below.

### 6.1 Harmonic Generation

#### 6.1.1 Magnetron Driven Ferrite Harmonic Generator

In the early stages of the development of the laboratory system it had been decided to use a 70 Gc magnetron as a source of fundamental power for the transmitter, and use ferrite harmonic generation. There had been many reports in the literature concerning successful ferrite harmonic generation, <sup>(28-34)</sup> some of these reporting conversion losses to third and higher harmonics (from X band) which were quite comparable with those achieved with point contact devices. There were also reports of successful frequency doubling from 35 Gc<sup>35</sup> and from 70 Gc<sup>36</sup>.

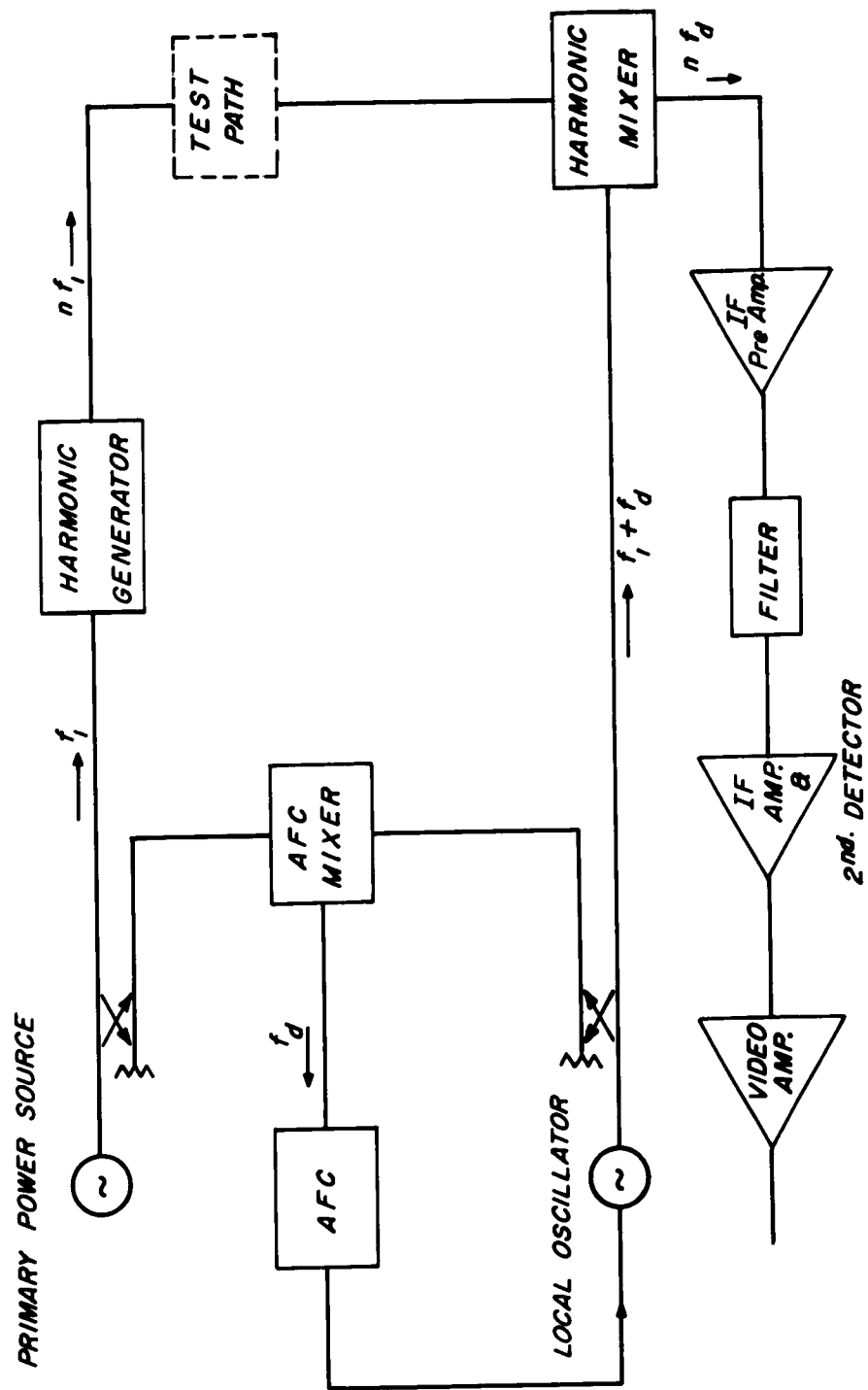


FIG. 41 - SUB-MILLIMETER WAVE PROPAGATION MEASUREMENT SYSTEM.

It was not within the scope or intent of this program to make a basic investigation of ferrite harmonic generation. We were, however, hopeful that by incorporating the techniques used in the previous work, and adding a sensitive high frequency receiver, we would be able to detect the higher harmonics. If the conversion efficiencies were found to be comparable to crystal devices, there would be considerable improvement in signal level since the power at the fundamental would be orders of magnitude greater than that which is possible to apply to a point contact device.

To this end, a Bomac BL-221 magnetron was purchased, which had a peak power output of 14 kw at 70 Gc. The modulator used to drive the magnetron was supposed to furnish a 0.25  $\mu$ sec pulse. This rather simple sounding requirement became quite problematical, and was in fact never satisfactorily resolved. The manufacturer's specifications on the RF bandwidth of the magnetron listed  $2.5 \text{ Mc}/\tau$  (where  $\tau$  = pulse width) as the maximum value. One essential to this measurement system as outlined was the AFC system holding the local oscillator at a fixed difference frequency from the transmitter. The circuitry involved here must be sufficiently wide to accommodate the pulse bandwidth. Hence, the 0.25  $\mu$ sec pulse, and a 10 Mc bandwidth were chosen.

The first pulse forming network used gave a pulse on the order of 90 nanoseconds. Efforts were made here to broaden the pulse, but when the width was increased, the top was not flat. This variation in peak anode current caused a pushing of the magnetron frequency of several megacycles, and the net effect on the RF bandwidth was as bad or perhaps worse than the narrow pulse.

A new pulse forming network was purchased with a 0.33  $\mu$ sec specification (maximum pulse allowable with this magnetron). This one gave a 0.4  $\mu$ sec pulse which was double peaked. The problem was then given to Bomac. Their claim was that the pulse transformer and pulse forming network had to be a matched assembly with the magnetron, in order to achieve a flat pulse of this length. They agreed to furnish these two units to provide a good flat pulse of 0.25  $\mu$ sec with their magnetron. This was never precisely achieved even though three attempts had been made and a considerable amount of time had been consumed.

During this period, experiments with harmonic generation were carried out using the original short pulse and crystal video detection. The magnetron itself produced sufficient third harmonic power for video detection, and it is clear that any ferrite generated harmonics must be of larger magnitude for the system to have any merit

The magnet used was a Varian 4" magnet with pole caps tapered to one inch and a capability across a 1/4" air gap of fields of 28,000 gauss.

The ferrite samples used were made into a variety of shapes from several materials. The criteria were narrow line width and high  $M_s$  materials such as Trans Tech TT-2-111 and Ferroxcube 5E1. Also some anisotropic single crystals were used on which very little information was available. (These latter were furnished by I. Bady of the Army Signal Research and Development Laboratories at Fort Monmouth, where similar materials had been successfully used at X band.)

The procedure followed was to set up the system with no ferrite in the guide and note the level of detectable third harmonic power coming directly from the magnetron. This third harmonic was estimated to be on the order of 60 to 70 db

below the fundamental i.e., one to two milliwatts peak power on the crystal. The ferrite sample would then be inserted. Generally this would reduce the amount of third harmonic power out. The magnetic biasing field would then be applied and slowly varied from zero to its maximum while observing the output. There was generally a value which would bring the output back to the level observed with no ferrite in the guide, but no higher values were seen. Both polarizations of the detector were used in these runs. The sample would then be moved a quarter guide wavelength and the process would be repeated.

In his analysis Jepsen<sup>37</sup> indicates that the optimum D.C. biasing field for third harmonic generation would be to bias the ferrite to resonance at the second harmonic. This would require a much larger field than we had available, however, and first harmonic resonance had to be used. Furthermore, his analysis did not consider shape factors and other variables which may well be even more significant.

Failing to see the third harmonic, a similar procedure was carried out for second harmonic. Here some flexibility was lacking as the available transitions did not permit viewing the cross polarized case. Here again, however, the results were negative.

Up to this point, the ferrite pieces had been in the shape of rectangular parallelepipeds or half-disks, and were held in position in the waveguide in teflon holders. Some of the first samples had been made full waveguide height hoping for a very snug fit inside the guide. Gold electrodes had been baked on the surfaces which contacted the guide walls. However, arcing occurred at the ferrite since the surface roughness of the guide precluded a sufficiently close fit. The pieces which did not extend full guide dimension in height but were held in

teflon did not cause breakdown in the waveguide.

At this time a sample holder was made up which would permit more flexibility in positioning of the ferrite in the waveguide. This was achieved by mounting the ferrite piece on a post which entered the narrow wall of the waveguide and which permitted independent adjustment of insertion distance and rotation of the post. The unit was designed so that waveguide pressurization could be maintained and such that different posts could be used with various ferrite samples attached. This system did suffer the disadvantage that the position could not be varied with respect to the short or effective short of the transition section, and the ferrite may not have been in the position of maximum r.f. magnetic field. Once again, results were negative.

In private communication with H. J. Shaw, it was then learned that experiments at X band were showing that unless the ferrite was located in a doubly resonant structure i.e., resonant both for the fundamental frequency and the desired harmonic, then harmonic generation was not predictable. This was apparently the cause of some lack of repeatability of experiments which had been carried out at lower frequencies also. It was his opinion that either by design or accident a resonance condition must exist at the ferrite sample.

For a while the fabrication of such a doubly resonant structure was contemplated. This would have involved some very critical and expensive machining problems, plus considerable experimentation to determine the effects of loading of the cavity by various shapes and types of ferrites. All considered, it was taking on more and more the aspects of a basic investigation in the applied physics field, which was precisely what we did not want to undertake. Our hope had been that ferrite

harmonic generation had advanced to the point where it was almost an engineering tool. Our attempts to repeat experiments carried out elsewhere showed that it was not. Furthermore, there was not assurance of success if further experimentation were followed, although it seemed much more likely.

It is felt that the resonance condition, or rather absence of it, was the most likely cause of the lack of success here. The earlier experiments at 70 Gc<sup>36</sup> had already shown an apparent shape and volume dependence with some samples yielding outputs which ranged down to zero as a dimension was changed. Without apology we had selected sample types, shapes and dimensions which had been used with success. Similarly, we pointedly avoided those already shown to have low or no detectable output. If the actual criterion was not this simple, however, and if the variation of electrical properties among samples of ostensibly the same material, and the variation of frequency between magnetrons, and the variation between positions of shorting and tuning elements in the waveguide, are all intimately related to the sample size and shape, then the basis used for selection does not signify.

In addition to these discouraging possibilities, there was the issue of the magnetron pulse itself. Here there was the apparently diminishing probability that the magnetron could be operated with the AFC circuitry as it had been built. This could no doubt be remedied by increasing the difference frequency and bandwidth of the AFC, but this in turn would have required changing the frequency of the receiver. This latter was financially impractical.

In the light of these considerations, it was decided to revise the harmonic generation component of the measurement system and proceed with a point contact

semiconductor device, with a klystron source.

#### 6.1.2 Klystron Driven Crystal Harmonic Generator

The cross guide configuration of the harmonic generator or mixer is shown in Figure 42. It is identical in structure to the harmonic mixer used as the receiver. The design is given in Figure 43. The input waveguide is RG-98/U; the crystal is silicon, 0.010" D and 0.004" thick; the whisker is 0.0015" tungsten; the output waveguide is RG-139/U. Using an input of 70 Gc, third and higher harmonics will be transmitted.

There are no techniques currently known for absolute measurement of low power levels above 200 Gc. This precludes any positive statement of conversion loss in a harmonic generator of this type. The approximate values, however, were arrived at by inference from other measurements which could be undertaken.

Since two of these mixers were available, the following method was used. With the small waveguide port terminated, the mixer was calibrated as a detector at 70 Gc. Then, assuming the law of the crystal would remain the same, and terminating the larger waveguide port, the mixer was used as a detector for the output of the harmonic generator. The figures thus achieved were used as representing power at the harmonic, and the conversion loss determined. The assumption made here is not exact. It is, however, the best choice available, since the precise deterioration of crystal efficiency with frequency is not known. It has been quite well established at lower frequencies that it is a deterioration, and the resulting figure should be conservative. This is to say that the direction of the error is known, but the magnitude is not.

The data taken in one particular junction made in the harmonic generator are shown in Figure 44. One



Figure 42 - Crossguide Crystal  
Harmonic Generator  
and Mixer



would expect from earlier work<sup>38</sup> that the conversion loss to the third harmonic would be approximately a function of the square of the input power, whereas the exponent here seems to be closer to  $2\frac{1}{2}$ . It would seem the prediction made was conservative since the "measured" values are conservative. The limitation was that the power available from the klystron was + 12 dbm at the crystal when this data was taken.

This type of measurement could not be made for the higher harmonics without the inclusion of a high pass filter in the waveguide. This could introduce even more uncertainty into the measurement, and it was considered impractical to build these filters solely for this purpose.

The alternative method for arriving at conversion loss, used for the higher harmonics, involved even more assumptions. Later discussion will show that the overall performance of the system will reduce the unknown quantities effectively to a sum of the harmonic generation conversion loss plus the harmonic mixing conversion loss (expressed in db). Neither can be absolutely measured. Any attempt to divide this sum into its separate parts would necessarily be quite arbitrary and essentially meaningless.

When using the completed system, it was found that the whisker-crystal junction which produced optimum power at the 4th harmonic was not necessarily optimum or even usable at 5th and 6th. In looking for the best overall dynamic range for the system, it would be necessary to find a crystal contact both in the harmonic generator and mixer which were the best available for the particular harmonic desired. Here, as in ferrite harmonic generation, one must contend with the "art" which accompanies the science, though not to the same degree. Each time a contact is broken in the harmonic generator, and

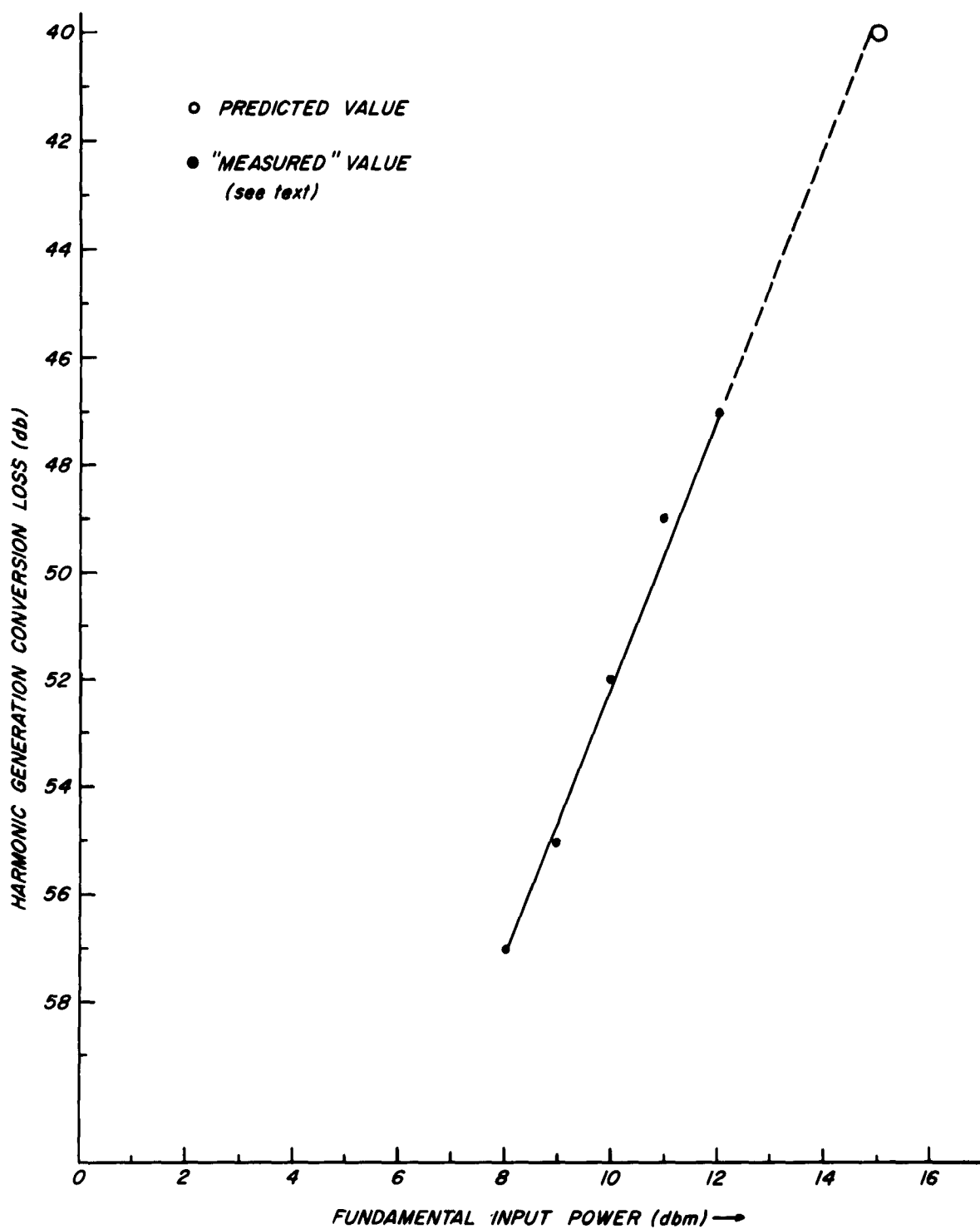


FIG. 44 - HARMONIC GENERATION CONVERSION LOSS TO THIRD HARMONIC

the whisker repointed and the crystal cleaned and a new contact made with probably a different pressure and at a different crystal location, it becomes impossible to separate the variables and ascribe improvement or degradation to any one with precision. A good point in the whisker is desirable, but if the whisker is to be repointed, all other variables change, and the net observable effect could be detrimental.

For most of the measurements made, contacts were made which simultaneously provided usable power at harmonics 4, 5, and 6 such that only the shorting plungers in the small guide had to be readjusted if a frequency change was made.

## 6.2 Harmonic Mixing

The use of harmonic mixing offered many advantages for the system. Primary among these were the capability of identifying a specified harmonic, and an increased sensitivity over crystal video detection. The mixer used had the same physical configuration as the harmonic generator shown in Figures 42 and 43.

Proper harmonic mixing requires relatively large amounts of power applied to the crystal when compared to conventional mixing. This in turn results in a higher crystal noise ratio, which arises principally from local oscillator noise. The frequency distribution of this noise is such that it is greatest at the frequency of the coherent local oscillator signal and decreases with increasing separation from this coherent output. It has also been reported<sup>(39, 40)</sup> that harmonic generation causes the ratio of coherent power to noise power to be less at the desired harmonic than at the fundamental input. These local oscillator noise sidebands beat with the signal harmonic and produce a substantial noise input to the IF amplifier. One method of reduction of this noise is operation at a higher frequency<sup>41</sup>. Within the

limits prescribed by other considerations (see section 6.4), this was done

When the system was assembled, the mixer IF impedance was measured with local oscillator drive applied, and found to be very nearly 250 ohms over the IF range. Since the amplifier input impedance was 50 ohms, this resulted in a loss of signal of only 2.6 db. Tuning stubs were tried for better matching, however, the 100 - 200 Mc range is not ideal for this technique. In most cases, the stubs were not used.

Some experimentation with output as a function of crystal bias current was also performed. Here the best output was achieved by using the self bias resulting from the L O. drive. This was generally about 3 ma with the local oscillator power at about +12 dbm. External bias applied in the forward direction effected little or no change, and in the reverse direction degraded the mixer performance.

The original estimates of conversion loss in the mixer were necessarily based on inference from performance at lower frequencies, and the generally accepted equivalent circuit of this point contact type of mixer. The minimum achievable conversion loss at low frequencies is determined by the action of the local oscillator on the barrier resistance of the point contact diode. This minimum conversion loss ( $L_b$ ) can be determined from the static current-voltage characteristics of the diode. The actual conversion loss at higher frequencies ( $L_c$ ) is larger than this minimum value due to the deteriorating effect of the barrier capacity ( $C_b$ ) and the crystal spreading resistance ( $R_s$ ). The frequency dependence of the actual conversion loss can be approximated by the equation

$$(1) \quad L_c = L_b (1 + 4 \pi f C_b R_s)$$

A similar increase in conversion loss occurs for the harmonic mixing case where  $f \approx nf_{LO}$ . For frequencies above 300 Gc, the first term of the previous equation becomes negligible and  $L_c \approx 4\pi n f_{LO} C_b R_s L_b$  where  $L_b$  is a corresponding value of minimum conversion loss for the harmonic mixing case. It is seen then that these quantities will increase with increasing harmonic number, but the incremental increase between adjacent harmonics becomes progressively less.

As mentioned earlier, it is not possible in the actual system to separate this conversion loss from the harmonic generation conversion loss by measurement. Agreement between the sum of the predicted losses and the measured sum is quite reasonable and is given in section 6.5.

### 6.3 AFC System

The AFC system used was patterned after that originally proposed by Pound<sup>42</sup> with modifications suggested by Johnson<sup>43</sup>. The block diagram is shown in Figure 45. The modulated klystron driving the harmonic generator is free running. The local oscillator for the harmonic mixer was operated c.w., and was locked in frequency to the primary source. This is done by sampling both signals and mixing in a crystal. As can be seen in the photograph of the system (Figure 48) the two signals were brought to the crystal through a hybrid tee. The transmitter signal enters port 1, the H arm; the local oscillator signal enters port 4, the E arm; the mixer crystal is on port 3, and an attenuator and shorting plunger on port 2. This was done to provide maximum isolation between the transmitter signal and the receiver crystal. With the attenuator and short, one can match any impedance in the opposite arm. When these were properly adjusted for the transmitter frequency, the signal coming in the H arm was down more than 40 db when detected out the E arm.

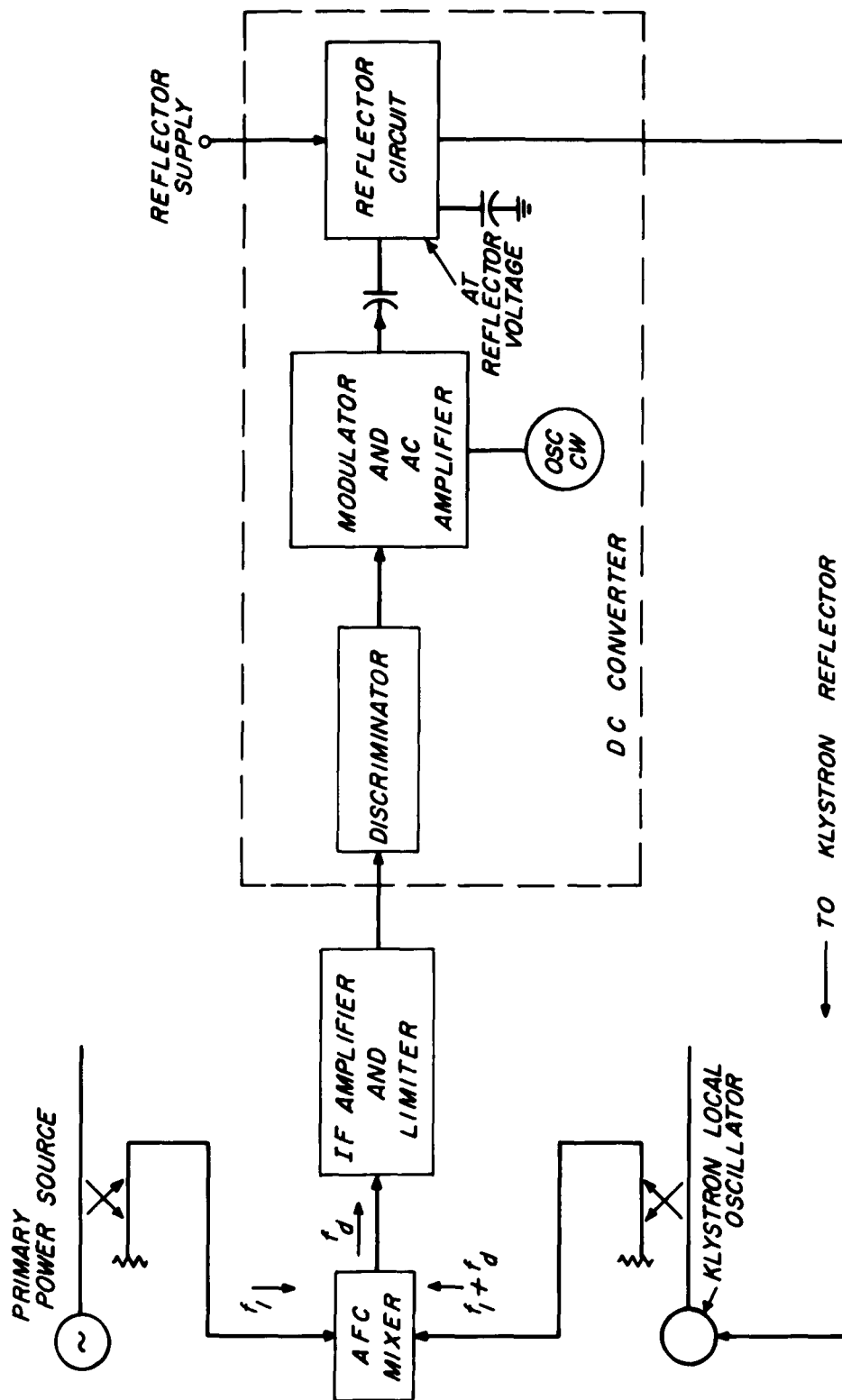


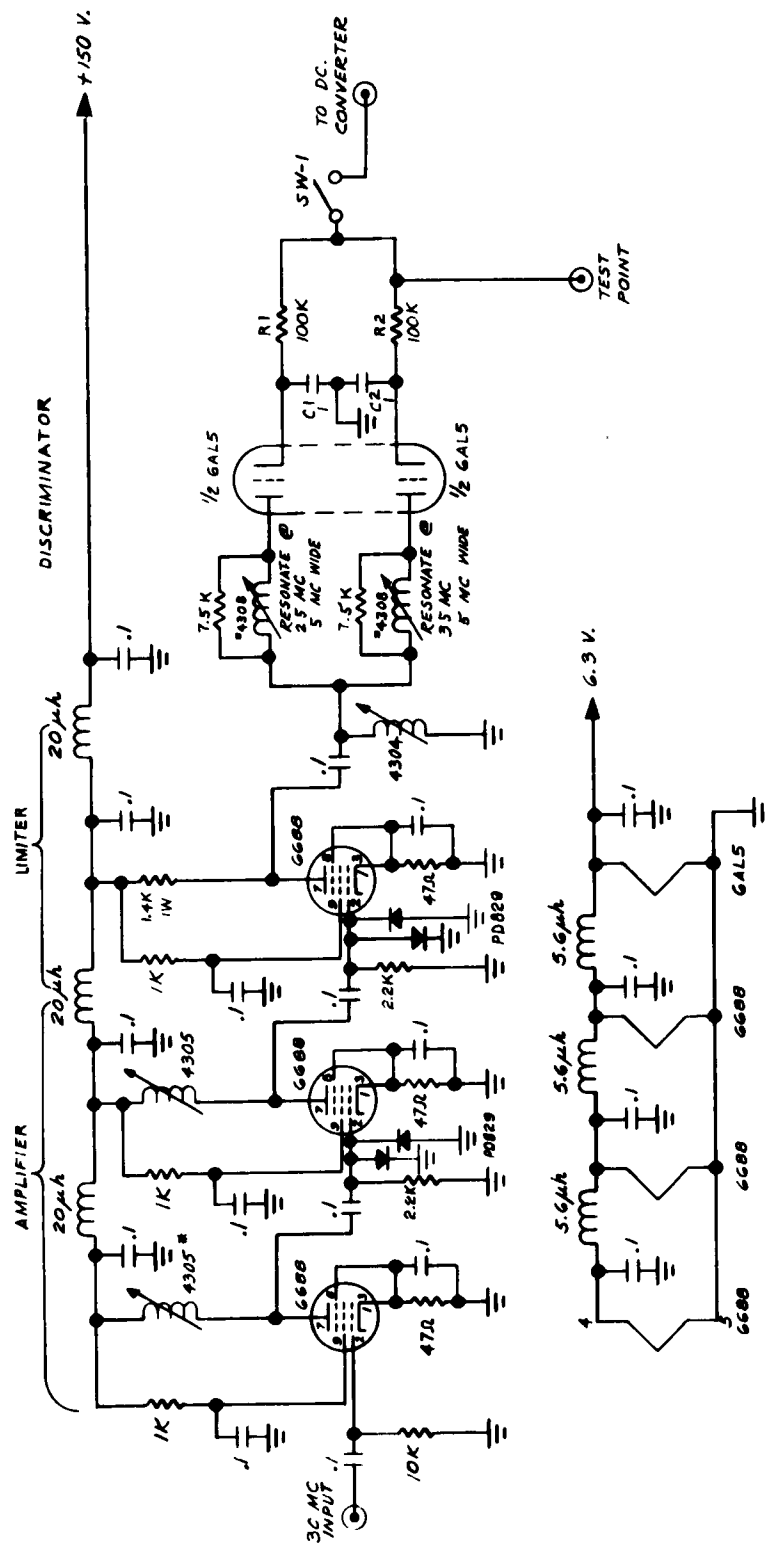
FIG. 45 - BLOCK DIAGRAM OF AFC SYSTEM

This attenuation plus the coupling and directivity of the coupler furnished adequate isolation for the receiver crystal. Earlier, a simple tee had been used, and it was found the isolation of the coupler alone was insufficient to prevent the detection of spurious signals at the mixer.

With both signals applied to the AFC mixer, the IF difference frequency,  $f_d$ , was amplified and applied to a discriminator. A drift in either source, resulting in a difference frequency other than  $f_d$ , would result in an error signal from the discriminator. This error voltage is then converted to an ac signal by using it to modulate a 5 Mc cw signal. This modulated signal is ac coupled to the reflector circuit where it is then demodulated by a peak detector and then filtered to extract the error signal once more. This is then applied to the reflector of the local oscillator klystron in the proper polarity to restore the difference frequency to  $f_d$ .

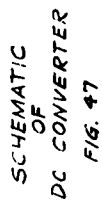
The circuit diagrams and operating characteristics given in an earlier report<sup>14</sup> were presented when efforts were being made to lock the local oscillator to the magnetron pulse. In changing over to the two klystron system, several circuit component modifications were made. Figures 46 and 47 show the final schematics incorporating these changes. Diodes FO 829 were added to improve the limiter characteristics. Also, the discriminator time constant was adjusted to provide a greater attenuation to the 1 kc signal modulation. The reflector driven circuit and the reflector filter were also modified to increase the output swing and to attenuate the 5 Mc chopper signal.

The final measured characteristics of the AFC system are as follows:



\* MILLER COMPANY NUMBER

SCHEMATIC OF  
IF AMPLIFIER  
FIG. 46



Input signal for "hard limiting"	10 mv
Center frequency	30 Mc
Discriminator sensitivity	1.85v/Mc
Discriminator output swing (peak to peak)	10.2 v
D.C. Amplifier gain	97
D.C. Amplifier swing	90 v
Amplified sensitivity	178 v/Mc
Klystron sensitivity	~1 v/Mc
System loop gain	178

Thus an open loop frequency drift of 35 Mc will be degenerated to approximately 200 kc when the loop is closed.

#### 6.4 Receiver

The criteria used in selection of the receiver amplifier were octave bandwidth, noise figure on the order of 5 db or less, and gain of 80 to 100 db. The octave bandwidth insured that at least three of the harmonics of interest could be used by selecting an appropriate difference frequency at the fundamental. At the time of purchase, octave amplifiers with center frequencies above 150 Mc were only available with low gain and high price. In the year which has since elapsed, substantial improvements have been made in both directions and transistorized or tunnel diode amplifiers are now available which would permit improvement in system sensitivity, or economy. One would now have the choice of selecting a higher frequency amplifier for the same investment, thereby improving the receiver noise figure, or selecting the same 100-200 Mc frequency range with considerably less expense.

For this investigation, however, the 100-200 Mc amplifier was somewhat dictated by economy. The fourth, fifth, and sixth harmonics could readily be included by choosing a 30 Mc difference frequency for the AFC system. When the amplifier

was received, the measured bandpass was actually 85 to 205 Mc, and hence, was also used for third harmonic as another point for checking the operating predictions of the system.

The amplifier was a conventional tube type, with an overall gain of 83 db and a noise figure of 5.5 db. It was built on two chassis in pre-amp and post-amp sections, with 20 db gain in the first section. This permitted the insertion of filters between the sections with little effect on the overall noise figure.

Bandpass filters were designed and built at center frequencies of 120 Mc, 150 Mc and 180 Mc. These were each 10 Mc wide with rejection of greater than 50 db for the undesired harmonics. Further details and schematics may be found in an earlier report<sup>14</sup>.

The overall noise figure of the receiver is a function of the conversion loss at the harmonic mixer, and hence is an indeterminant quantity in so far as direct measurement is concerned. It was predicted to be on the order of 50 to 55 db, and agreement with prediction seems to warrant acceptance of this as at least a proper order of magnitude figure.

#### 6.5 System Performance

Figure 48 shows the completed waveguide system. The klystron at the top left of the photograph was used as the transmitter source, the klystron at left center was the local oscillator. The harmonic generator and harmonic mixer are here butted together, thus reducing the transmission path at the harmonic to three inches, which is the minimum physically realizable here. The chassis for the AFC system are in the center foreground.

The transmitter klystron is followed by an isolator. In this system where all available power from the klystrons is desired at the crystals, and essentially no padding is present in

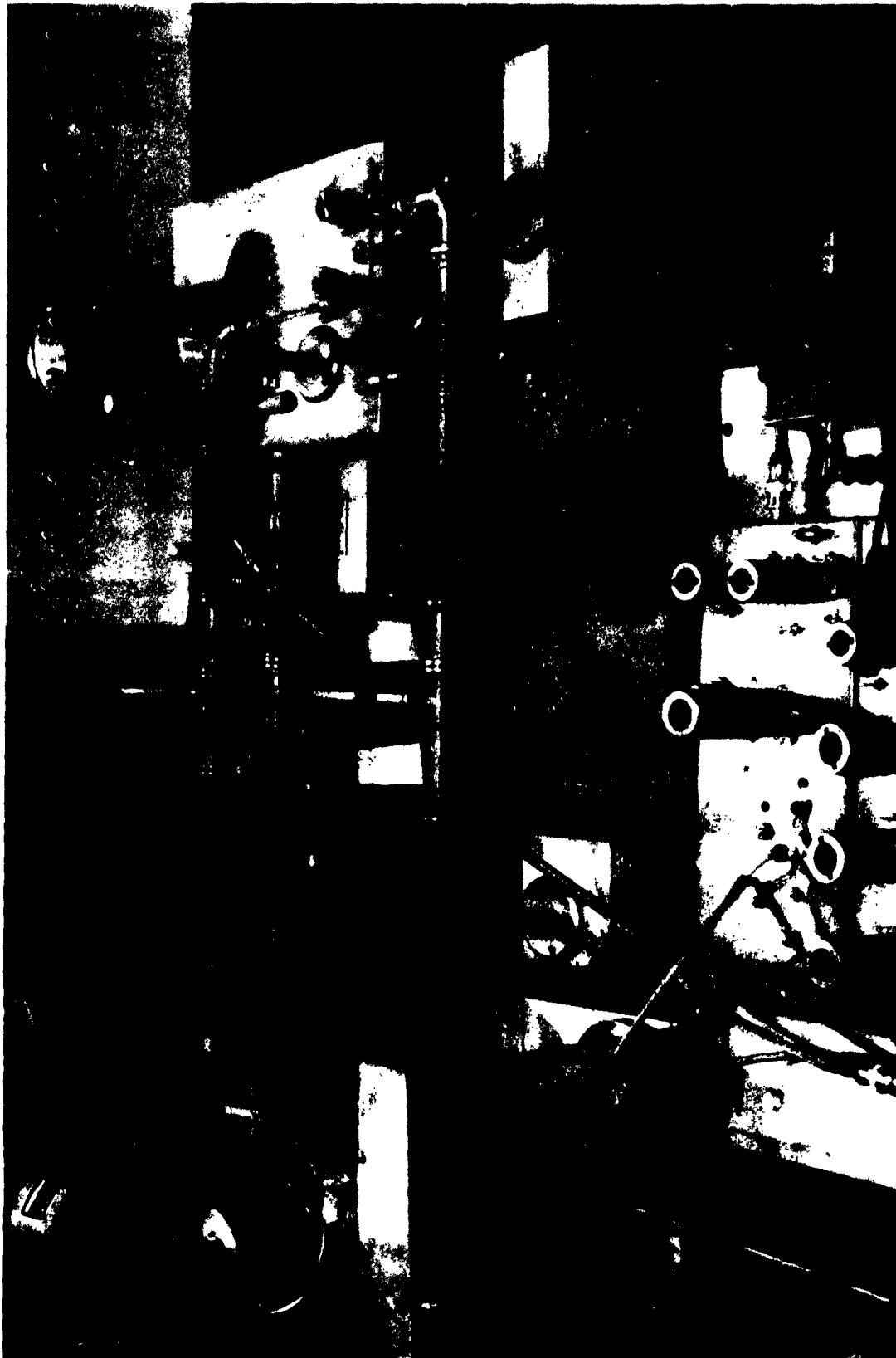


Figure 48 - Submillimeter  
Wavelength Measure-  
ment System

the waveguide, the use of an isolator is strongly recommended. Without the isolator, any adjustments made at the mixers would generally result in a pulling of the klystron frequency due to the impedance changes seen by the klystron. Such pulling effects were frequently beyond the hold-in capability of the AFC system. This was particularly true when new contacts were being made in a mixer while the system was operating. In any future system built on these lines, two isolators would be desirable.

For discussion of the overall performance of the measurement system we define the following symbols:

Amplifier Noise Figure	$F_{IF}$
Crystal Noise Ratio	$t$
Harmonic Mixing Conversion Loss	$L_{C(M)}$
Receiver Noise Figure	$F^* = L_{C(M)}(F_{IF}^{t+1})$
Effective Bandwidth	$B_{eff} = B_{IF} \times B_{video}$
Receiver Sensitivity	$S_n = F^* k T B_{eff}$
Power at the Fundamental	$P_f$
Harmonic Generation Conversion Loss	$L_{C(G)}$
Power at the $n^{th}$ Harmonic	$P_n$
System Dynamic Range	$(P_n - S_n) \text{ in db}$

Among these, the measurable quantities are the power at the fundamental (+12 dbm), the video and IF bandwidths (40 cycles and 10 Mc, respectively), the amplifier noise figure (5.5 db), the crystal noise ratio and the system dynamic range, or signal above noise. The latter two are a function of the harmonic being used. Expressing each term in db, we have

$$(2) \quad P_n = P_f - L_{C(G)}$$

and

$$(3) \quad S_n = F + kTB_{\text{eff}} = L_{C(M)} + (F_{IF} + t - 1) + kTB_{\text{eff}}$$

hence from (2) and (3)

$$(4) \quad P_n - S_n = P_f - (F_{IF} + t - 1) - kTB_{\text{eff}} - L_{C(G)} - L_{C(M)}$$

or

$$(5) \quad L_{C(G)} + L_{C(M)} = P_f - (F_{IF} + t - 1) - kTB_{\text{eff}} - (P_n - S_n)$$

Here we have the sum of the conversion losses expressed in terms of measurable quantities. This, however, is as far as one can go without an absolute measure of the power at the harmonic.

Using this expression, and the measured values of crystal noise ratio and dynamic range at the specified harmonic, one can arrive at the figures in Table III. The predicted values are there listed beyond the range which was actually checked. It is felt that the agreement is sufficiently good that these figures could be used with reasonable confidence in predicting the behavior of an extension of the system.

As was pointed out in the section on harmonic generation, the conversion loss in the transmitter could be improved significantly by having more power available at the fundamental. Indeed, at the sixth harmonic, using the relationship that  $L_{C(G)}$  is proportional to  $(P_f)^{n-1}$ , a 3 db increase in fundamental power should show up as a 15 db increase in the dynamic range. For the measurements made here, there was sufficient signal at 420 Gc. To extend this above 500 Gc, however, would have required higher power at the fundamental, and would be desirable on both the harmonic generator and mixer crystals.

Harmonic Number (n)	Frequency (Gc)	t (ratio)	MEASURED					PREDICTED				
			(F <sub>IF</sub> +t-1) (db)	kTB <sub>eff</sub> (dbm)	P <sub>f</sub> (dbm)	P <sub>n</sub> -S <sub>n</sub> (db)	L <sub>C(G)</sub> +L <sub>C(M)</sub>	L <sub>C(G)</sub>	L <sub>C(M)</sub>	L <sub>C(G)</sub> +L <sub>C(M)</sub>		
3	210	50	+17	-126	+12	61	60	39	16	55		
4	280	37	+16	-131	+12	46	81	52	20	72		
5	350	15	+12	-131	+12	32	99	65	24	89		
6	420	8	+10	-131	+12	29	104	73	26	99		
7	490	-	-	-	-	-	-	81	28	109		
8	560	-	-	-	-	-	-	89	30	119		

129

TABLE III  
Comparison of Operational System with Prediction

## 6.6 Measurements

Inspection of Figure 48 shows one feature of the measurement system which must always be borne in mind when a measurement is proposed. This is the fact that there exists a closed loop of waveguide which must always be maintained. One could consider this as starting at the hybrid tee and proceeding in two directions to the mixers where the loop must again be closed. This is to say that the transmission line for the harmonic signal cannot be changed without some compensatory adjustment in the fundamental waveguide length. Since measurements at these frequencies must necessarily be of the insertion loss type, it is essential that the system not be interrupted in a fashion which would result in a breaking of the frequency lock between the klystrons. When such an interruption occurs, and the AFC loop is readjusted to a lock-in range and closed once more, there is always the possibility that the original reference level is no longer valid. In general practice it was found that the change in the reference level which occurred as a result of this was less than one db. On occasion, however, it was greater than this and could then require a frequency adjustment on both klystrons to return to the original level. This is not surprising, since the hold-in range of the AFC loop exceeds the lock-in range. If the open loop frequency drift would have been 20 Mc, without the AFC (degenerated by the loop to something on the order of 115 kc), then when the loop is opened this separation appears and one or the other of the klystrons must be adjusted in frequency either by a change in reflector voltage or in the cavity tuning, before the lock can be achieved again. This can result in operation at a different point on the klystron mode with a resultant change in power on the crystal. When the loop was undisturbed, the output power level was usually stable over thirty

minute periods to  $\pm 0.3$  db.

Measurements were made on loss in RG-139/U waveguide which were quite straightforward in procedure. The measurement was begun with the system as shown in Figure 48. Then sections of RG-139/U and RG-98/U of equivalent length could be inserted between the mixers and in the local oscillator waveguide line, respectively, thus effectively displacing the receiver mixer crystal to the right, as seen in the photograph. The insertion loss of the RG-139/U could then be measured. For several reasons, only short lengths of guide were used. One of these was a comment <sup>\*</sup> that a section of this guide had been measured to have a 5 db loss in a two inch section at 300 Gc. If this were true, long lengths of guide could have exceeded the limitations of the system dynamic range. Furthermore, long lengths of guide inserted in the fundamental line could possibly change the power level on the local oscillator crystal sufficiently to affect the measurement. Bends which would have enabled the forming of a "U" in the harmonic guide to eliminate the latter objection, were unobtainable. As a result, 4" and 8-1/2" lengths were made (to correspond to lengths of RG-98/U already available). The results of the measurements of the two pieces are shown in Figure 49 expressed on a db/foot basis. The shorter section showed the higher loss. There is a remote possibility that some of this could be the result of losses at the joints being sufficiently high that they would affect the extrapolated data. It seems more likely, however, that the actual variation from piece to piece in surface finish and corresponding loss is really as much as is indicated.

---

\* Private communication with M. de Thomasson of American Radio Company, Inc.

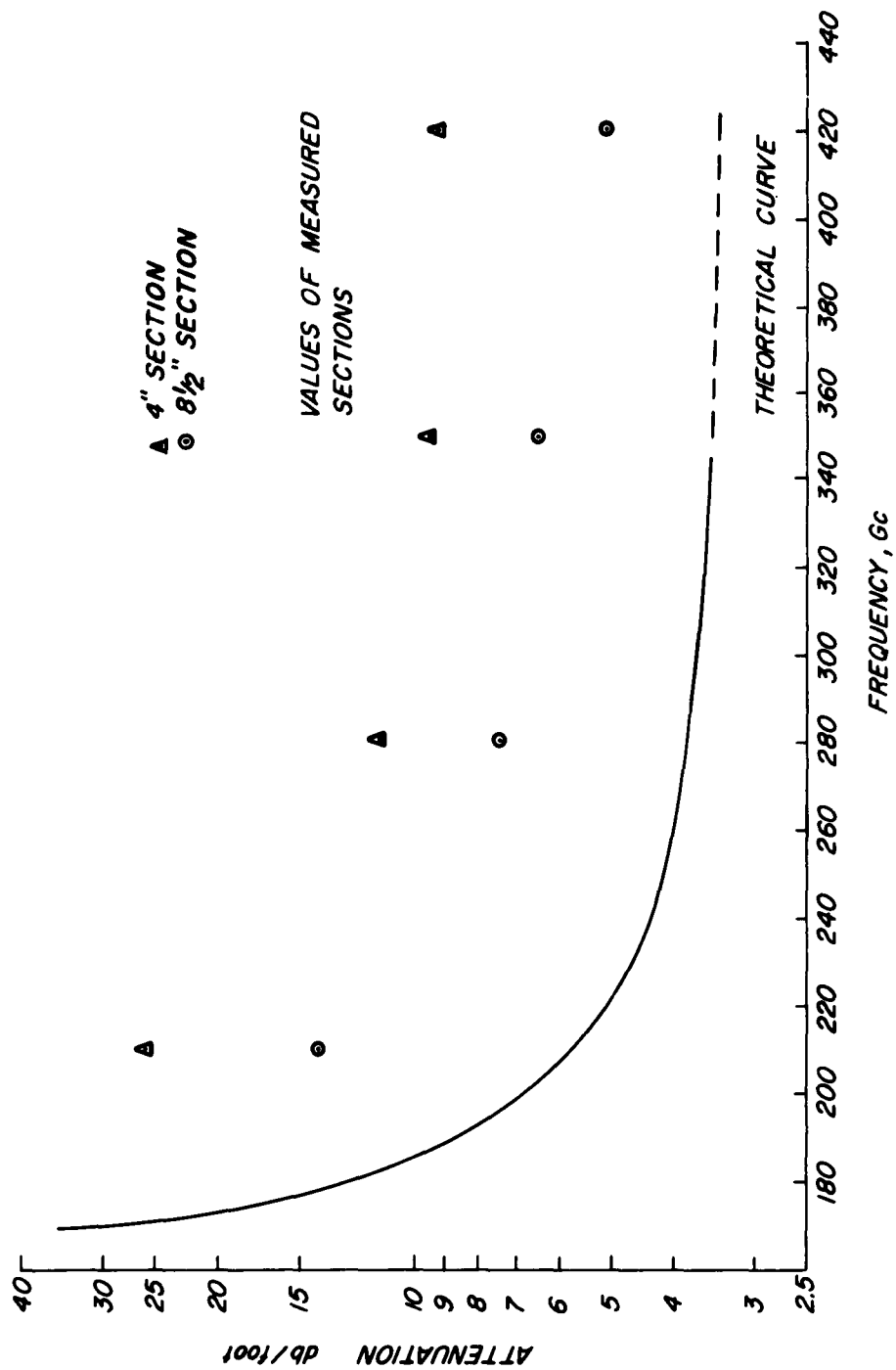


FIG. 49 - ATTENUATION IN RG-139/U WAVEGUIDE

The measurement of the oversized and overmoded waveguide was much more complicated. The test set up is shown in Figure 50. Since long lengths of line were necessarily involved here, a "U" of the oversized waveguide was necessitated. Each of the longer straight sections are four feet in length; six of these were made. The bends pictured were made with a  $45^{\circ}$  miter and were constructed to be interchangeable with two radius bends which were available. The short section was then made up to compensate for the displacement in the mixers and also the different lengths in the bends. The original plan was to obtain a reference level with just the one small section and the bends in place. The launching and bend losses would then be assumed fixed, and the loss per unit length measured by inserting pairs of the four foot sections, thus obtaining data for lengths of 8, 16 and 24 feet of guide.

The launching technique used was a horn and lens combination. Pyramidal horns were fabricated for the RG-139/U waveguide which were designed to have a pattern which would confine most of the energy within a  $1\text{-}1/2'' \times 3''$  aperture 3" from the horn apex. The focal length of the quartz lenses was 2.93". The lenses were attached to the S-band guide. The mixers and the first S-band guide flanges were then fixed in place such that the horns would be at the focal point of the lenses. All flanges on the S-band guide were modified to accept locating dowel pins to insure proper waveguide alignment.

The optical launching was used since multimode propagation was desired, but with a preferential launching of the lowest order modes as indicated in Section 5.

The results of one of the first experiments performed at 280 Gc are shown in Figure 51. The initial losses of launching, collecting and the two mitered bends amounted to 10 db. The



Figure 50 - Experimental  
Arrangement for  
Measurement on  
RG-48/U Waveguide

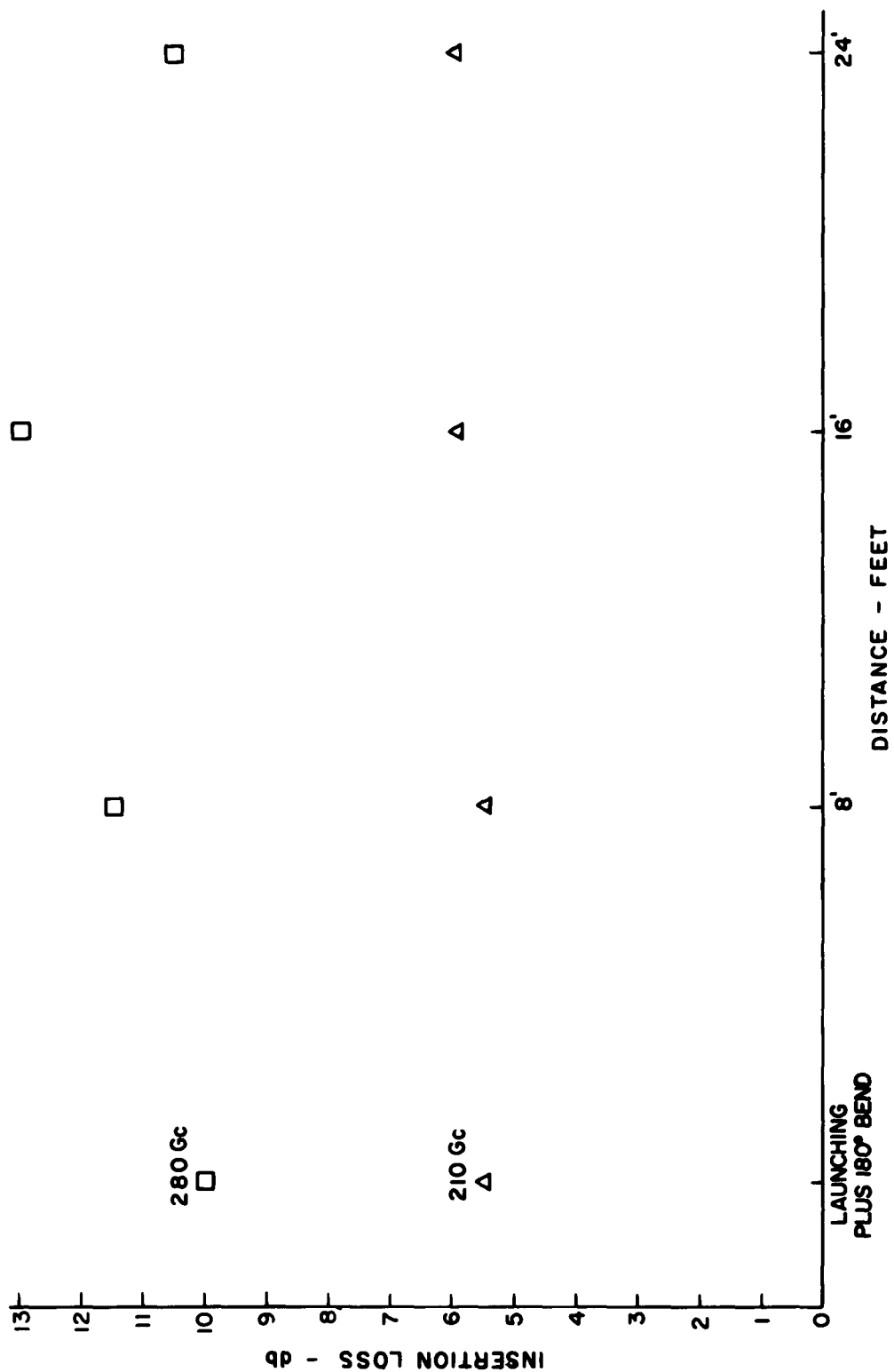


FIG. 51 -MEASURED LOSSES IN RG-48/U WAVEGUIDE AT 210 AND 280Gc

addition of the first lengths indicated an insertion loss in the waveguide, but the insertion of the final lengths reversed this trend indicating a net loss over 24' of only 1/2 db. These data were repeated many times. An investigation was then made at 210 Gc using crystal video detection thereby providing complete freedom of adjustment of the detector relative to the lens. It was found in this fashion that extreme care was required in the axial adjustment of the large waveguide in order to assure maximum signal at the focus of the lens. That is to say, that misalignment of the waveguide with respect to the axis of the launching horn could result in the off axis focusing of the received energy. The crystal video detector was then used to align the axis of the oversized waveguide as closely as possible with the axis of the transmitting horn, and the receiver mixer could then be fixed in the proper position for maximum received signal. (The results of the crystal video detection are also shown in Figure 51.) With the waveguide thus aligned; the 280 Gc measurement showed the total losses for launching, collecting, bends and 24' transmission path of 8-1/2db. The measurements at lesser length, however, continued to show greater losses.

It was then apparent that this beam was extremely well collimated, and in spite of the path length, most of the transmission was occurring within the first Rayleigh distance of the lens aperture. ( $D^2/\lambda$  for 280 Gc with the S-band aperture is approximately 20 feet ) Over this distance, even if the waveguide were not present, a simple horn lens arrangement would show very little transmission path loss. In order to have more significant data, either the path length had to be increased, or the Rayleigh distance shortened.

For this reason the lenses were stopped down to smaller aperture, so that more of the effect of the actual wall

losses could be seen. Two apertures were made measuring  $1\text{-}1/2'' \times 1''$ , and  $1'' \times 3/4''$ . The Rayleigh distances at 350 Gc were now very nearly 8 feet and 4 feet respectively. Hence transmission could now be effected over several Rayleigh distances of the lens aperture where straight optical considerations would indicate power loss would be proportional to the inverse square of the distance. The data obtained here are shown in Figure 52. Here it is seen that with the full aperture (Rayleigh distance of slightly more than 24 feet) the path loss was barely detectable. When the apertures were inserted, some anomalous behavior developed in the intermediate lengths. The high losses measured over the 16 foot path are obviously not dissipative losses but apparent losses which must be due to some interference pattern within the guide. The losses over the entire path would seem to set an upper limit on dissipative losses of the order of 0.1db/foot. The observed deviation from this on the other hand suggest that extreme care must be exercised when optical and oversized guide techniques are combined. A most interesting experiment would be one in which the path length of the oversized guide could be changed in very small increments such that the existence and behavior of interference patterns, if any, could be observed. With the modal distribution entirely unknown, this behavior and existence is now purely speculative. However, this phenomenon, coupled with the lack of flexibility in the horn-lens combinations of the transmitter and receiver, seem to provide the only plausible explanation for observed results.

It should also be noted here that when the radius bends were inserted in place of the mitered bends, the losses were extremely high, as was expected. The bends tried had radii (measured to the centerline) of  $3\text{-}1/2''$  and  $5\text{-}1/4''$ . Both exhibited losses in excess of 15 db. This type of behavior was predictable

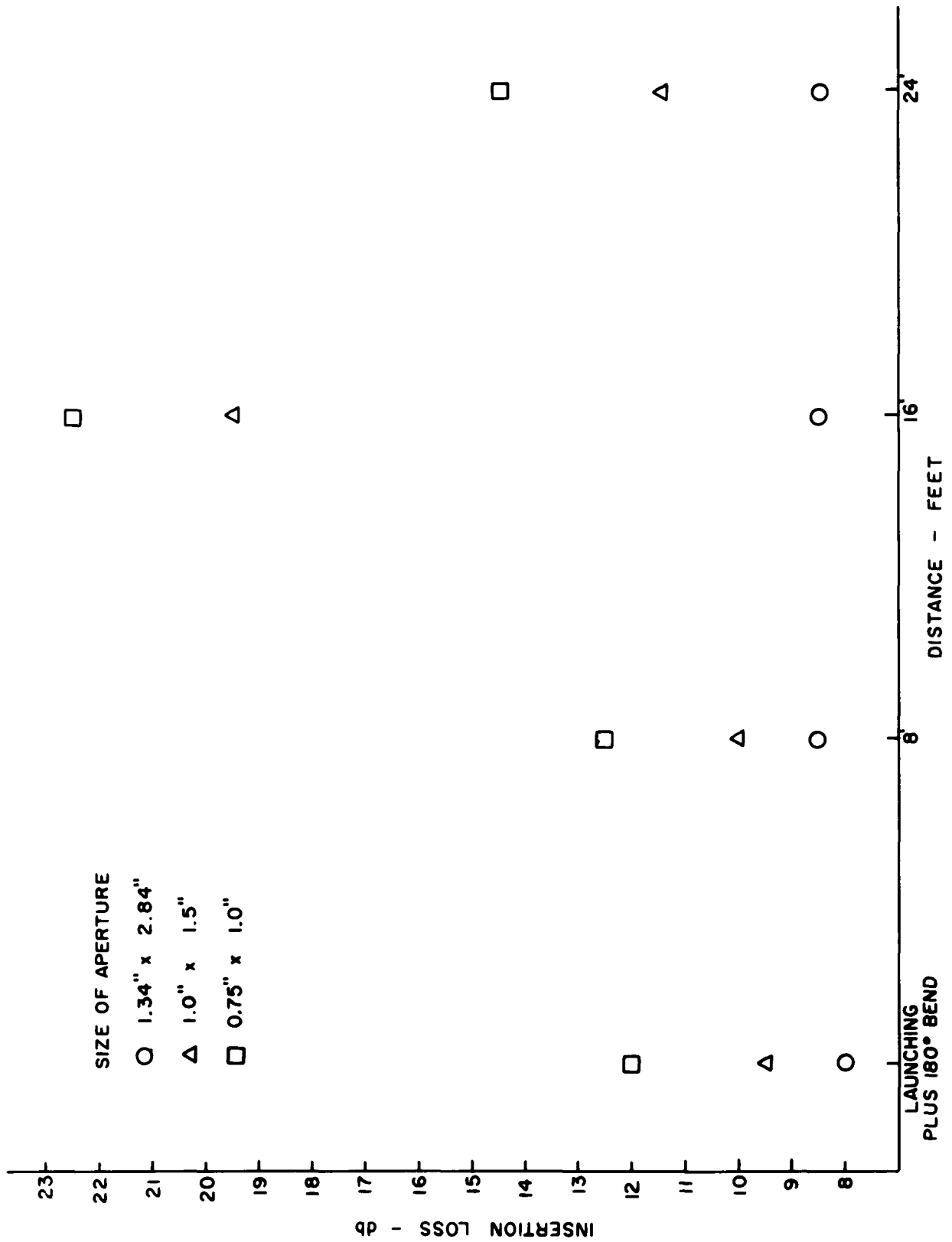


FIG. 52 - MEASURED LOSSES IN RG-48/U WAVEGUIDE AT 350 Gc

from a ray tracing basis which indicated that the radius bend would create a considerable amount of mode conversion to the higher order modes. These modes not only have higher loss in linear transmission, but also, if the order is sufficiently high, they will not be properly focused by the lens. Hence, in the optical type system used here, such mode conversion shows up immediately as lost energy.

One fact was clearly demonstrated: the overmoded guide with optical launching can offer a very significant improvement over the purely optical case, and a vast improvement over standard rectangular guide over moderate distances of tens of feet where delay distortion is a negligible factor.

## 7. CONCLUSIONS AND RECOMMENDATIONS

In the preceding sections, a variety of possible transmission methods applicable to the submillimeter wavelength region have been described briefly or in detail. No one method represents the panacea for submillimeter systems. In all cases some trade-offs must be made among such desirable features as low loss transmission, simplicity of construction of the transmission line and compatible components, power handling capabilities, lack of frequency limitations, etc. Working within the constraints thus imposed, however, some recommendations can be made and conclusions formed.

Of the several transmission lines surveyed in Section 2 of this report, it is felt that the three types selected for most thorough investigation offer the most advantages for general use. All of them will require further experimental investigation to determine the precise extent of their limitations.

The trough guide does have some upper frequency limit of usefulness due to the very small dielectric thickness required. Now that the launching efficiency has been demonstrated to be realistically predictable, a program will be required which would determine with what accuracy and to what limits of thickness a very thin dielectric surface can be deposited. It is felt that this program would show this line to be useful to frequencies on the order of 600 Gc, and possibly higher. The trough guide offers the advantages of partial shielding, rigidity, ease of support and low loss transmission. The oversized multimoded trough guide has the favorable point that fewer higher order modes can propagate than in a comparably oversized circular or rectangular guide. Here again, some experimental investigation would be required regarding launching into the guide in such a fashion that preferential mode excitation is assured.

Another phenomenon not readily predictable in surface wave structures is the radiation which will result when the field is perturbed, such as by the presence of a component structure. The problem will always be that of finding techniques whereby this effect can be minimized. This will be true regardless of the surface wave structure used. Any discontinuities arising from junctions or components must be investigated experimentally before definitive statements can be made concerning their practical usage.

Optical techniques using zone plates or lenses have the obvious advantage of frequency extension up through the visible region. When Fresnel region propagation is used, low loss can be realized, and the power capability is excellent. However, radiation (just as for surface wave structures) or beam distortion (asymmetry in the transverse plane) may occur as a result of diffraction, refraction, or reflection effects at components. If components such as prisms are to be used, and diffraction effects are to be overcome, these components must at least be large enough to subtend the entire beam. This either imposes a limitation on the beamwidth or dictates components of awkward size. Straight optical methods also have the disadvantage of a lack of inherent shielding. If shielding is not a problem, this is no doubt one of the most simply constructed short range transmission lines available.

The lack of adequate electrical and physical shielding is, of course, a disadvantage common to optical waveguides and most surface wave structures. Hence there may be undesired coupling between transmission lines, and pressurization or protection from weather may be difficult. If necessary, artificial shielding can be provided by enclosing the line or waveguide with an absorbent non-reflecting cover at a location where the field

components have decayed to negligible values. Such shields have been used successfully in several earlier investigations of open-type waveguides.

The oversized rectangular guide incorporates the advantages of a simple and readily available structure, good shielding, low loss and good power capacity. It introduces its own problem of distortion. As was pointed out there exist combinations of modulation frequency and distance traveled within which this problem becomes negligible, however. Once more, an experimental study on launching in preferential modal distributions is certainly desirable. Also, if quasi-optical components such as double prism attenuators and couplers are to be used within the guide, their effects on this modal distribution are not readily calculable.

Some recommendations have been given in the text concerning the types of components which afford the most promise for use in conjunction with the transmission lines. A notable exception is that of detectors. It has been tacitly assumed that the detectors, like the sources, would be built with conventional waveguide of the shortest possible length, since at the present state of the art these are necessarily small devices having dimensions on the order of a wavelength. There exist area detectors of the thermal variety; however, their response time precludes their use with high modulating frequencies. The Golay cell, for example, when air filled has a time constant of approximately three milliseconds, and when helium filled this can be reduced (with some sacrifice of sensitivity) to 600 microseconds. Until there is significant improvement made in detectors of this type, the superheterodyne receiver employing a mixer diode in dominant mode waveguide remains the best available detection method. This, however, is essentially the only

component for which standard waveguide packaging can be recommended. The optical and quasi-optical components seem to be the most plausible for extension to still shorter wavelengths.

A measurement system was designed for frequencies as high as 420 Gc. This system was completed and data taken successfully at 210, 280, 350, and 420 Gc. If similar systems are to be built in the future, it is recommended that the same general principles be applied. Some modifications could be made which would improve sensitivity and general performance, but still adhere to the original concepts. One such modification which is recommended is operation at a higher IF. There exist traveling wave tubes and other low-noise amplifiers which could be used to provide a receiver IF of 250 to 750 Mc. This would permit operation with a 70 Mc difference frequency at the fundamental and include in the receiver bandwidth harmonics four through ten. Coaxial bandpass filters (readily available commercially) could be used for harmonic selection. A higher IF would also reduce the effects of local oscillator noise contributions to the mixer noise figure, thus improving sensitivity.

The use of higher frequency signal sources for the local oscillator and the transmitter would also improve the receiver sensitivity and the system dynamic range. Klystrons having tens of milliwatts of power have recently become available at frequencies as high as 140 Gc. Carcinotrons have also become available, and can provide about a watt of power at 140 Gc and tens of milliwatts of power at selected frequencies as high as 330 Gc. The carcinotrons are admittedly quite expensive, but the higher frequency klystrons are only moderately more expensive than the 70 Gc klystrons that were purchased for this program. A compromise system of moderate cost and improved dynamic range could be built for operation at 280 and 420 Gc by the use of

140 Gc klystrons for harmonic mixing and harmonic generation.

It is also quite possible that a similar system could be improved by use of a different mixer design. There was no certainty here that the harmonic mixer and generator which were designed and used represent the optimum, although their performance is essentially as good as predicted. However a separate program for study of mixer and detector designs for submillimeter use is certainly recommended.

In summary, the measurement system has been shown to be practicable, with good dynamic range, and to have potential for further improvement. Systems of this type can be readily used at frequencies to about 400 Gc for a wide variety of applications, including, for example, the measurement of atmospheric attenuation and the general development of short-millimeter wave components.

## BIBLIOGRAPHY

1. J.C. Wiltse, "Some Characteristics of Dielectric Image Lines at Millimeter Wavelength", IRE Trans., Vol. MTT-7, p. 65; January, 1959.
2. M.J. King and J.C. Wiltse, "Surface Wave Propagation on a Dielectric Rod of Elliptic Cross Section", Electronic Communications, Inc., Scientific Report No. 1 on AFCRL Contract No. AF 19(604)-5475; August, 1960.
3. M.J. King, J.D. Rodgers, F. Sobel, F. Wentworth and J.C. Wiltse, "Quasi-Optical Components and Surface Waveguides for the 100 to 300 Gc Frequency Range", Electronic Communications, Inc., Scientific Report No. 2 on Contract No. AF 19(604)-5475; November, 1960.  
  
F. Sobel, F.L. Wentworth and J.C. Wiltse, "Quasi-Optical Surface Waveguide and Other Components for the 100 to 300 Gc Region", Trans. IRE, Vol. MTT-9, pp. 512-518; November, 1961.  
  
M.J. King and J.C. Wiltse, "Surface Wave Propagation on Coated or Uncoated Metal Wires at Millimeter Wavelengths", Trans. IRE, Vol. AP-10, pp. 246-254; May, 1962.
4. M. Cohn and M.J. King, "Selected Surface Wave Excitation Studies", Electronic Communications, Inc., Scientific Report No. 3 on Contract No. AF 19(604)-5475; March, 1962.
5. E.K. Damon and W.S.C. Chang, "Submillimeter Techniques", Proceedings of the Ohio State University - Wright Air Development Division Symposium on Electromagnetic Windows, WADD TR 60-274, Vol. I, June, 1960. See Figure 7, page 24.
6. G. Goubau and F. Schwering, "Guided Propagation of Electromagnetic Wave Beams", Trans. IRE Vol. AP-9, 248-256; May, 1961.
7. J.R. Christian and G. Goubau, "Experimental Studies on a Beam Waveguide for Millimeter Waves", ibid., pp. 256-263.
8. M. Cohn, "Propagation in Partially Dielectric Loaded Parallel Plane and Trough Waveguides", The Johns Hopkins University Radiation Lab., Technical Report No. AF-78, Contract No. AF 33(616)-6753; July, 1960.
9. Contract No. DA 36-039 sc-90750, "Investigation of Improved Airborne Antenna Techniques for Combat Surveillance", issued by USAERDL, Fort Monmouth, New Jersey.

10. K. Tomiyasu, "Intrinsic Insertion Loss of a Mismatched Microwave Network", Trans. IRE, Vol. MTT-3, pp. 40-44; January, 1955.
11. M. Born and E. Wolf, "Principles of Optics", Pergamon Press, New York, 1959.
12. M. Cohn, M. J. King, F. Sobel, and J. C. Wiltse, "Millimeter Wave Research", Electronic Communications, Inc. Technical Note No. 1 on Contract No. AF 30(602)-2457, August 31, 1961.
13. L. F. Van Buskirk and C. E. Hendrix, "The Zone Plate as a Radio Frequency Focusing Element", IRE Trans., Vol. AP-9 p. 319; May, 1961.
14. J. M. Cotton, F. Sobel, and J. O. Wedel, "Millimeter Wave Research", Electronic Communications, Inc., Technical Note No. 3 on Contract No. AF 30(602)-2457; February 28, 1962.
15. F. Sobel, F. L. Wentworth, and J. C. Wiltse, "Quasi-Optical Surface Waveguide and Other Components for the 100 to 300 Gc Region", IRE Trans., Vol. MTT-9, pp. 512-518; November, 1961.
16. M. Cohn, J. M. Cotton, and F. Sobel, "Millimeter Wave Research", Electronic Communications, Inc., Technical Note No. 2 on Contract No. AF 30(602)-2457; November 30, 1961.
17. F. Sobel, F. L. Wentworth, M. Cohn and J. C. Wiltse, "Millimeter Wave Component Research", Electronic Communications, Inc., Final Report on Contract No. AF 19(604)-5474; March, 1962.
18. F. A. Jenkins and H. E. White, "Fundamentals of Physical Optics", McGraw-Hill Book Co., Inc.; New York, 1937.
19. R. G. Fellers, "Applications of Dielectric Prisms at Millimeter Wavelengths", University of South Carolina, Dept. of Electrical Engineering, Contract AF 19(603)-43, AFOSR-TN-59-687; July 16, 1959.
20. R. G. Fellers, "Millimeter Wave Transmission by Non-Waveguide Means", The Microwave Journal, 5, pp. 80-86; May, 1962.
21. L. Lewin, "A Note on Quasi-Optical Methods at Millimeter Wavelength", Proc. of the Symposium on Millimeter Waves, Polytechnic Press of the Polytechnic Institute of Brooklyn, pp. 469-475; 1959.

22. R.H. Garnham, "Optical and Quasi-Optical Transmission Techniques and Component Systems for Millimeter Wavelengths", R.R.E. Report No. 3020, Royal Radar Establishment, Malvern, England; March, 1958.
23. A.E. Karbowiak, "Guided Wave Propagation in Submillimetric Region", Proc. IRE, 46, pp. 1706-1711; October, 1958.
24. C.A. Martin, "TM Waves in Submillimetric Region", Correspondence to Proc. IRE, 48, pp. 250-251; February, 1960.
25. A.E. Karbowiak, "TM Waves in Submillimeter Region", Correspondence to Proc. IRE, 48, p. 251; February, 1960.
26. S. Ramo and J.R. Whinnery, "Fields and Waves in Modern Radio", 2<sup>nd</sup> Edition, John Wiley and Sons, Inc., New York; 1953.
27. C.C. Eaglesfield, "Optical Pipeline, a Tentative Assessment", Proc. IEE, Vol. 109B, No. 243, pp. 26-32; January, 1962.
28. W.P. Ayres, P.H. Vartanian, and J.L. Melchor, "Frequency Doubling in Ferrites", JAP, 27, pp. 188-189; February, 1956.
29. J.L. Melchor, W.P. Ayres, and P.H. Vartanian, "Microwave Frequency Doubling from 9 to 18 KMC in Ferrites", Proc. IRE, 45, pp. 643-646; May, 1957.
30. W.P. Ayres, "Millimeter-Wave Generation Experiment Utilizing Ferrites", Trans. IRE, Vol. MTT-7, pp. 62-65; January, 1959.
31. B.A. Auld, H.J. Shaw, and D.K. Winslow, "Traveling Wave Frequency Doubling in Ferrites", JAP, 32, pp. 3175-3185; March, 1961.
32. D.D. Douthett, I. Kaufman, and A.S. Risley, "Microwave Harmonic Generation by Ferrimagnetic Crystals", JAP, 32, pp. 1905-1912; October, 1961.
33. I. Bady, "Frequency Doubling Using Ferrite Slabs, Particularly Planar Ferrites", Trans. IRE, Vol. MTT-10, pp. 55-64; January, 1962.
34. D.D. Douthett, I. Kaufman, and A.S. Risley, "Frequency Doubling in Anisotropic Ferrites", JAP, 33, pp. 1935-1936; April, 1962.

35. C.S. Gaskell, "Millimeter Wave Harmonic Generation in Ferrites", Proc. IRE, 50, p. 326; March, 1962.
36. "Investigation of Microwave Non-Linear Effects Utilizing Ferromagnetic Materials", Final Report on Signal Corps Contract No. DA 36-039 sc-73278; Melabs, Palo Alto, Calif.
37. R.L. Jepsen, "Harmonic Generation and Frequency Mixing in Ferromagnetic Insulators", Scientific Report No. 15, Gordon McKay Laboratory of Applied Science; May 25, 1958.
38. C.M. Johnson, D.M. Slager, and D.D. King, "Millimeter Waves from Harmonic Generators", Rev. Sci. Instr., 25, pp. 213-217; March, 1954.
39. J.M. Richardson and R.B. Riley, "Performance of three Millimeter Harmonic Generators and Crystal Detectors", Trans. IRE, Vol. MTT-5, pp. 131-135; 1957.
40. J.M. Richardson and J.J. Faris, "Excess Noise in Microwave Crystal Diodes Used as Rectifiers and Harmonic Generators", Trans. IRE, Vol. MTT-5, pp. 208-212; 1957.
41. M. Cohn and J.B. Newman, "Microwave Mixer Performance at Higher Intermediate Frequencies", 1959 IRE National Convention Record, Part 3, pp. 169-176; March, 1959.
42. R.V. Pound, "Frequency Stabilization of Microwave Oscillators, Proc. of the IRE., 35, p. 1405; 1947.
43. C.M. Johnson, "Frequency Stabilization Circuit for High Voltage Klystrons," Johns Hopkins University Radiation Laboratory, Internal Memorandum RL/53/IM-42; June 17, 1953.

# DISTRIBUTION LIST

<u>RADC-TDR-62-626</u>	<u>Nr. of Copies</u>
RADC (RALTM) Griffiss AFB NY	3
RADC (RAAP) Griffiss AFB NY	1
RADC (RAWED/Mr. R. Davis) Griffiss AFB NY	1
RADC (RASGR/M. D. Nicholson) Griffiss AFB NY	1
RADC (RAALD) Griffiss AFB NY	1
Commanding Officer USASRDL (SIGRA/ST-ADT) Ft Monmouth NJ	1
ASD (WWAD-Library) Wright-Patterson AFB Ohio	1
AU (Library) Maxwell AFB Ala	1
Chief, Naval Research Labs Code 2021 Wash 25 DC	1
AFSC (SCSE) Andrews AFB Wash 25 DC	1
ASTIA (TIPCA) Arlington Hall Station Arlington 12, Va.	10
Commanding General USASRDL (SIGRA/SL-PEE/Mr. N. Lipetz) Ft Monmouth NJ	1
Commanding Officer Diamond Ordnance Fuze Lab ATTN: Mr. J. A. Kaiser Wash 25 DC	1
Bureau of Ships (691B2C) Electronic Division ATTN: Mr L. V. Gumina Wash 25 DC	1

DISTRIBUTION LIST CONT'D

Commander ASD (WWDPVE-1/Mr. G.F. Durie) Wright-Patterson AFB Ohio	1
Commander Hq Detachment 2 AFRD ATTN: Mr. C.E. Ellis LG Hanscom Fld Bedford Mass	1
Commander ASD (ASRNRE-1/Mr. R.B. Leasure) Wright-Patterson AFB Ohio	1
University of Illinois ATTN: Dr. P.D. Coleman College of Engineering Urbana Ill	1
Raytheon Corporation ATTN: Mr. F. McVay 6380 Hollister Ave. Santa Barbara Calif	1
Polytechnic Institute of Brooklyn ATTN: Dr. A.A. Oliner Microwave Research Institute 55 Johnson St. Brooklyn NY	1
FXR ATTN: Mr. L. Bertan 26-12 Borough Pl Woodside 77 NY	1
Sperry Microwave Co ATTN: Mr. R. Duncan Clearwater Fla	1
Microwave Associates ATTN: Dr. L. Gould Burlington Mass	1
University of Wisconsin ATTN: Dr. Scheibe Dept of Elec Eng Madison Wisconsin	1
Director Ballistic Research Lab Aberdeen Proving Ground Aberdeen Md	1

DISTRIBUTION LIST CONT'D

AFCRL ATTN: Mr. F. J. Zucker Electromagnetic Radiation Lab Bedford Mass	1
NASA ATTN: Dr. Robert Coates, Code 520.1 Goddard Space Flight Center Greenbelt Md	1
Aerospace Corporation ATTN: Dr. R. C. Hansen Electronics Lab PO Box 95085 Los Angeles 25 Calif	1
MIT Lincoln Laboratory ATTN: Dr. Gerald Heller Lexington 73 Mass	1
The Martin Co ATTN: Dr. Vernon E. Derr Orlando Fla	1
Lawrence Radiation Laboratory ATTN: Mr. Charles B. Wharton University of Calif PO Box 808 Livermore Calif	1
Princeton University ATTN: Mr. William P. Ernst Project Staff Engineer Project Matterhorn Princeton NJ	1
Thompson-Ramo-Wooldridge ATTN: Dr. Irving Kaufman 8433 Fallbrook Ave Canoga Park Calif	1
Boulder Laboratories ATTN: Dr. J. M. Richardson National Bureau of Standards Boulder Colorado	1
US Army Signal Research & Development Lab ATTN: Mr. Leonard Hatkin Chief, Antenna & Microwave Circuitry Section Belmar NJ	1

DISTRIBUTION LIST CONT'D

Department of Electrical Engineering  
ATTN: Dr. Harvey Palmer  
The Johns Hopkins University  
Balto. 18 Md

Massachusetts Institute of Technology  
ATTN: Dr. Alan H. Barrett  
Room 26-459  
Cambridge Mass

US Army Signal Research & Development Lab  
ATTN: Dr. Georg Goubau  
Fort Monmouth NJ

Columbia University  
ATTN: Dr. S.P. Schlesinger  
Department of Electrical Engineering  
New York 27 NY

<p>Rome Air Development Center, Griffiss A. F. Base, N. Y. Rpt. No. RADG-TDR-62-626 MILLIMETER WAVE RESEARCH, Final Tech. Rpt., 16 December 1962; 148 pp. Incl. Figs.</p> <p>Unclassified Report</p> <p>The report includes a study of propagation methods for possible use in the submillimeter wavelength region (1.0 to 0.1 mm) of the electromagnetic spectrum. The more promising among these (through waveguide, oversized waveguide and Fresnel region propagation using Fresnel zone plates) are given a more comprehensive analytical treatment. Recommendations are given for some designs which would appear to have the highest probability for success.</p> <p>A measurement system consisting of a harmonic generator signal source and a harmonic-mixing superheterodyne receiver was built which was used for data taking at 210, 280, 350, and 420 Gc. The fundamental signals for harmonic generation and mixing were obtained from 70 Gc klystrons. An AFC system was developed to hold the frequency of one klystron stable with respect to the frequency of the second. The theory and instrumentation of the system is presented with some data taken on standard and oversized rectangular waveguides.</p>	<ol style="list-style-type: none"> <li>1. Microwaves</li> <li>2. Microwave Equipment</li> <li>3. Waveguides</li> <li>4. Transmission</li> <li>5. Analysis</li> <li>6. Extremely High Frequency</li> </ol> <p>I. AFSC Project No. 4506 Task No. 450602</p> <p>II. Contract No. AF30(602)-2457</p> <p>III. E. C. I., Timonium, Md.</p> <p>IV. Cotton, J. M., Cohn, M., Sobel, F., Wiltse, J. C.</p> <p>V. In ASTIA Collection</p>
<p>Rome Air Development Center, Griffiss A. F. Base, N. Y. Rpt. No. RADG-TDR-62-626 MILLIMETER WAVE RESEARCH, Final Tech. Rpt., 16 December 1962; 148 pp. Incl. Figs.</p> <p>Unclassified Report</p> <p>The report includes a study of propagation methods for possible use in the submillimeter wavelength region (1.0 to 0.1 mm) of the electromagnetic spectrum. The more promising among these (through waveguide, oversized waveguide and Fresnel region propagation using Fresnel zone plates) are given a more comprehensive analytical treatment. Recommendations are given for some designs which would appear to have the highest probability for success.</p> <p>A measurement system consisting of a harmonic generator signal source and a harmonic-mixing superheterodyne receiver was built which was used for data taking at 210, 280, 350, and 420 Gc. The fundamental signals for harmonic generation and mixing were obtained from 70 Gc klystrons. An AFC system was developed to hold the frequency of one klystron stable with respect to the frequency of the second. The theory and instrumentation of the system is presented with some data taken on standard and oversized rectangular waveguides.</p>	<ol style="list-style-type: none"> <li>1. Microwaves</li> <li>2. Microwave Equipment</li> <li>3. Waveguides</li> <li>4. Transmission</li> <li>5. Analysis</li> <li>6. Extremely High Frequency</li> </ol> <p>I. AFSC Project No. 4506 Task No. 450602</p> <p>II. Contract No. AF30(602)-2457</p> <p>III. E. C. I., Timonium, Md.</p> <p>IV. Cotton, J. M., Cohn, M., Sobel, F., Wiltse, J. C.</p> <p>V. In ASTIA Collection</p>